

Late-transition-state metal catalyzed polymerizations of olefins in supercritical carbon dioxide

Citation for published version (APA):

Vries, de, T. J. (2003). *Late-transition-state metal catalyzed polymerizations of olefins in supercritical carbon dioxide*. [Phd Thesis 1 (Research TU/e / Graduation TU/e), Chemical Engineering and Chemistry]. Technische Universiteit Eindhoven. <https://doi.org/10.6100/IR566708>

DOI:

[10.6100/IR566708](https://doi.org/10.6100/IR566708)

Document status and date:

Published: 01/01/2003

Document Version:

Publisher's PDF, also known as Version of Record (includes final page, issue and volume numbers)

Please check the document version of this publication:

- A submitted manuscript is the version of the article upon submission and before peer-review. There can be important differences between the submitted version and the official published version of record. People interested in the research are advised to contact the author for the final version of the publication, or visit the DOI to the publisher's website.
- The final author version and the galley proof are versions of the publication after peer review.
- The final published version features the final layout of the paper including the volume, issue and page numbers.

[Link to publication](#)

General rights

Copyright and moral rights for the publications made accessible in the public portal are retained by the authors and/or other copyright owners and it is a condition of accessing publications that users recognise and abide by the legal requirements associated with these rights.

- Users may download and print one copy of any publication from the public portal for the purpose of private study or research.
- You may not further distribute the material or use it for any profit-making activity or commercial gain
- You may freely distribute the URL identifying the publication in the public portal.

If the publication is distributed under the terms of Article 25fa of the Dutch Copyright Act, indicated by the "Taverne" license above, please follow below link for the End User Agreement:

www.tue.nl/taverne

Take down policy

If you believe that this document breaches copyright please contact us at:

openaccess@tue.nl

providing details and we will investigate your claim.

Late-transition-state metal catalyzed polymerizations of olefins in supercritical carbon dioxide

PROEFSCHRIFT

ter verkrijging van de graad van doctor aan de
Technische Universiteit Eindhoven, op gezag van de
Rector Magnificus, prof.dr. R.A. van Santen voor een
commissie aangewezen door het College voor
Promoties in het openbaar te verdedigen
op dinsdag 2 september 2003 om 16.00 uur

door

Tjerk Jan de Vries

geboren te De Bilt

Dit proefschrift is goedgekeurd door de promotoren:

prof.dr.ir. J.T.F. Keurentjes

en

prof.dr. C.E. Koning

Copromotor:

dr.ir. M.F. Kemmere

CIP-DATA LIBRARY TECHNISCHE UNIVERSITEIT EINDHOVEN

Vries, Tjerk J. de

Late-transition-state metal catalyzed polymerizations of olefins in supercritical carbon dioxide / by Tjerk J. de Vries. – Eindhoven : Technische Universiteit Eindhoven, 2003.

Proefschrift. – ISBN 90-386-2605-3

NUR 913

Trefwoorden: polymerisatie / overgangsmetaalkatalysatoren ; palladium / superkritische vloeistoffen ; koolstofdioxide / polyolefinen / thermodynamica ; fase-evenwicht / fysisch-chemische simulatie en modellering / statistische associërende vloeistof theorie ; SAFT

Subject headings: polymerization / transition-state metal catalysts ; palladium / supercritical fluids ; carbon dioxide / polyolefins / thermodynamics ; phase equilibrium / physicochemical simulation and modeling / statistical associating fluid theory ; SAFT

© Copyright 2003, T.J. de Vries

Druk: Universiteitsdrukkerij, Technische Universiteit Eindhoven

Samenvatting

Tegenwoordig worden veel elastomeren op grote schaal geproduceerd in organische oplosmiddelen. Bezorgdheid over veiligheid en milieu heeft geleid tot een zoektocht naar meer milieuvriendelijkere processen. Het vervangen van de organische oplosmiddelen door een meer milieuvriendelijk alternatief, zoals superkritisch koolstofdioxide (skCO₂), is één van de oplossingen. skCO₂ is een goed oplosmiddel voor kleine apolaire moleculen en tal van kleine polaire moleculen, echter niet voor polymeren. Hierdoor is skCO₂ zeer geschikt voor precipitatiepolymerisaties. Het is niet mogelijk om conventionele katalysatoren toe te passen voor de productie van elastische polyolefinen in skCO₂, omdat CO₂ deze katalysatoren inactieveert. Late-overgangsmetaal katalysatoren zijn stabiel in CO₂. Katalysatoren op basis van overgangsmetalen worden echter nog zeer weinig gebruikt voor polymerisaties in skCO₂ en zeker niet voor polymerisaties van olefinen in skCO₂.

Voor toepassing van skCO₂ als medium voor polymerisaties en als hulpmiddel voor het verwerken van polymeren is het belangrijk om over thermodynamische gegevens van de betreffende systemen te beschikken. Experimentele vlokpunten van binaire systemen van etheen en poly(etheen-co-propeen) (PEP) zijn bepaald voor verschillende molecuulgewichten. Tevens is de invloed van CO₂ op het binaire systeem etheen-PEP bepaald. De experimentele resultaten zijn gemodelleerd met de statistische associërende vloeistof theorie (SAFT) toestandsvergelijking. Het fasegedrag van tussenliggende samenstellingen kan goed worden voorspeld wanneer één enkele isopleet wordt gebruikt om de binaire interactie parameter van CO₂ en PEP te bepalen.

Een op palladium gebaseerde katalysator is gebruikt om 1-hexeen te polymeriseren in CO₂, hetgeen hoogmoleculaire polymeren opleverde. Uit referentiepolymerisaties in dichloormethaan blijkt dat polymeren met identieke molecuulgewichten en -gewichtverdelingen kunnen worden gevormd in skCO₂. Vervolgens zijn precipitatiepolymerisaties van etheen met de op palladium gebaseerde katalysator uitgevoerd in skCO₂ bij verschillende temperaturen, drukken en monomeerconcentraties. Daarnaast zijn

referentiepolymerisaties uitgevoerd in dichloormethaan. Hoogmoleculaire polymeren met smalle molecuulgewichtsverdelingen worden gevormd met redelijk goede opbrengsten, ofschoon de polymerisatie in skCO₂ een precipitatiepolymerisatie is, terwijl de polymerisatie in dichloormethaan een solutiepolymerisatie is. De gemeten drukval tijdens de polymerisatie is gemodelleerd om de reactiesnelheid te bepalen. De SAFT toestandsvergelijking is gebruikt om de neergeslagen gezwollen polymeerfase te beschrijven. Om de superkritische vloeistoffase te beschrijven zijn de Peng-Robinson en de Lee-Kesler-Plöcker toestandsvergelijking gebruikt. Gedurende de polymerisaties neemt de reactiesnelheid initieel sterk af, gevolgd door een meer geleidelijke afname. De berekeningen geven sterke aanwijzingen dat de inactivatie van de katalysator wordt veroorzaakt door een lokaal tekort aan monomeer.

De polymeren op basis van etheen zijn geanalyseerd met gelpermeatiechromatografie, differentiële scanning calorimetrie en ¹H en ¹³C kernspinresonantie. De polymerisaties in skCO₂ en in dichloormethaan leveren zeer sterk vertakte amorfe polymeren op met hoge molecuulgewichten en smalle molecuulgewichtsverdelingen. Bovendien blijkt dat de polymeren die gevormd zijn in skCO₂ een hoger gehalte aan korte keten vertakkingen bezitten. Dit wordt waarschijnlijk veroorzaakt doordat CO₂ een apolair karakter heeft, terwijl dichloormethaan polair is. Binnen het experimentele meetbereik heeft de statische druk geen invloed op het molecuulgewicht of de vertakkingen van de polymeren. Temperatuur en etheenconcentratie hebben daarentegen wel invloed op het molecuulgewicht, echter niet op de korte keten vertakkingen van de polymeren. Bovendien geven analyses van de polyetheenpolymeren met behulp van ¹³C kernspinresonantie een sterke indicatie voor een nieuwe vertakking-op-vertakking structuur die nog niet eerder is beschreven.

Co-polymerisaties van methylacrylaat en etheen met de op palladium gebaseerde katalysator zijn succesvol uitgevoerd in vloeibaar CO₂ als functie van verschillende monomeer concentraties en concentratieverhoudingen. De inbouw van methylacrylaat en de molecuulgewichten van de verkregen polymeren zijn vergeleken met literatuurwaarden van polymerisaties uitgevoerd in dichloormethaan. In vergelijking met dichloormethaan kunnen vergelijkbare molecuulmassa's worden verkregen. De inbouw van methylacrylaat in het copolymeer bij gelijke monomeer verhoudingen is hoger in vloeibaar CO₂ dan in dichloormethaan. Dit kan worden toegeschreven aan een hogere methylacrylaat concentratie

dichtbij de katalysator, òf aan een energetisch gunstiger katalysator-methylacrylaat complex vergeleken met het katalysator-etheen complex.

Velerlei aspecten van de late-overgangsmetaal complex gekatalyseerde polymerisatie van olefinen in $skCO_2$ zijn behandeld in dit werk. Desondanks dienen enkele zaken nog opgelost te worden of in meer detail te worden uitgezocht voordat een uitvoerbaar proces ontworpen kan worden. Katalysatoractiviteit en oplosbaarheid moeten verbeterd worden. Vele aspecten van het fasegedrag en van de reologische eigenschappen van de vaak heterogene polymeer-monomeer- CO_2 mengsels zijn nog niet helder en het massa- en warmtetransport in dit soort mengsels is complex. Desondanks is er een concept voor een toekomstig procesontwerp gegeven. De methodiek en de resultaten in dit proefschrift kunnen gebruikt worden voor het ontwerp van milieuvriendelijkere polymerisatieprocessen in $skCO_2$.

Summary

Many elastomers are currently being synthesized on a large scale in organic solvents. Safety and environmental concerns have induced a search for more environmentally sound processes. One solution is replacement of the organic solvent with a more environmentally benign alternative such as supercritical carbon dioxide (scCO₂). ScCO₂ is a good solvent for small non-polar and many small polar molecules, however, not for most polymers. This makes scCO₂ a suitable medium for precipitation polymerizations. Many polymerizations using various mechanisms have already successfully been performed in scCO₂. However, synthesis of elastomeric polyolefins using conventional early-transition-state metal based catalysts is impossible due to the incompatibility of these catalysts with CO₂. Late-transition-state metal catalysts are more stable in scCO₂. Up till now, catalysts based on transition-state metals are rarely used for polymerizations in scCO₂ and certainly not for polymerizations of olefins.

For the application of scCO₂ as a medium for polymerization and as processing aid, it is important to have reliable thermodynamic data of the systems involved. Experimental cloud-point data of binary systems of ethylene-poly(ethylene-co-propylene) (PEP) are presented for different molecular weights. Also, the influence of CO₂ on the phase behaviour of the binary system ethylene-PEP has been studied. The experimental results have been modeled using the statistical associating fluid theory (SAFT) equation-of-state (eos). The phase behavior of the intermediate compositions can adequately be predicted using one single isopleth to determine the binary interaction parameter between PEP and CO₂.

A palladium-based catalyst has been used to polymerize 1-hexene in scCO₂ yielding high molecular weight polymers. A comparison with polymerizations in dichloromethane reveals that polymers with identical molecular weight and polydispersity are formed. Precipitation polymerizations of ethylene have also been carried out in scCO₂ with this palladium-based catalyst at different pressures, temperatures and monomer concentrations. Reference experiments have been performed in dichloromethane. High molecular weight polymers with

low polydispersities have been obtained in reasonably good yields, although the polymerization in scCO₂ is a precipitation polymerization whereas the polymerization in dichloromethane is a solution polymerization. The measured pressure decrease upon polymerization has been modeled to determine the reaction rate. The SAFT eos has been used to describe the precipitated swollen polymer phase and the Peng-Robinson eos or the Lee-Kesler-Plöcker eos have been used to describe the supercritical fluid phase. During the polymerization, the calculated reaction rate initially decreases fast, followed by a gradual decrease in activity. The calculations strongly suggest that the catalyst decay is induced by monomer starvation.

The polymers have been analyzed with gel permeation chromatography, differential scanning calorimetry and ¹H and ¹³C nuclear magnetic resonance. The polymerizations in scCO₂ and dichloromethane result in highly branched amorphous polymers of high molecular weight and narrow molecular weight distributions. Moreover, the polymers produced in scCO₂ show a higher degree of short chain branching (SCB), which likely originates from the non-polar environment compared to the polar dichloromethane. Within the investigated range, the static pressure does not influence the polymer weight nor the SCB. Temperature and ethylene concentration have an effect on the polymer weight, however, not on the SCB of the polymers. Furthermore, analysis of the ¹³C nuclear magnetic resonance spectra of the polyethylenes gives a strong indication of a new branch-on-branch structure, which has not been assigned before.

Copolymerizations of methyl acrylate and ethylene with a palladium-based catalyst have successfully been carried out in compressed carbon dioxide at different monomer concentrations and monomer ratios. The incorporation of methyl acrylate and the molecular weight of the polymers have been compared to literature values of polymerizations conducted in dichloromethane. In comparison with dichloromethane, similar molecular weights can be obtained. The incorporation of methyl acrylate in the copolymer at the same monomer ratio is higher in compressed CO₂, which can be attributed to a higher methyl acrylate concentration near the catalyst or to an energetically more favorable catalyst-methyl acrylate complex compared to a catalyst-ethylene complex.

A number of issues regarding the late-transition-state metal catalyzed olefin polymerizations in scCO₂ have been discussed in this thesis. Nevertheless, some issues have to be resolved or investigated in more detail before a viable process can be designed. Catalyst activity and solubility still need improvement. Many aspects of the phase behavior and the rheological properties of the often heterogeneous polymer-monomer-CO₂ mixtures are not completely clear and the mass and heat transport phenomena in these mixtures are complex. Nevertheless, a concept for a future process design has been given. The methodology and results presented in this thesis provide guidelines for the design of environmentally benign polymerization processes in scCO₂.

Contents

Samenvatting	3
Summary	7
1. Catalytic polymerizations in supercritical carbon dioxide	13
2. Phase behavior of poly(ethylene-co-propylene) in ethylene and carbon dioxide: experimental results and modeling with the Statistical Associating Fluid Theory equation of state	23
3. Polymerization of olefins catalyzed by a palladium complex in supercritical carbon dioxide	41
4. Late-transition-state metal catalyzed polymerization of ethylene in supercritical carbon dioxide; determination of reaction rate by modeling the pressure	47
5. Characterization of polyethylenes produced in supercritical carbon dioxide by a late transition metal catalyst	63
6. Late-transition-metal catalyzed copolymerization of ethylene and methyl acrylate in compressed carbon dioxide	77
7. Prospects and issues for transition-metal catalyzed polymerizations in scCO ₂	87
Appendix 1: Programs to calculate overall pressure as function of conversion in batch precipitation polymerizations	107
Appendix 2: Program for calculation of sorption and swelling of polymers	119
Dankwoord	123
Curriculum Vitae	124
	11

Chapter 1

Catalytic polymerizations in supercritical carbon dioxide

Abstract

In this chapter, current polymerization processes for elastomer production are described. In order to make these processes more sustainable, replacement of the commonly used organic solvents, e.g. by supercritical carbon dioxide (scCO₂), represents a major challenge. The properties of supercritical fluids are discussed with emphasis on scCO₂. Small non-polar and many small polar molecules have a high solubility in scCO₂. However, most polymers do not dissolve in scCO₂. Polymerizations in scCO₂ are discussed, mainly focusing on processes which use transition-metal-based catalysts. Finally, the objective and outline of this thesis are given.

1.1 General introduction

Many elastomers, in particular poly(ethylene-co- α -olefin(-co-diolefins)) are currently being synthesized on a large scale in organic solvents¹, e.g. the production of EPDM in hexane. From an environmental point of view, these processes are undesired, due to inevitable losses of the solvent. Another major drawback of polymerizations in organic solvents is the inefficient removal and recovery of the solvents and monomers, as illustrated in Figure 1.1. The solvent recovery after polymerization often requires more process steps and energy than the actual polymerization.

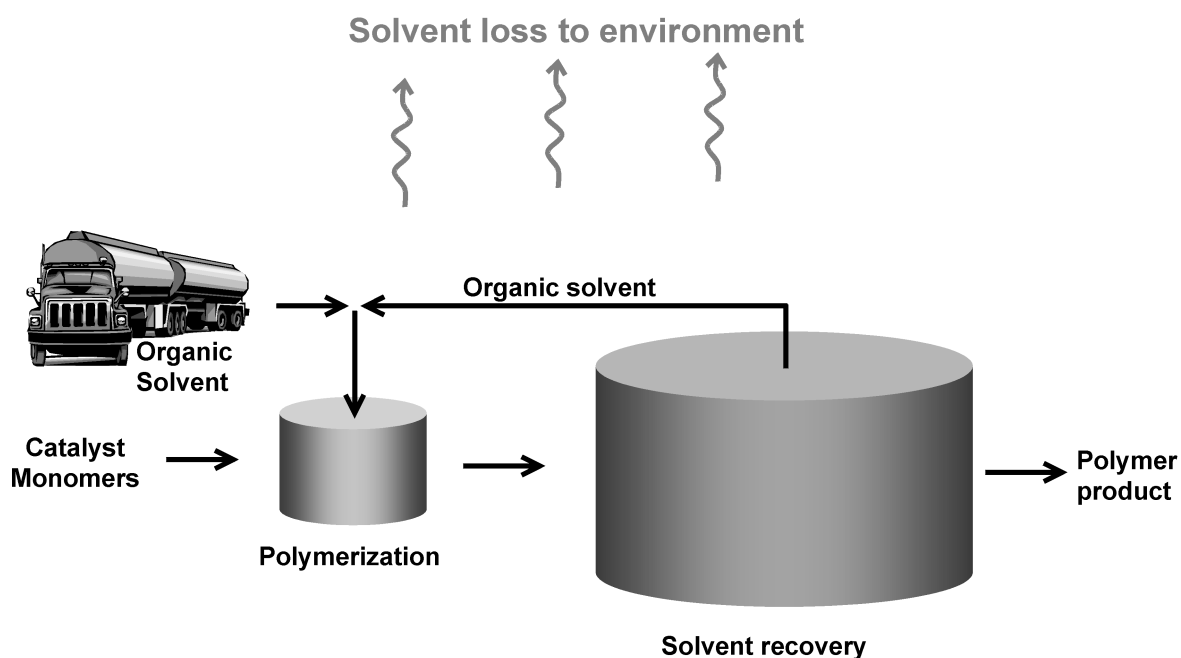


Figure 1.1. Schematic view of polymerization and solvent recovery in conventional polymerization processes for the production of poly(ethylene-co- α -olefin(-co-diolefins)).

The existing slurry and gas phase processes for the production of these polymers represent an improvement with respect to the solvent recovery step. However, in the gas phase processes, incorporation of high amounts of heavier monomers is limited due to the low vapor pressures of these monomers. Furthermore, conventional slurry processes use aliphatic diluents such as iso-butane or in some processes (supercritical) propane, which are highly flammable. To make these processes more sustainable, the organic solvents have to be replaced by environmentally benign alternatives. In this thesis, the use of supercritical carbon dioxide (scCO₂) will be explored for this purpose.

1.2 Supercritical carbon dioxide

A supercritical fluid is defined as a substance for which the temperature and pressure are above their critical values, see Figure 1.2. Above the critical temperature, the vapor-liquid coexistence line no longer exists. Therefore, a supercritical fluid can be tuned from liquid-like to gas-like without crossing a phase boundary, simply by changing the pressure or the temperature.

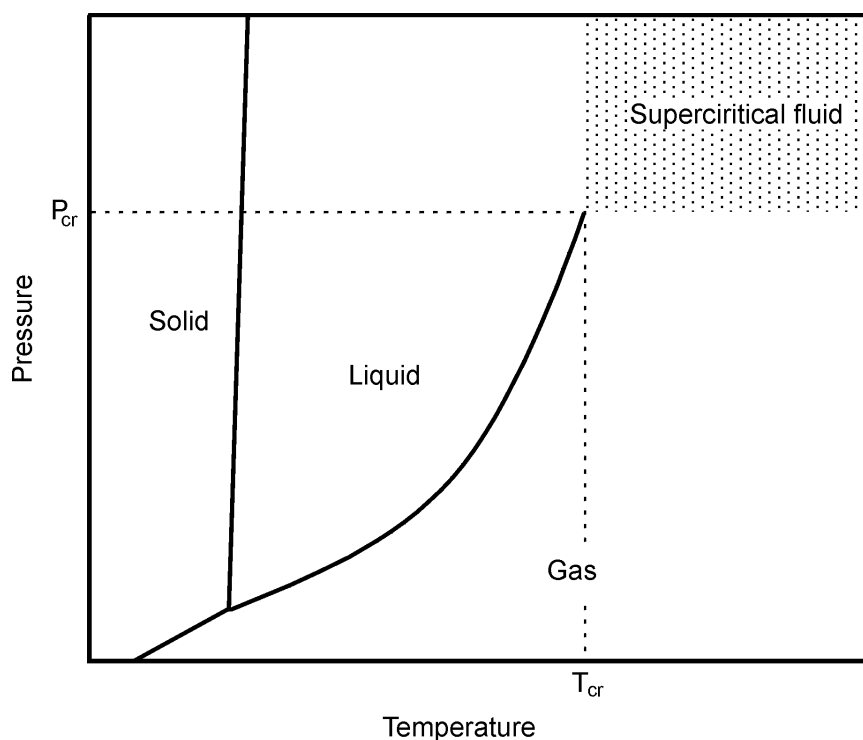


Figure 1.2. Schematic phase diagram for a pure component. The critical temperature, T_{cr} , and the critical pressure, P_{cr} , mark the end of the vapor-liquid equilibrium line and the beginning of the supercritical fluid region.

From a process technology point-of-view, the interesting pressure and temperature range is close to the critical point, because the physical properties in this range can be altered significantly by small changes in pressure or temperature. As an example, the solvent strength is closely related to the density of the fluid, therefore, compounds can be precipitated from solution by reducing the pressure. This has for example been used to fractionate polydisperse polymers^{2,3} and to induce crystallization in polymers⁴. Furthermore, the removal of the supercritical solvent after reaction is relatively simple.

One of the most commonly used supercritical fluids is scCO_2 , as it is environmentally benign, non-toxic, non-flammable, inexpensive and has a relatively low supercritical point. The critical temperature and pressure of pure CO_2 are 31.1°C and 73.8 bar , respectively. In Figure 1.3, the density of CO_2 at different temperatures is plotted as a function of pressure. It clearly shows that the modification of the density only requires small temperature or pressure changes just above the critical point.

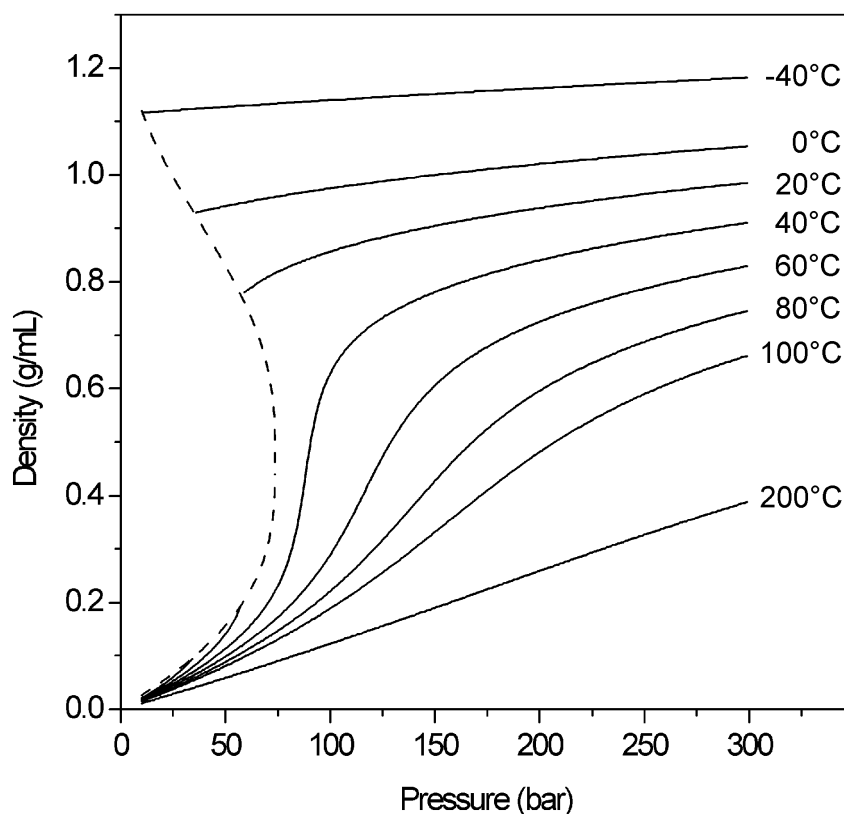
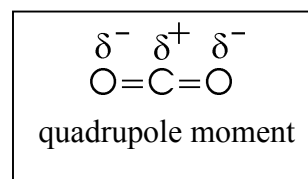


Figure 1.3. Density of CO_2 as a function of pressure at different temperatures (solid lines) and at the vapor-liquid equilibrium line (dashed line)⁵.

In general terms, scCO_2 is a solvent with low viscosity, high diffusion rates and no surface tension⁶. The viscosity of scCO_2 is in the range of 0.02 to 0.1 cP, which is one order of magnitude lower than the viscosity of a liquid (0.5 to 1 cP) and one order of magnitude higher than the viscosity of a vapor (0.01 cP). Diffusion coefficients in scCO_2 are a factor 5 to 10 higher than in common liquids⁷.

The solvent strength of scCO₂ has for a long time been considered to be in the range of n-hexane. However, due to the strong quadrupole-moment of CO₂ and its low polarizability, any comparison to conventional solvents is inaccurate. In some cases,



CO₂ can best be compared to perfluorinated solvents, which are non-polar and have a low polarizability like CO₂. Furthermore, the acidity of CO₂ has a beneficial effect on the solubility of weakly basic molecules. Generally, small molecules show high solubility in supercritical or liquid carbon dioxide⁸. In Figure 1.4, the phase diagrams of some small non-polar and polar molecules in CO₂ are given. Although the polarity of the molecules vary considerably, all compounds show complete miscibility above 90 bar. It should be noted that the critical temperature of the compounds is significantly higher than that of CO₂. Therefore, the mixtures are in the liquid state, except at very high CO₂ content. In many industrial applications, the concentrations of reactants are as high as possible to achieve high efficiencies, which implies that critical properties of the mixture have to be considered instead of the critical pressure and temperature of pure CO₂.

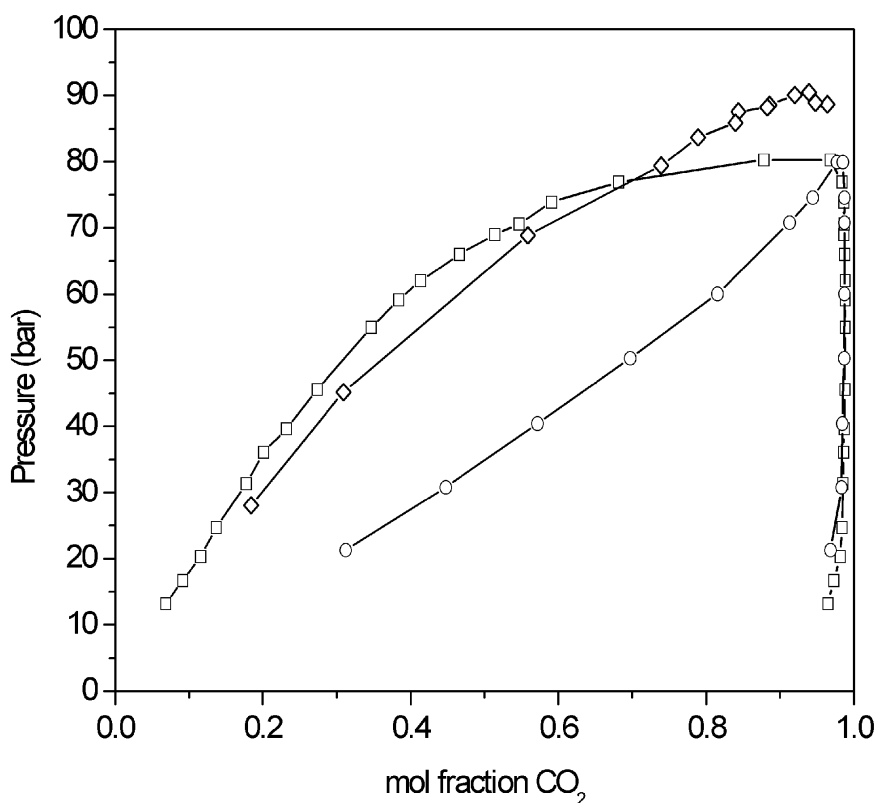


Figure 1.4. Phase diagrams of selected non-polar and polar molecules in CO₂; (◇) acrylic acid⁹, (□) methanol¹⁰, (○) 1-hexene¹¹.

1.3 Polymers in (supercritical) carbon dioxide

In general, large molecules and polymers have a rather limited solubility in (sc)CO₂^{12,13}. A few examples of exceptions are shown in Figure 1.5. The polymers in this Figure all have a flexible backbone and very weak interactions between the polymer chains. The expensive perfluorinated polymers and the cheaper polydimethylsiloxanes have been recognized early on as being highly soluble in (sc)CO₂ whereas the poly(ether carbonate)s have recently been discovered¹⁴. The second requirement for solubility in CO₂ is an attractive interaction between CO₂ and the polymer. The weak basic carbonyl moieties in Figure 1.5d and 1.5e positively influence the solubility in CO₂¹⁵. All the prerequisites are met by the polymer in Figure 1.5e, making this polymer the most soluble in (sc)CO₂ to date.

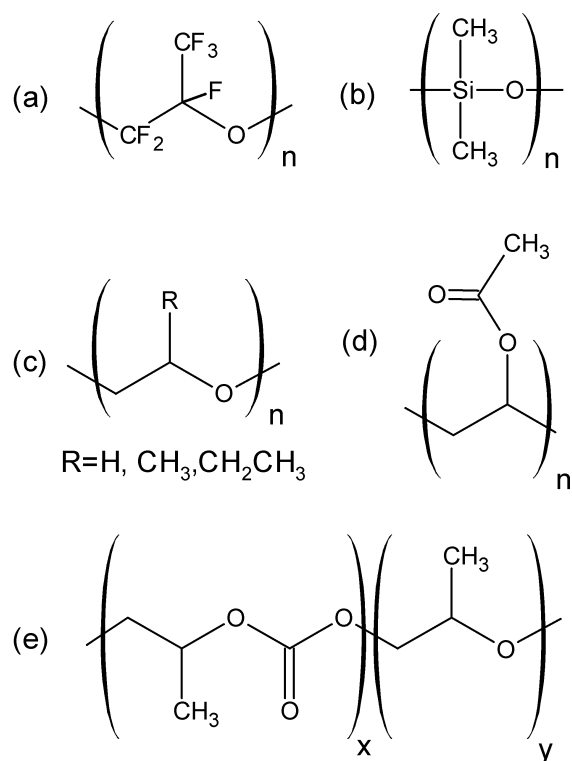


Figure 1.5. Polymeric structures soluble in scCO₂. (a) Perfluoropoly(propylene oxide), (b) Polydimethylsiloxane, (c) poly(ethylene-oxide) (R = H), poly(propyleneoxide) (R = CH₃) and poly(butyleneoxide) (R = CH₂CH₃), (d) polyvinylacetate, (e) poly(propyleneether carbonate).

1.4 Polymerization in supercritical carbon dioxide

Figure 1.6 shows the number of papers and patents that have been published over the years concerning polymerizations in scCO₂. In the last ten years, a substantial increase in publications can be observed. Free-radical or cationic chain growth polymerizations are the most common mechanisms employed for polymerization in scCO₂^{16,17}. Many industrially

A polymerization catalyst used for ring-opening metathesis polymerization (ROMP) of norbornene is shown in Figure 1.7a. The catalyst is not soluble in scCO_2 , therefore, methanol has been used as a cosolvent to improve the solubility of the catalyst. A general method to enhance the solubility in scCO_2 is modification of the catalyst with fluorinated tails, see Figure 1.7b and d. These catalysts are especially designed for polymerization in CO_2 and have a high solubility in scCO_2 . The catalysts shown in Figure 1.7b and c have been used for the copolymerization of epoxides and CO_2 . In these systems, CO_2 acts both as a reactant and as a solvent for the polymerizations.

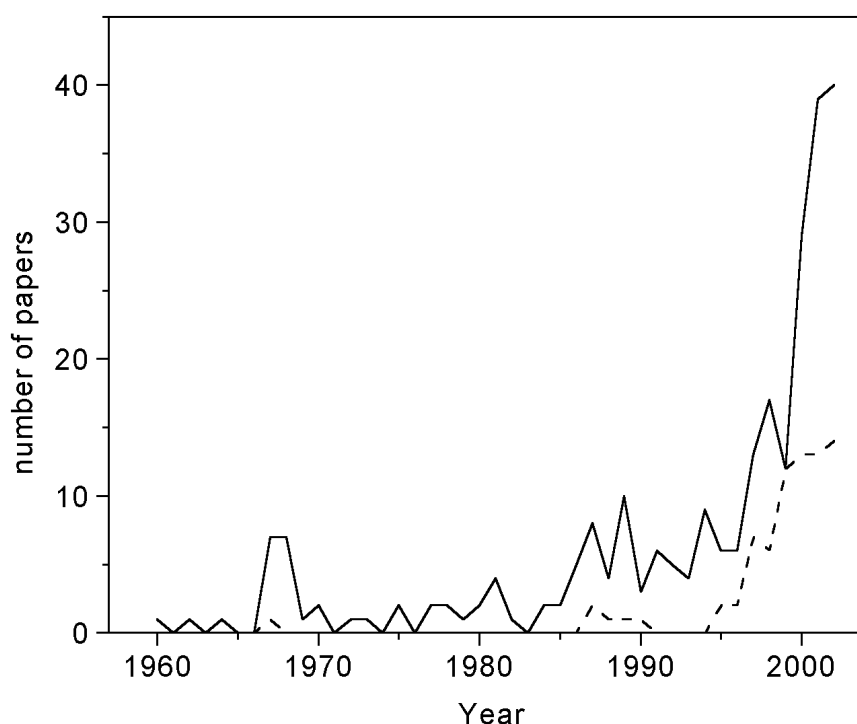


Figure 1.8. Number of papers concerning polymerization using nickel (solid line) and palladium catalysts (dashed line).

Another important issue for catalytic polymerizations is the compatibility of the catalyst with the mildly acidic CO_2 . The acidity of CO_2 poisons catalysts based on early-transition-state metals, which are often used for olefin polymerizations. Therefore, these catalysts can not be used in scCO_2 . Late-transition-metal based catalysts show more resistance to heteroatom based functional groups^{22,23,24}. These catalysts are interesting for their high tolerance towards impurities and the ability to (co)polymerize monomers with heteroatom functionalities.

However, in contrast to the early-transition-state metal based olefin catalysts, the research on late-transition-metal based catalysts has just begun. Figure 1.8 shows the number of papers since 1957 dealing with polymerization catalysts based on nickel and palladium¹⁸.

1.4 Aim and outline of this thesis

The objective of this thesis is to use scCO₂ as an environmentally benign alternative for organic solvents used in the production of elastomers. Chapter 2 describes the experimentally observed phase behavior of poly(ethylene-co-propylene) in CO₂ and ethylene, and the modeling of the phase behavior with the Statistical Associating Fluid Theory equation-of-state. In Chapter 3, the solubility and polymerization activity of a cationic late-transition-metal catalyst in CO₂ is discussed and compared to its performance in dichloromethane. The influence of pressure and temperature on the batch polymerization of ethylene in scCO₂ has been studied in Chapter 4. Additionally, a method has been described to derive the reaction rate from experiments by modeling the phase behavior. In Chapter 5, polyethylenes obtained in Chapter 4 at various conditions are compared with each other and with polyethylene produced in dichloromethane. The copolymerization of ethylene with methyl acrylate is described in Chapter 6. Finally, important issues for a future process design are discussed in Chapter 7.

1.5 References

- (1) Balk, R. *Condensed course on Polymer Reaction Engineering* **2002**, September 24-26, TU/e, Eindhoven.
- (2) Folie, B.; Kelchtermans, M.; Shutt, J. R.; Schonemann, H.; Krukoniš, V. *J. Appl. Polym. Sci.* **1997**, *64*, 2015.
- (3) Han, S. J.; Gregg, C. J.; Radosz, M. *Ind. Eng. Chem. Res.* **1997**, *36*, 5520.
- (4) Stejny, J.; Whitfield, A. F.; Pritchard, G. M.; Hill, M. J. *Polymer* **1998**, *39*, 4175.
- (5) Bush, D. *Equation of state for Windows 95 version 1.0.14*, Georgia Institute of Technology, **1994**.
- (6) McHugh, M. A.; Krukoniš, V. J. *Supercritical Fluid Extractions: Principles and Practice*, 2nd ed. **1994**, Butterworth-Heinemann, Stoneham, MA.

- (7) Suarez, J. J.; Medina, I.; Bueno, J.L. *Fluid Phase Equilibria* **1998**, *153*, 167.
- (8) Dandge, D. K.; Heller, J. P.; Wilson, K. V. *Ind. Eng. Chem. Prod. Res. Dev.* **1985**, *24*, 162.
- (9) Byun, H. S.; B.M.Hasch; M.A.McHugh *Fluid Phase Equilib.* **1996**, *115*, 179.
- (10) Chang, C. J.; C. Y. Day; C. M. Ko; K. L. Chiu *Fluid Phase Equilib.* **1997**, *131*, 243.
- (11) Wagner, Z.; I. Wichterle *Fluid Phase Equilib.* **1987**, *33*, 109.
- (12) O'Neill, M. L.; Cao, Q.; Fang, M.; Johnston, K. P.; Wilkinson, S. P.; Smith, C. D.; Kerschner, J. L.; Jureller, S. H. *Ind. Eng. Chem. Res.* **1998**, *37*, 3067.
- (13) Kirby, C. F.; McHugh, M. A. *Chem. Rev.* **1999**, *99*, 565.
- (14) Sarbu, T.; Styrane T.; Beckman, E. J. *Nature* **2000**, *405*, 165.
- (15) Kazarian, S. G.; Vincent, M. F.; Bright, F. V.; Liotta, C. L.; Eckert, C. A. *J. Am. Chem. Soc.* **1996**, *118*, 1729.
- (16) Kendall, J. L.; Canelas, D. A.; Young, J. F.; DeSimone, J. M. *Chem. Rev.* **1999**, *99*, 543.
- (17) Cooper, A. I. *J. Mater. Chem.* **2000**, *10*, 207.
- (18) SciFinder Scholar 2002, <http://www.cas.org/SCIFINDER/SCHOLAR/index.html>.
- (19) Mistele, C. D.; Thorp, H. H.; DeSimone, J. M. *Pure Appl. Chem.* **1996**, *A33*, 953.
- (20) Super, M. S.; Berluche, E.; Costello, C. A.; Beckman, E. *Macromolecules* **1997**, *30*, 368.
- (21) Hori, H.; Six, C.; Leitner, W. *Macromolecules* **1999**, *32*, 3178.
- (22) Boffa, L. S.; Novak, B. M. *Chem. Rev.* **2000**, *100*, 1479.
- (23) Ittel, S. D.; Johnson, L. K.; Brookhart, M. *Chem. Rev.* **2000**, *100*, 1169.
- (24) Younkin, T. R.; Conner, E. F.; Henderson, J. I.; Friedrich, S. K.; Grubbs, R. H.; Bansleben, D. A. *Science* **2001**, *287*, 460.

Chapter 2

Phase behavior of poly(ethylene-*co*-propylene) in ethylene and carbon dioxide: experimental results and modeling with the Statistical Associating Fluid Theory equation of state

Abstract

For the application of supercritical carbon dioxide as a medium for polymer synthesis and processing, it is important to have reliable thermodynamic data of the systems involved. In this study, experimental cloud-point data of binary systems of ethylene-poly(ethylene-*co*-propylene) (PEP) are presented for different molecular weights, 8.7 and 51 kg/mol, respectively. Also, the influence of carbon dioxide on the binary system ethylene-PEP51 is studied. Additionally, the experimental results have been modeled using the statistical associating fluid theory equation-of-state. Using a single isopleth to determine the binary interaction parameter between PEP and CO₂, intermediate compositions can adequately be predicted.

2.1 Introduction

An increasing number of processes deal with high pressure polymer-solvent systems in which phase behavior is a key issue. These include polymerization reactions¹ and various polymer processing operations, such as polymer shaping², fractionation^{3,4} and modification⁵. In these processes, it is important to know whether the polymer precipitates, dissolves, or swells and how reactive components are distributed between phases. Even more important, especially in the case where one of the components is a supercritical fluid, is to know how these processes can be manipulated.

The use of carbon dioxide as a polymerization reaction medium can be regarded as an environmentally friendly alternative for organic solvents, e.g. for the production of ethylene-propylene diene copolymer (EPDM) and other elastomers. For this purpose, we have developed a system for precipitation polymerizations of olefins in carbon dioxide using a late-transition-metal-based catalyst.⁶ To allow for the design of a process based on this system, the phase behavior of the binary system ethylene-poly(ethylene-co-propylene) (PEP) and the ternary system ethylene-PEP-CO₂ is studied. Most of the work described in the literature has focused on polymer-solvent systems rather than non-solvents. Binary systems of linear and branched polyethylenes in ethylene have been studied experimentally.^{7,8} Also, the effect of carbon dioxide as a nonsolvent on polymer-solvent systems has been described.⁹⁻¹¹ The available literature on the phase behavior of polymers in supercritical fluids has recently been reviewed in more detail.¹² In this work, the effect of molecular weight of the polymer in systems containing PEP and ethylene and the influence of CO₂ on the phase behavior are studied experimentally.

To describe the experimental results, we use the statistical associating fluid theory (SAFT) equation-of-state (EOS).¹³ The SAFT EOS is based on statistical thermodynamics and despite the rather complex derivation of the model equations, the basic idea and the application of the model are less complex. The SAFT EOS can be written as a sum of Helmholtz energies. The first contribution is the Helmholtz energy of an ideal gas, followed by a correction for a mixture of hard spheres, a correction for chain formation and a correction for the dispersion and association forces:

$$a = a_{\text{ideal gas}} + a_{\text{hard sphere}} + a_{\text{chain}} + a_{\text{dispersion}} (+a_{\text{association}}) \quad (2.1)$$

Because of the absence of strong specific interactions in our systems, like hydrogen bonding, the association contribution is omitted in our calculations. Without the association term, the SAFT EOS requires three parameters for pure components: a segment volume, v° , a segment-segment interaction energy, u°/k , and the number of segments, m . The dispersion energy is incorporated in the model as a square-well potential. Additionally, in multicomponent systems, a binary interaction parameter is needed for each pair of components and mixing rules have to be applied. In this chapter, mixing rules based on the Van der Waals one-fluid theory are used as described by Huang and Radosz¹⁴. The binary interaction parameter, k_{ij} , is used as a correction on the segment-segment interaction energy between the two different segments:

$$u_{ij} = (u_{ii} \cdot u_{jj})^{1/2} \cdot (1 - k_{ij}) \quad (2.2)$$

2.2 Experimental Section

2.2.1 Materials

Carbon dioxide (Messer Nederland, grade 4.5) and ethylene (Aga Gas, grade 3.5) were used as received. A few parts per million of hydroquinone was added to prevent polymerization of ethylene. The properties of the completely amorphous PEP are listed in Table 2.1.

Table 2.1. Characterization of poly(ethylene-co-propylene)

Sample	M_n (kg mol ⁻¹) ^a	M_w (kg mol ⁻¹) ^a	M_z (kg mol ⁻¹) ^a	Me/ 100C ^b	Tg (°C) ^c
PEP8.7	8.7	24	47	22	-60.2
PEP51	51	120	210	21	-54.5

^a measured with high temperature GPC experiments. ^b Me/100C is the number of methyl branches per 100 carbon atoms determined from overall propylene content of the polymer. ^c DSC measurements were performed at 10 °C/min. using 13-17 mg polymer samples, which were vacuum dried in an oven at 60°C for 24 hours. The calorimetric glass transition temperatures Tg were determined using the midpoint of heat capacity change as a criterion. No melting peak was observed in the range -80°C to 100°C.

2.2.2 Methods

Cloud-point measurements. The phase behavior of ethylene-PEP51, ethylene-PEP51-CO₂ and ethylene-PEP8.7 was studied in an optical high-pressure cell designed for pressures up to 4000 bar and temperatures up to 450 K. The cell, which is provided with sapphire windows and magnetic stirring, is a modification of the one described by Van Hest and Diepen¹⁵. For a detailed description of this apparatus and of the experimental techniques used, we refer to De Loos et al.¹⁶.

The cloud-point pressures of mixtures of known composition were measured as a function of temperature by visual observation of the onset of phase separation of the homogeneous phase upon lowering the pressure (cloud-point isopleths). The cloud points were determined with an absolute error of ± 0.03 °C in temperature and ± 1 bar in pressure. The sample preparation was carried out at ambient pressure and temperature. The estimated relative error in the amount of the components in the mixtures is less than 2% for PEP8.7, less than 0.1% for PEP51 and for ethylene, and less than 0.7 % for CO₂.

SAFT calculations The SAFT EOS requires pure-component parameters and binary interaction parameters for calculations. The pure-component parameters for small molecules (carbon dioxide and ethylene) are obtained by fitting to experimental vapor pressure data and saturated liquid densities. The procedure to obtain parameters for large molecules or polymers is less evident. In the SAFT EOS, this can elegantly be achieved by extrapolation of the parameters of a homologous series. This has previously been performed by Huang and Radosz¹³ for a series of n-alkanes and has been used for calculation of the phase behavior of systems containing PEP.^{17,18} In addition to this method, we fitted the parameters to *PVT* data of the polymer by minimization of the residual squares of calculated and measured densities or pressures. Binary interaction parameters were determined using vapor-liquid or liquid-liquid composition equilibrium data.

The core of the iterative method used to calculate the binary and ternary systems is described in Koak and Heidemann.¹⁹ This method calculates molar phase ratios and phase compositions of two-phase multicomponent systems at given temperature, pressure, overall composition, pure- component parameters and binary interaction parameters. This procedure needs initial guesses for the distribution coefficients, e.g. $k_i = y_i/x_i$. The polymer PEP was described as a pure component with molecular weight equal to M_n . To calculate cloud-point pressures in a ternary system using this flash algorithm, a second iterative procedure was used as a shell to approach the condition that $\Sigma(x_i - z_i)^2 = 0$, where x_i is the weight fraction of component i in

one phase and z_i is the weight fraction of component i in the feed. A similar procedure was used to calculate k_{ij} s of the binary system CO₂-PEP51 from ternary cloud-point data of the system CO₂-ethylene-PEP51.

Table 2.2. Isoleths for the systems PEP51-ethylene and PEP8.7-ethylene

T (°C)	P (bar)						
$w_{\text{pep51}}=0.0357$		$w_{\text{pep51}}=0.0498$		$w_{\text{pep51}}=0.0756$		$w_{\text{pep51}}=0.0989$	
39.39	2181	39.47	2163	39.61	2115	39.39	2083
44.54	2077	44.43	2057	44.76	2006	44.56	1977
49.36	1985	49.38	1961	49.12	1926	49.49	1890
54.33	1897	53.95	1885	54.32	1843	54.35	1811
59.51	1816	58.94	1809	59.07	1776	59.06	1749
64.13	1756	64.25	1741	63.95	1715	64.21	1687
68.98	1702	69.15	1684	68.81	1661	69.1	1634
$w_{\text{pep51}}=0.1230$		$w_{\text{pep51}}=0.1491$					
39.23	2061	39.47	2011				
44.26	1960	44.39	1917				
49.25	1874	49.18	1837				
54.05	1797	54.13	1765				
59.16	1730	59.01	1703				
63.98	1673	63.88	1647				
68.91	1619	68.62	1597				
$w_{\text{pep8.7}}=0.0468$		$w_{\text{pep8.7}}=0.1168$		$w_{\text{pep8.7}}=0.1503$		$w_{\text{pep8.7}}=0.1983$	
39.67	1827	39.51	1759	39.60	1715	39.51	1615
44.41	1748	44.56	1682	44.45	1646	44.44	1553
50.01	1666	49.36	1617	49.13	1586	49.83	1492
54.57	1610	54.23	1559	54.61	1524	54.33	1447
59.59	1555	59.11	1505	59.10	1480	59.64	1399
64.14	1512	64.13	1457	64.44	1432	64.11	1364
69.40	1465	68.86	1413	69.37	1395	69.54	1325

Table 2.3. Isopleths for the system ethylene-PEP51-CO₂

T (°C)	P (bar)	T (°C)	P (bar)	T (°C)	P (bar)	T (°C)	P (bar)
$w_{\text{pep51}} = 0.050$							
$w_{\text{CO}_2} = 0.050$		$w_{\text{CO}_2} = 0.100$		$w_{\text{CO}_2} = 0.150$		$w_{\text{CO}_2} = 0.200$	
39.44	2342	39.29	2585	39.52	2959	39.28	3705
44.54	2204	44.30	2413	44.46	2712	44.37	3240
49.30	2094	49.44	2263	49.23	2519	49.27	2913
54.16	1996	54.21	2144	54.09	2355	54.18	2666
59.05	1910	59.07	2041	59.00	2218	59.04	2470
63.95	1844	63.92	1949	63.89	2101	64.00	2311
68.90	1764	68.86	1871	68.71	2001	68.85	2181
$w_{\text{pep51}} = 0.100$							
$w_{\text{CO}_2} = 0.050$		$w_{\text{CO}_2} = 0.100$		$w_{\text{CO}_2} = 0.150$		$w_{\text{CO}_2} = 0.200$	
39.42	2265	39.53	2496	39.49	2900	39.35	3665
44.33	2140	44.42	2334	44.44	2654	44.33	3191
49.17	2032	49.23	2193	49.25	2457	49.2	2867
54.06	1938	54.11	2081	54.26	2290	54.13	2618
59.03	1858	58.99	1981	59.02	2166	59.01	2419
63.68	1785	63.91	1894	63.84	2055	64.15	2258
68.93	1718	68.71	1818	69.08	1950	68.97	2132

2.3 Results and discussion

2.3.1 Experimental results for the ethylene - PEP systems

The experimental results for the system PEP51-ethylene and PEP8.7-ethylene are presented in Table 2.2. In Figure 2.1, the experimental cloud-point isopleths of the PEP51-ethylene and PEP8.7-ethylene systems are shown. This figure shows that, at the experimental conditions, the cloud-point pressure decreases upon an increase in the temperature or in the polymer weight fraction (w_p) or upon a decrease in molecular weight of the polymer. A similar trend has been observed in systems based on linear polyethylene and ethylene⁷.

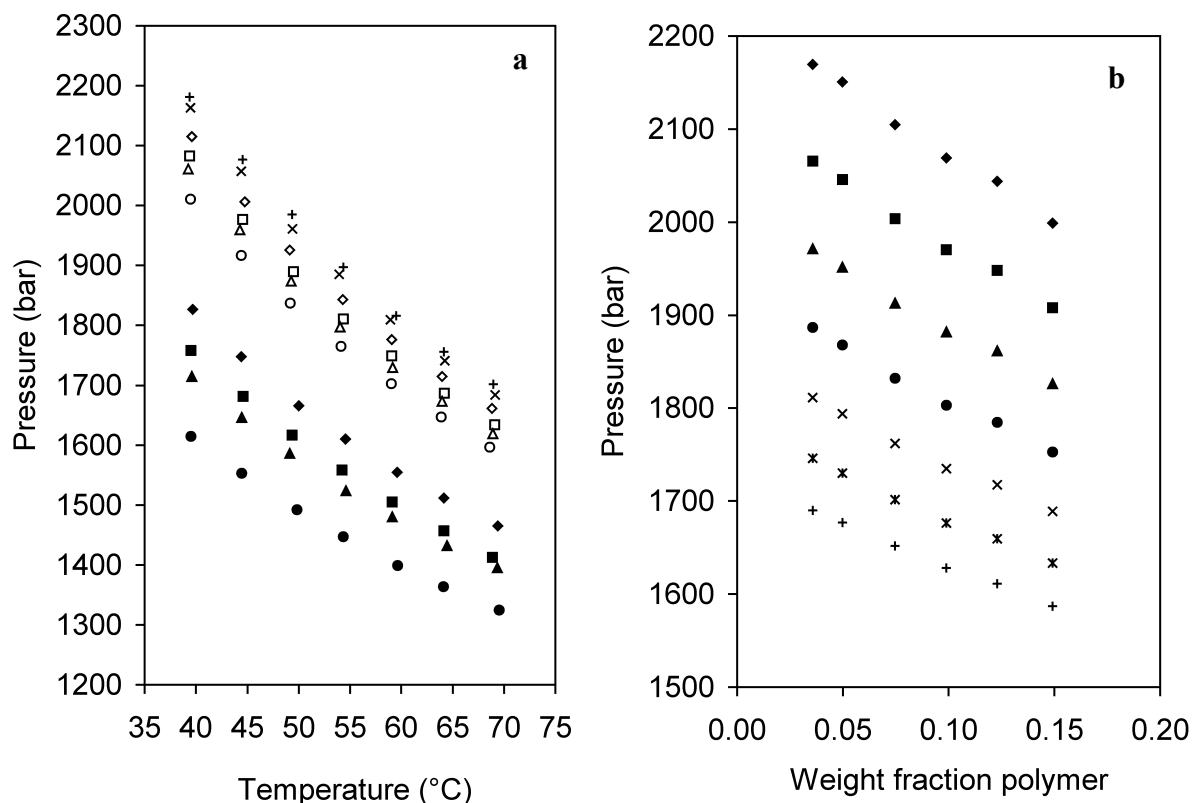


Figure 2.1. Cloud-point measurements of (a) PEP51 and PEP8.7 in ethylene and (b) pressure-composition sections for PEP51-ethylene system. (a) PEP51: (+) $w_p = 0.0357$; (x) $w_p = 0.0498$; (\diamond) $w_p = 0.0756$; (\square) $w_p = 0.0989$; (Δ) $w_p = 0.1230$; (\circ) $w_p = 0.1491$; PEP8.7: (\blacklozenge) $w_p = 0.0468$; (\blacksquare) $w_p = 0.1168$; (\blacktriangle) $w_p = 0.1503$; (\bullet) $w_p = 0.1983$. (b) (\blacklozenge) $T = 40$ °C; (\blacksquare) $T = 45$ °C; (\blacktriangle) $T = 50$ °C; (\bullet) $T = 55$ °C; (x) $T = 60$ °C; (\times) $T = 65$ °C; (+) $T = 70$ °C.

2.3.2 Experimental results for the system ethylene – PEP51 – CO₂

The binary system CO₂-PEP51 could not be determined experimentally as expected. No homogeneous phase could be detected for a sample containing 9.8 wt % PEP51 in CO₂ for pressures up to 4000 bar and temperatures between 40 to 170 °C. To examine the interaction between CO₂ and PEP51 indirectly, the ternary system ethylene-PEP51-CO₂ was measured. The experimental results for this system are presented in Table 2.3. Figures 2.2 and 2.3 show experimental cloud-point isopleths for the system ethylene-PEP51-CO₂. From these data it can be concluded that an increase in the weight fraction CO₂ (w_{CO_2}) leads to a higher cloud-point pressure. This effect can be attributed to the lower permittivity and the higher quadrupole moment of CO₂ when compared to ethylene. Both properties lower the dispersion

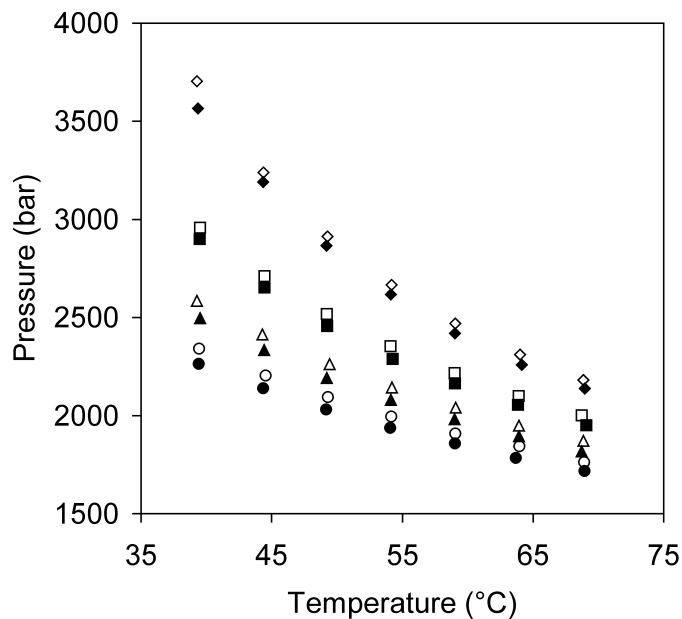


Figure 2.2. Cloud-point pressures of the ethylene-PEP51-CO₂ system with 5 wt % PEP51 (open symbols) and 10 wt % PEP51 (closed symbols). (\diamond, \blacklozenge) $w_{\text{CO}_2} = 0.20$; (\square, \blacksquare) $w_{\text{CO}_2} = 0.15$; ($\triangle, \blacktriangle$) $w_{\text{CO}_2} = 0.10$; (\circ, \bullet) $w_{\text{CO}_2} = 0.05$.

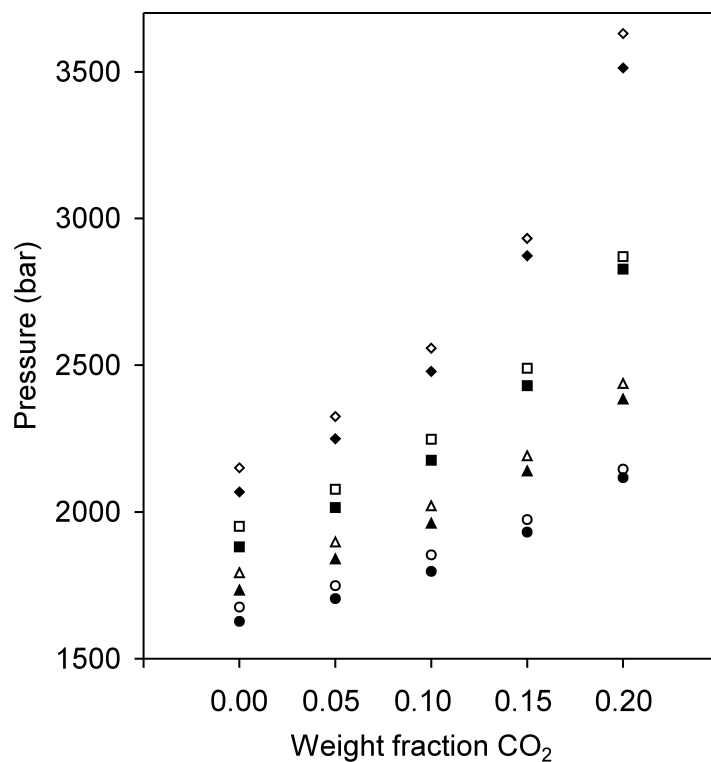


Figure 2.3. Selected pressure composition sections for the ethylene-PEP51-CO₂ system with 5 wt % PEP51 (open symbols) and 10 wt % PEP51 (closed symbols). (\diamond, \blacklozenge) $T = 40$ °C; (\square, \blacksquare) $T = 50$ °C; ($\triangle, \blacktriangle$) $T = 60$ °C; (\circ, \bullet) $T = 70$ °C.

interaction with the polymer, because the polymer has a much higher permittivity. The increase in the slope (dP/dT) of the isopleths with increasing weight fraction CO_2 can be attributed to the higher quadrupole moment of CO_2 , because interactions due to quadrupole moments are more temperature sensitive. These results strongly suggest that the polymerization of olefins in CO_2 can only be performed as a precipitation polymerization.

2.3.3 Pure-component SAFT parameters

The pure-component SAFT parameters used are summarized in Table 2.4. For PEP two different sets of pure-component parameters were used. The first set was taken from Huang and Radosz¹³, determined from extrapolation of a homologous series of n -alkanes. These pure-component parameters have been used to model the phase behavior of systems containing PEP and various olefins^{17,18}, and it appears plausible to use them for our system as well. The second set of PEP parameters was obtained by fitting to PEP PVT data.²⁰ Figure 2.4 shows the PVT behavior of PEP using both the Huang and Radosz parameters for the pure polymers and the calculated pure- component parameters fitted to density.

Table 2.4. SAFT pure-component parameters

Component	u^0/k (K)	v^{00} (mL/mol)	m	e/k^c	M_n (g/mol)	Source
Carbon dioxide	216.08	13.578	1.417	40	44.01	13
Ethylene	212.06	18.157	1.464	10	28.054	13
PEP51	210.00	12.000	$0.05096 \cdot M_n$	10	51000	13
PEP51 ^a	471.44	21.690	$0.034265 \cdot M_n$	10	51000	this work
PEP51 ^b	469.86	21.618	$0.034365 \cdot M_n$	10	51000	this work
PEP8.7	210.00	12.000	$0.05096 \cdot M_n$	10	8700	13
PEP8.7 ^a	471.44	21.690	$0.034265 \cdot M_n$	10	8700	this work
PEP8.7 ^b	469.86	21.618	$0.034365 \cdot M_n$	10	8700	this work

^aLiterature PVT data of a PEP polymer ($M_w=134$ kg/mol, $M_w/M_n=2.6$, 22 methyl groups per 100 carbon atoms) fitted by minimization of $\Sigma(P_{\text{experiment}} - P_{\text{calculated}})^2$. ^bSame as a , except fitted by minimization of $\Sigma(\rho_{\text{experiment}} - \rho_{\text{calculated}})^2$. ^cParameter for temperature dependency of the interaction energy, u , see Huang and Radosz¹³.

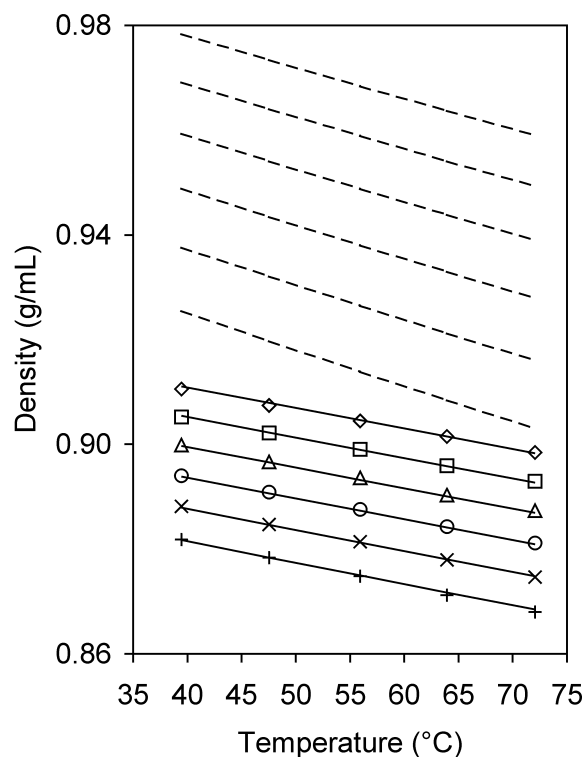


Figure 2.4. Experimental *PVT* data of a PEP polymer (symbols), SAFT prediction with Radosz parameters extrapolated from a homologous series of n-alkanes (dashed lines) and SAFT calculation with parameters fitted to the experimental *PVT* data (solid lines). (\diamond) $P = 2000$ bar; (\square) $P = 1800$ bar; (Δ) $P = 1600$ bar; (\circ) $P = 1400$ bar; (\times) $P = 1200$ bar; ($+$) $P = 1000$ bar.

2.3.4 Binary interaction parameter for ethylene-PEP

A binary interaction parameter, k_{12} , was calculated for each cloud point of the ethylene-PEP51 system using different pure-component parameters for PEP. Using the pure-component parameters for PEP of Huang and Radosz¹³, the k_{12} values determined for different temperatures and compositions are shown in Figure 2.5. The interaction parameter appears to be composition and temperature dependent. Although the variations in the values of k_{12} appear to be relatively small, the cloud-point pressure is extremely sensitive to the interaction parameter; sensitivity analysis of the parameters show that dP_{cp}/dk_{12} varies between $1 \cdot 10^5$ to $3 \cdot 10^5$ bar. As a result, the difference between calculated and experimental cloud-point pressures ranges from 200 to 600 bars, even when k_{12} is allowed to be a function of temperature. Another problem with the Radosz parameters is the occurrence of a critical point near 5 wt % PEP51, which is not found experimentally.

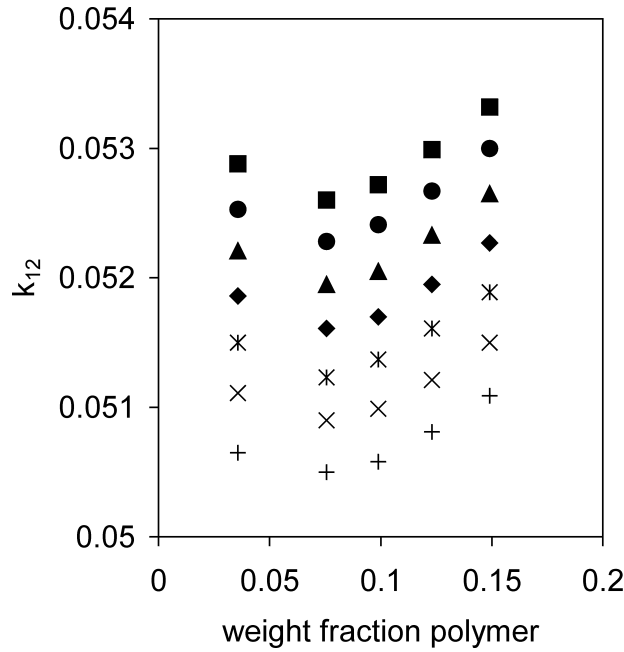


Figure 2.5. Interaction parameter calculated for each cloud point of the PEP51-ethylene system, using pure-component parameters for PEP51 from Huang and Radosz: (■) $T = 39.5$ °C; (●) $T = 44.5$ °C; (▲) $T = 49.3$ °C; (◆) $T = 54.2$ °C; (*) $T = 59.1$ °C; (×) $T = 64.1$ °C; (+) $T = 69.0$ °C.

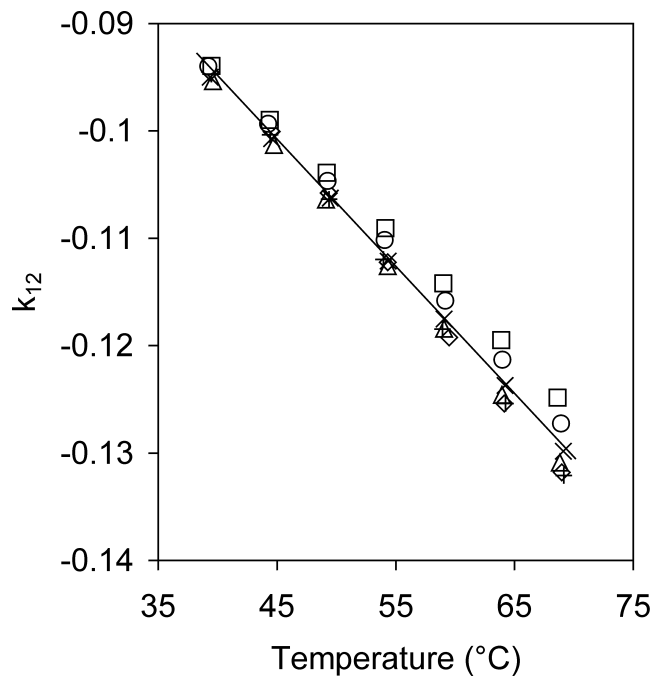


Figure 2.6. An interaction parameter is correlated to each cloud point of the PEP51-ethylene system. Pure-component parameters for PEP51 are fitted to *PVT* data. (◇) $w_p = 0.0357$; (+) $w_p = 0.0498$; (Δ) $w_p = 0.0756$; (×) $w_p = 0.0989$; (○) $w_p = 0.1230$; (□) $w_p = 0.1491$.

Table 2.5. Temperature dependence of binary interaction parameters

System	Binary interaction parameter
Ethylene-PEP51	$k_{12} = -0.0011847 \cdot T(\text{K}) + 0.27616$
Ethylene-CO ₂	$k_{13} = 0.000491 \cdot T(\text{K}) - 0.0669$
PEP51-CO ₂	$k_{23} = -0.001043 \cdot T(\text{K}) + 0.49125$

Next, the set of pure-component parameters obtained by fitting to *PVT* data was used. Figure 2.6 shows the temperature dependence for the different isopleths. Large negative values for k_{12} are obtained, and absolute differences between k_{12} values are larger than those for the first set of pure-component parameters. However, the calculation of cloud points is much less sensitive to k_{12} , and a simple linear dependence of k_{12} on temperature (see Table 2.5), is sufficient to describe all the cloud points of the ethylene-PEP51 system (see Figure 2.7). The slight difference in pure-component parameters fitted to the density and to the pressure lead to almost identical values of k_{12} and cloud points. Therefore, the pure-component parameters obtained from fitting to the density were used in subsequent calculations.

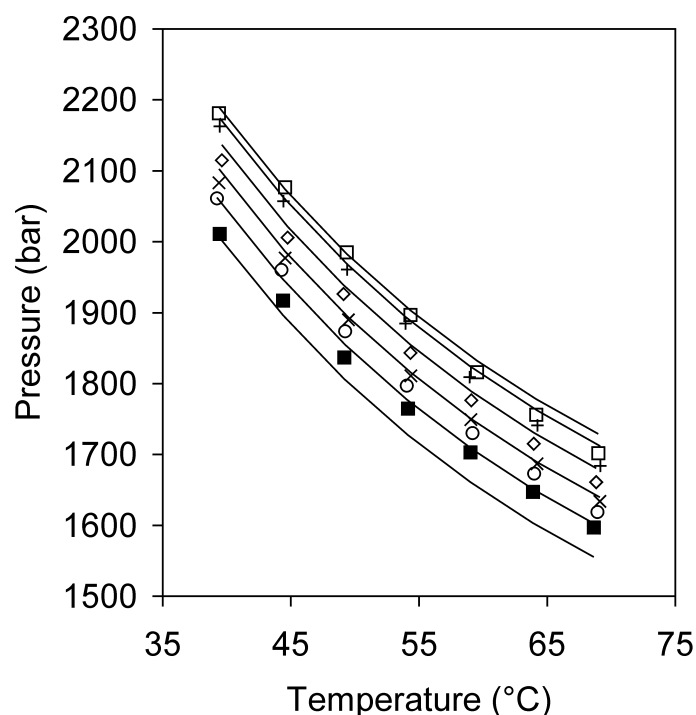


Figure 2.7. SAFT calculation of the cloud-point isopleths of the ethylene-PEP51 system using pure-component parameters for PEP51 derived from polymer *PVT* data. (□) $w_p = 0.0357$; (+) $w_p = 0.0498$; (◇) $w_p = 0.0756$; (×) $w_p = 0.0989$; (○) $w_p = 0.1230$; (■) $w_p = 0.1491$.

To examine the extrapolation capability of SAFT, the previously determined interaction parameters for ethylene-PEP51 were used to model the ethylene-PEP8.7 system. The calculated cloud-point pressures using the Huang and Radosz pure polymer parameters show a larger decrease than measured. The differences between calculated and measured cloud-point pressures for the PEP8.7-ethylene system were approximately 200 bar. Strictly speaking, it is thermodynamically not allowed to use a concentration-dependent binary interaction parameter without adjusting the expression for the chemical potential. Nevertheless, we used k_{12} from Figure 2.5 in these calculations.

The calculation with polymer parameters obtained from PVT data show a smaller decrease in cloud-point pressure than experimentally observed, approximately 100-200 bar above the measured cloud-point pressure. Furthermore, a critical point was calculated near 5 wt % PEP8.7.

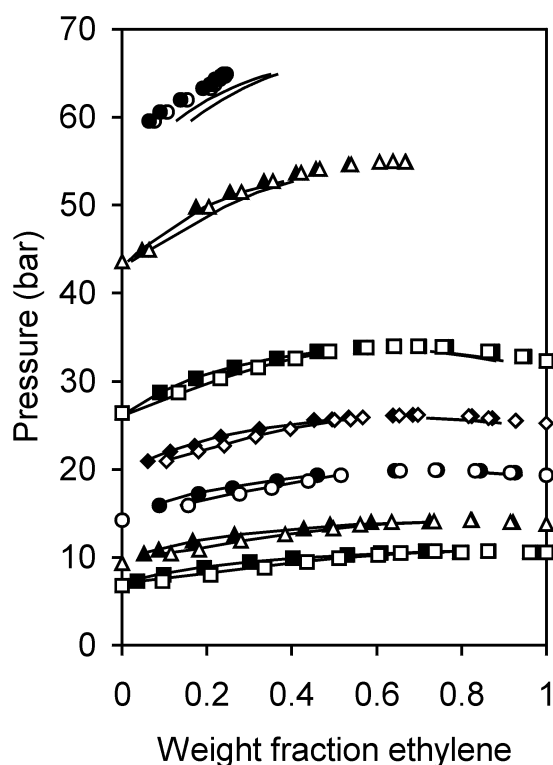


Figure 2.8. Vapor-liquid composition equilibrium data of ethylene-CO₂ system at different temperatures (open and closed symbols represent respectively gas and fluid phases) and SAFT modeling (lines). (●,○) $T = 293.15$ K; (▲,△) $T = 283.15$ K; (■,□) $T = 263.15$ K; (◆,◇) $T = 252.95$ K; (●,○) $T = 243.15$ K; (▲,△) $T = 231.55$ K; (■,□) $T = 223.15$ K.

2.3.5 Binary interaction parameter for ethylene - CO₂

Figure 2.8 shows the vapor-liquid equilibrium data²¹ and the modeling results for the ethylene-CO₂ mixtures. The binary interaction parameter, k_{13} , was fitted to the compositions of the liquid and the vapor phases, respectively. The experimental data near the critical points (283 K and 293 K) have not been incorporated into the fit, because a reasonable fit could no longer be obtained. The correlation with the experimental data was excellent when an interaction parameter was used that linearly depended on temperature (see Table 2.5). Differences between calculated and experimental values were not large when a temperature-independent interaction parameter was used. However, k_{13} was clearly temperature-dependent and our cloud-point measurements of the PEP-ethylene-carbon dioxide system were performed at much higher temperatures. Therefore, a temperature dependent k_{13} was used to describe this system.

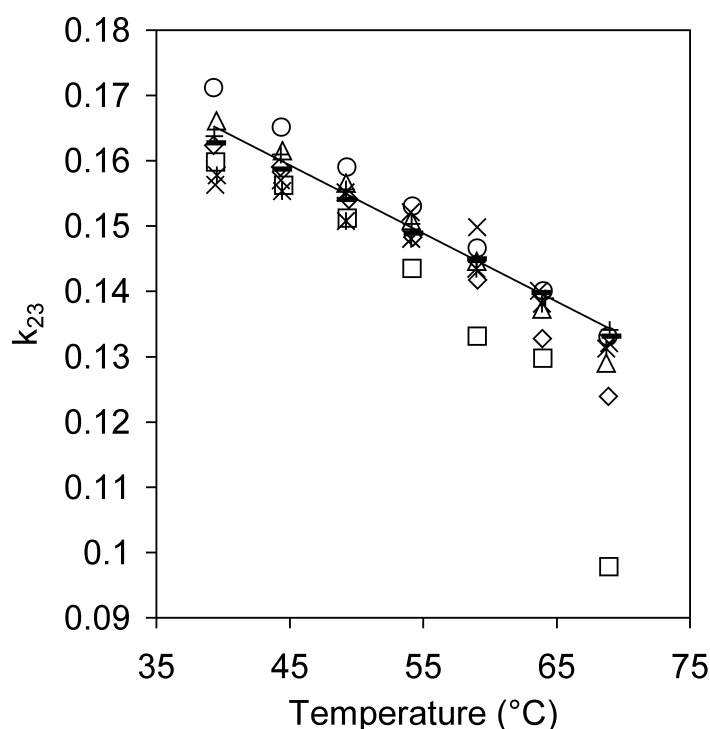


Figure 2.9. Determination of binary interaction parameter for PEP51-CO₂. Symbols are binary interaction parameters fitted to cloud points. The line is the linear regression through the isopleth with a sample composition of 70 wt % ethylene, 20 wt % CO₂, and 10 wt % PEP51. Weight fraction PEP51 = 0.050: (□) $w_{\text{CO}_2} = 0.05$; (◇) $w_{\text{CO}_2} = 0.10$; (△) $w_{\text{CO}_2} = 0.15$; (○) $w_{\text{CO}_2} = 0.20$; Weight fraction PEP51=0.100: (×) $w_{\text{CO}_2} = 0.05$; (✱) $w_{\text{CO}_2} = 0.10$; (-) $w_{\text{CO}_2} = 0.15$; (+) $w_{\text{CO}_2} = 0.20$.

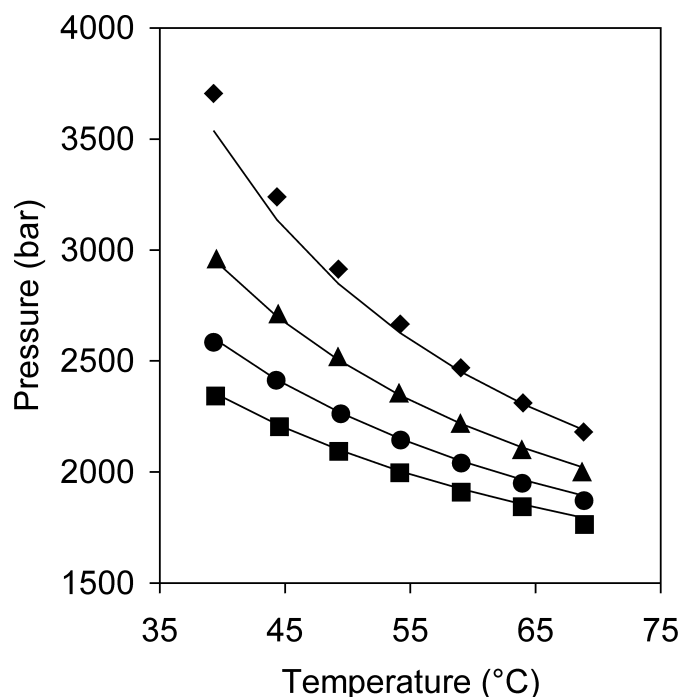


Figure 2.10. Cloud points (symbols) of 5 wt % PEP51 in x wt % CO_2 and $1 - x$ wt % ethylene. SAFT modeling (lines) with k_{23} fitted to the isopleth containing 10 wt % PEP51, 20 wt % CO_2 and 70 wt % ethylene. (◆) $w_{CO_2} = 0.20$; (▲) $w_{CO_2} = 0.15$; (●) $w_{CO_2} = 0.10$; (■) $w_{CO_2} = 0.05$.

2.3.6 Binary interaction parameter for PEP- CO_2

The determination of the interaction parameter for PEP- CO_2 , k_{23} , is complicated because PEP is insoluble in pure CO_2 . Therefore, k_{23} was fitted to all cloud points of the ternary ethylene-PEP51- CO_2 system. Figure 2.9 shows that k_{23} decreases with increasing temperature for all concentrations. At low CO_2 concentrations, the calculated cloud point is significantly less sensitive to k_{23} than at high CO_2 concentrations. Therefore, we used the isopleth with the highest CO_2 concentration (20 wt %) and 10 wt % PEP51 to obtain a fit of k_{23} , linearly dependent on temperature (see table 2.5). This temperature-dependent k_{23} was used to predict the other isopleths. The calculated ternary cloud points containing 5 wt % PEP51 are shown in Figure 2.10. As can be seen from this figure, the predictions agree very well with the experimental data. The SAFT calculation for systems containing 10 wt % PEP51 is not shown but showed an even better agreement with the cloud-point measurements.

2.4 Acknowledgements

The authors thank Naveen Koak for help with the SAFT calculations and the flash algorithm. We also thank DSM for measuring the molecular weight distributions of the polymer samples and Wim Poot for experimental assistance.

2.5 References

- (1) Kendall, J. L.; Canelas, D. A.; Young, J. F.; DeSimone, J. M. Polymerizations in Supercritical Carbon Dioxide. *Chem. Rev.*, **1999**, *99*, 543-563.
- (2) Benedetti, L.; Bertucco, A.; Pallado, P. Production of Micronic Particles of Biocompatible Polymer using Supercritical Carbon Dioxide. *Biotechnol. Bioeng.* **1997**, *53*, 232-237.
- (3) Pradhan, D.; Chen, C.; Radosz, M. Fractionation of Polystyrene with Supercritical Propane and Ethane - Characterization, Semibatch Solubility Experiments, and SAFT Simulations. *Ind. Eng. Chem. Res.* **1994**, *33*, 1984-1988.
- (4) Folie, B.; Kelchtermans, M.; Shutt, J. R.; Schonemann, H.; Krukonis, V. Fractionation of Poly(ethylene-co-vinyl acetate) in Supercritical Propylene: Towards a Molecular Understanding of a Complex Macromolecule. *J. Appl. Polym. Sci.* **1997**, *64*, 2015-2030.
- (5) Han, S. J.; Lohse, D. J.; Radosz, M.; Sperling, L. H. Preparation of a Thermoplastic Interpenetrating Polymer Network (IPN) from Isotactic Polypropylene and Epdm Terpolymer in Supercritical Propane. *Polym. Prepr.* **1997**, *38*, 432-433.
- (6) De Vries, T. J.; Duchateau, R.; Vorstman, M. A. G.; Keurentjes, J. T. F. Polymerisation of Olefins Catalysed by a Palladium Complex in Supercritical Carbon Dioxide. *Chem. Commun.* **2000**, 263-264.
- (7) De Loos, Th. W.; Poot, W.; Diepen, G. A. M. Fluid Phase Equilibria in the System Polyethylene + Ethylene. 1. Systems of Linear Polyethylene + Ethylene at High Pressure. *Macromolecules* **1983**, *16*, 111-117.
- (8) De Loos, Th. W.; Poot, W.; Lichtenthaler, R. N. The Influence of Branching on High-Pressure Vapor-Liquid Equilibria in Systems of Ethylene and Polyethylene. *J. Supercrit. Fluids* **1995**, *8*, 282-286.

- (9) Kiamos, A. A.; Donohue, M. D. The Effect of Supercritical Carbon Dioxide on Polymer-Solvent Mixtures. *Macromolecules* **1994**, *27*, 357-364.
- (10) Xiong, Y.; Kiran, E. High-Pressure Phase Behavior in Polyethylene/n-Butane Binary and Polyethylene/n-Butane/CO₂ Ternary Systems. *J. Appl. Polym. Sci.* **1994**, *53*, 1179-1190.
- (11) Martin, T. M.; Lateef, A. A.; Roberts, C. B. Measurements and Modeling of Cloud Point Behavior for Polypropylene/n-Pentane and Polypropylene/n-Pentane/Carbon Dioxide at High Pressure. *Fluid Phase Equilib.* **1999**, *154*, 241-259.
- (12) Kirby, C. F.; McHugh, M. A. Phase Behavior of Polymers in Supercritical Fluid Solvents. *Chem. Rev.* **1999**, *99*, 565-602.
- (13) Huang, S. H.; Radosz, M. Equation of State for Small, Large, Polydisperse, and Associating Molecules. *Ind. Eng. Chem. Res.* **1990**, *29*, 2284-2294.
- (14) Huang, S. H.; Radosz, M. Equation of State for Small, Large, Polydisperse, and Associating Molecules: Extension to Fluid Mixtures. *Ind. Eng. Chem. Res.* **1991**, *30*, 1994-2005.
- (15) Van Hest, J. A. M.; Diepen, G. A. M. Solubility of naphthalene in supercritical methane. In *The Physics and Chemistry of High Pressures*, Symposium Papers, London, England, June 27-29, 1962; Soc. Chem. Ind., 1963, 10-18.
- (16) De Loos, Th. W.; Poot, W.; Diepen, G. A. M. Fluid Phase Equilibria in the System Polyethylene + Ethylene. 1. Systems of Linear Polyethylene + Ethylene at High Pressure. *Macromolecules* **1983**, *16*, 111- 117.
- (17) Chen, S. J.; Economou, I. G.; Radosz, M. Density-Tuned Polyolefin Phase-Equilibria .1. Binary Solutions of Alternating Poly(ethylene-propylene) in Subcritical and Supercritical Propylene, 1-Butene, and 1-Hexene. Experiment and Flory-Patterson Model. *Macromolecules* **1992**, *25*, 4987-4995.
- (18) Han, S. J.; Gregg, C. J.; Radosz, M. How the Solute Polydispersity Affects the Cloud-Point and Coexistence Pressures in Propylene and Ethylene Solutions of Alternating Poly(ethylene-co-propylene). *Ind. Eng. Chem. Res.* **1997**, *36*, 5520-5525.
- (19) Koak, N.; Heidemann, R. A. Phase boundary calculations for solutions of a polydisperse polymer. *AIChE J.* **2001**, *47*, 1219.
- (20) Zoller, P.; Walsh, D. J. *Standard Pressure-Volume-Temperature Data for Polymers*; Technomic: Lancaster, Pennsylvania, 1995, 69-70.

Chapter 2

- (21) Gmehling, J.; Onken, U.; Arlt, W. *Vapor-liquid equilibrium data collection*; DECHEMA: Frankfurt/Main, 1980.

Chapter 3

Polymerization of olefins catalyzed by a palladium complex in supercritical carbon dioxide

Abstract

A late transition metal catalyst has been used to homopolymerize 1-hexene and ethylene in supercritical carbon dioxide yielding high molecular weight polymers; a comparison with polymerizations in dichloromethane reveals that polymers with identical molecular weight and polydispersity are formed.

3.1 Introduction

Supercritical carbon dioxide (scCO₂) has recently emerged as an interesting substitute for organic solvents. CO₂ is environmentally friendly compared to organic solvents and has a low critical temperature (31.1°C) and pressure (73.8 bar). The physical properties of scCO₂ range from liquid-like to gas-like and can be manipulated by changing the pressure and the temperature. Physical properties like gas-like viscosities and diffusion rates, coupled with the liquid-like densities, can result in significant advantages in combined reaction, separation and purification processes. A drawback of scCO₂ is that only volatile or relatively non-polar compounds are soluble, as CO₂ is non-polar and has a low polarizability and relative permittivity¹.

Polymerization reactions using radical initiators and step growth mechanisms have been carried out in scCO₂². More recently homogeneous catalysts have successfully been applied in scCO₂ for the preparation of small molecules³ and polymers⁴⁻⁶. An interesting extension in the application of CO₂ is the use of CO₂ both as a reactant and as a solvent in a copolymerization with cyclohexene oxide⁷. The goal of our research is to copolymerize α -olefins in scCO₂. Traditional catalysts for poly(olefin) production are based on early-transition-state metals, which are highly oxophilic and therefore not suitable for polymerizations in CO₂. As late-transition-state metal complexes are less oxophilic, they are more likely to be effective polymerization catalysts in scCO₂. Here we describe the catalytic polymerization of ethylene and 1-hexene catalyzed by a homogeneous diimine palladium complex^{8,9}, also known as the Brookhart system, see Figure 3.1.

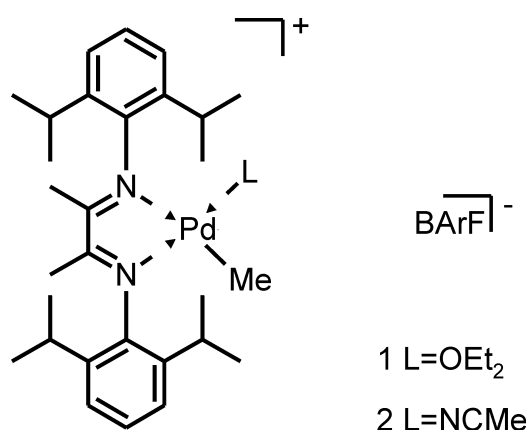


Figure 3.1 Catalyst precursors used for polymerizations, BArF = tetrakis-(3,5-bis(trifluoromethyl)phenyl)borate.

3.2 Results and Discussion

In our polymerization experiments, we were primarily interested to see if high molecular weight polymers could be produced and whether or not the active catalyst would exhibit complexation behavior with CO₂. The results of the polymerizations in CO₂ and in dichloromethane are listed in Table 3.1. The values of the turnover frequencies (TOFs) show that the activity of the catalyst is similar in both solvents, despite the large difference in phase behavior of the reaction mixtures. Both the catalyst and the polymers are soluble in dichloromethane. As expected, the polymer does not dissolve in scCO₂. Consequently, the polymerizations performed in CO₂ were all precipitation polymerizations as has been observed in the experiments. Although the differences in phase behavior are rather large, the polymers produced are very similar, both in molecular weight and in molecular weight distribution. This behavior indicates that there is no diffusion limitation, despite the precipitation in CO₂, suggesting strong swelling of the polymer, either by CO₂ or by the monomers used. More importantly, a similar molecular weight indicates that the active catalyst does not exhibit complexation behavior with CO₂, since this would have resulted in a lower molecular weight.

To study the effect of catalyst concentration on the poly(1-hexene) yield two sets of experiments were conducted, one set with a relatively high catalyst concentration in dichloromethane and CO₂ (experiments 2 and 3, respectively) and one set with a low catalyst concentration (experiments 4 and 5, respectively). When the experiments were carried out with the high catalyst concentration, the TOF in CO₂ was lower than in the corresponding experiment in dichloromethane. The experiments in the two solvents using the low catalyst concentration showed identical values for TOF, M_n and M_w/M_n, taking into account experimental error. In order to explain the effect of catalyst concentration to the TOF, the solubility of the catalyst precursor was measured in scCO₂. The solubility experiments were conducted in a 1.4 mL high-pressure view cell equipped with sapphire windows and a heating jacket. The cell was filled with about 3 mg (2 μmol) solid catalyst precursor 2. The air was removed by flushing with CO₂ at low pressure. The cell was then heated, filled with CO₂ at high pressure and placed in a UV spectrophotometer. Although scCO₂ is a poor solvent for ionic compounds, the solubility at 35 and 40 °C was found to be in the order of 1·10⁻⁴ mol/l, see Figure 3.2.

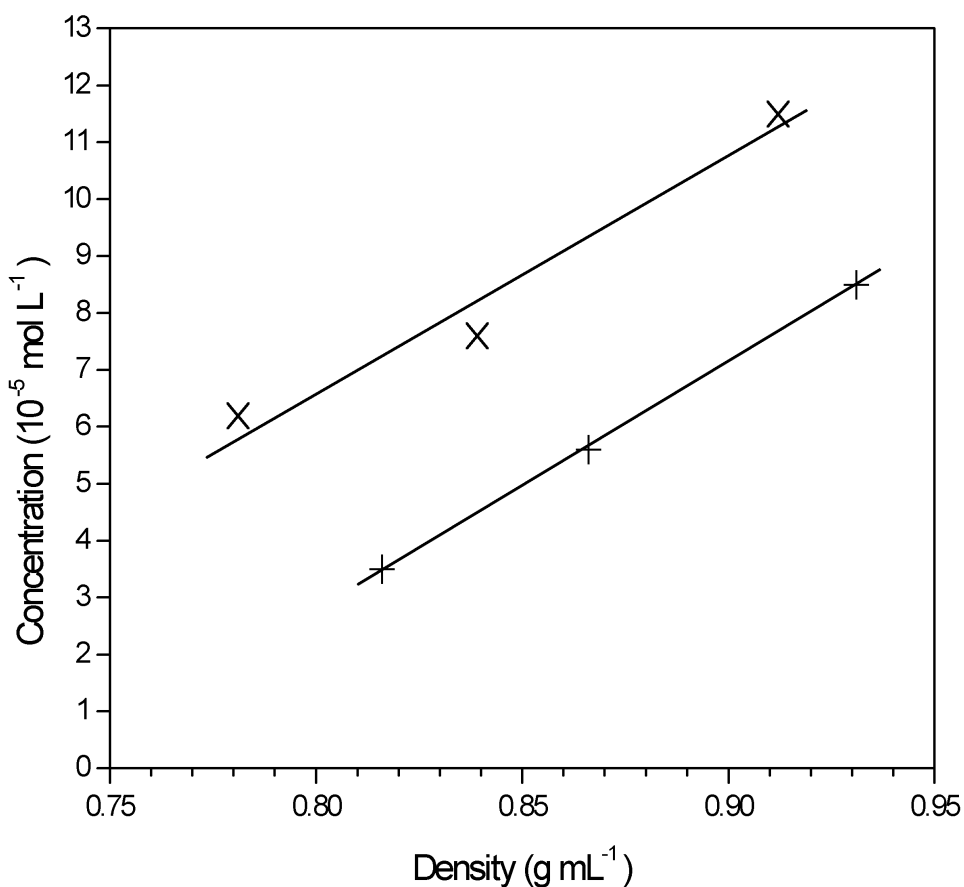


Figure 3.2. Solubility of catalyst precursor 2 as a function of scCO₂ density. (+) T = 35°C; (×) T = 40°C.

However, the rate of solubilization was low, as it typically took 1 hour to reach equilibrium. The relatively high solubility can be ascribed to the bulky anion (BArF). Generally, the solubility of an anion in hydrocarbon solvents is known to increase with increasing distribution of charge, e.g. the solubility increases in the order BF₄, PF₆, SbF₆, BArF and this is likely to apply for the apolar scCO₂ as well. All polymerizations of 1-hexene in CO₂ were performed above the maximum solubility of the catalyst. Even in experiment 5 with the lowest catalyst concentration, only half of the added amount of catalyst is dissolved in the initial stage of the polymerization, according to Figure 3.2 and the density of the reaction mixture. During polymerization, however, the solubility of the catalyst will be different from that in pure CO₂, since the catalyst is attached to a growing polymer chain. Moreover, 1-hexene can act as a cosolvent. When the experiments with the low catalyst concentration are

compared, no difference in TOF is observed. Obviously, the catalyst solubilization is not limiting during experiment 5 in CO₂ as the activity was similar in experiment 4 using dichloromethane. Comparing experiment 2 and 3 with the higher catalyst concentration, a significant difference in TOF is observed, which can be explained by the slow solubilization and low solubility of the catalyst in CO₂. Because of the amount of 1-hexene used, the mixture of 1-hexene and CO₂ is not supercritical during the polymerizations. Therefore, in experiment 6, ethylene was polymerized in scCO₂ to high molecular weight polymer. It follows from this experiment that the catalyst is also active in scCO₂. In principle, this opens the possibility to copolymerize in scCO₂ with monomers such as ethylene and propylene.

Table 3.1. Polymerization of ethylene and 1-hexene in CO₂ and CH₂Cl₂ for 2 h^a.

Experiment	Catalyst precursor	Catalyst (10 ⁻⁵ mol L ⁻¹)	Solvent	Pressure (bar)	Monomer ^b (mol L ⁻¹)	TOF ^c (h ⁻¹)	M _n ^d (kg mol ⁻¹)	M _w /M _n
1	1	42	CO ₂	239	1.7	450	135	2.1
2	2	30	CH ₂ Cl ₂	-	2.7	1010	93	1.5
3	2	30	CO ₂	194	2.9	560	102	1.5
4	2	13	CH ₂ Cl ₂	-	2.3	810	101	1.7
5	2	13	CO ₂	193	2.1	990	103	2.0
6	2	2.6	CO ₂	156	0.27	2250	88	2.0

^a High-pressure polymerizations were conducted in a 75 mL stainless steel high-pressure reactor equipped with sapphire windows, a heating jacket and a magnetic stirring bar. The solid catalyst precursor 1 (air and temperature sensitive) was put in the reactor in a glass ampulla, which broke under pressure; catalyst precursor 2 (stable at room temperature in air) was placed directly in the reactor. The air was carefully removed by flushing with CO₂ at low pressure and the reactor was heated. In case of 1-hexene as the monomer, the reactor was first filled with CO₂ and then the monomer was added. In the case of ethylene, the reactor was flushed and filled with ethylene after which CO₂ was added. ^b Experiments 1-5: 1-hexene, reaction temperature 35°C; experiment 6: ethylene starting pressure 6.9 bar, reaction temperature 40°C. ^c Turnover Frequency: mol monomer converted / mol catalyst / hour. ^d GPC (against polystyrene standards).

From the foregoing, it can be concluded that polymerization of ethylene and alpha-olefins can effectively be carried out in scCO₂. In the case of 1-hexene, a comparison was made with polymerization behavior in an organic solvent, which yielded similar molecular weights and molecular weight distributions. In order to improve the solubility of the catalysts, the ligands can be modified to enhance the solubility in scCO₂^{10,11}. Another extension of our work is the evaluation of other late-transition-state olefin polymerization catalysts known from literature^{12,13} for their application in scCO₂.

3.3 References

- (1) McHugh, M. A.; Krukonis, V. J. *Supercritical Fluid Extractions: Principles and Practice*, 2nd ed. **1994**, Butterworth-Heinemann, Stoneham, MA.
- (2) Kendall, J. L.; Canelas, D. A.; Young, J. F.; DeSimone, J. M. *Chem. Rev.* **1999**, *99*, 543.
- (3) Jessop, P. G.; Ikariya, T.; Noyori, R. *Chem. Rev.* **1999**, *99*, 475.
- (4) Mistele, C. D.; Thorp, H. H.; DeSimone, J. M. *Pure Appl. Chem.* **1996**, *A33*, 953.
- (5) Fürstner, A.; Koch, D.; Langemann, K.; Leitner, W.; Six, C. *Angew. Chem., Int. Ed. Engl.* **1997**, *36*, 2466.
- (6) Hori, H.; Six, C.; Leitner, W. *Macromolecules* **1999**, *32*, 3178.
- (7) Super, M.; Berluche, E.; Costello, C.; Beckman, E. *Macromolecules* **1997**, *30*, 368.
- (8) Johnson, L. K.; Killian, C. M.; Brookhart, M. *J. Am. Chem. Soc.* **1995**, *117*, 6414.
- (9) Mecking, S.; Johnson, L. K.; Wang, L.; Brookhart, M. *J. Am. Chem. Soc.*, 1998, **120**, 888.
- (10) Kainz, S.; Koch, D.; Baumann, W.; Leitner, W. *Angewandte Chemie, Int. Ed. Engl.*, **1997**, *36*, 1628.
- (11) Carroll, M. A.; Holmes, A. B. *Chem. Commun.* **1998**, 1395.
- (12) Klabunde, U.; Ittel, S. D. *J. Mol. Catal.* **1987**, *41*, 123.
- (13) Wang, C.; Friedrich, S.; Younkin, T. R.; Li, R. T.; Grubbs, R. H.; Bansleben, D. A.; Day, M. W. *Organometallics* **1998**, *17*, 3149.

Chapter 4

Late-transition-state metal catalyzed polymerization of ethylene in supercritical carbon dioxide; determination of reaction rate by modeling the pressure

Abstract

Precipitation polymerizations of ethylene have been carried out in supercritical carbon dioxide (scCO₂) with a palladium-based catalyst at different pressures, temperatures and monomer concentrations. High molecular weight polymers with low polydispersities have been obtained in reasonably good yields. The pressure decrease upon polymerization has been modeled to determine the reaction rate. The Statistical Association Fluid Theory (SAFT) equation-of-state (eos) has been used to describe the precipitated swollen polymer phase and the Peng-Robinson (PR) eos or the Lee-Kesler-Plöcker (LKP) eos to describe the supercritical phase. The calculations strongly indicate that the catalyst decay is induced by starvation.

4.1 Introduction

Many polymers are currently being synthesized on a large scale in organic solvents. From an environmental point of view, these processes are undesired, due to inevitable losses of the solvent during removal and recovery of the solvent. CO₂ offers an environmentally benign, non-toxic, non-flammable and inexpensive alternative as a reaction medium with a relatively low critical temperature (31.1°C) and pressure (73.8 bar). Use of CO₂ above the critical temperature has the advantage that the behavior of CO₂ ranges from liquid-like to gas-like. In this way, the physical properties of the reaction medium can easily be tuned, simply by changing pressure and/or temperature. Thus, lower viscosities and higher mass and heat transfer rates during polymerization can be achieved. Furthermore, removal of the reaction medium is simple as compared to traditional solvents used in polymerization processes.

Many polymerizations have already successfully been performed in scCO₂¹. Examples are the radical polymerization of styrene² and methyl acrylate³ as well as the transition-metal-catalyzed polymerization of CO₂ and cyclohexene oxide to produce polycarbonate⁴. In most cases, the monomers are highly soluble in scCO₂, whereas the resulting polymer is not and phase separations occur. On-line measurement of the reaction rate is very difficult due to the high pressures involved. Also, the polymerizations in scCO₂ are often heterogeneous, which hampers the use of most spectroscopic techniques. However, turbidimetry measurements have been performed to study the reaction rate in an early stage of the radical polymerization of methyl methacrylate (MMA) in scCO₂⁵. It should be noted, however, that the actual mixture of the MMA and CO₂ is a liquid phase instead of a supercritical fluid phase due to the high concentration of MMA used in these experiments.

A conventional method for following the rate of reaction in polymerization experiments in traditional organic solvents is to correlate the decrease in pressure of a supply of gaseous monomer to the conversion. Heller⁶ describes a method in which the decrease in pressure is correlated to the reaction rate with a virial equation-of-state. A similar method can be used for reactions in supercritical media, which are often subject to a pressure change upon reaction.

In this study, the precipitation polymerization of olefins in scCO₂ is investigated using a late-transition-state metal complex as a catalyst⁷. The current chapter describes the polymerizations of ethylene in scCO₂ at different pressures and temperatures. Moreover, a model is developed to determine the reaction rate indirectly based on the measured pressure

Polymerization of ethylene in scCO₂; determination of reaction rate by modeling the pressure during polymerization and a description of the phase behavior of the polymer and supercritical fluid phase.

4.2 Theory

We have developed a model to calculate the pressure as a function of conversion. It is assumed that the reaction mixture consists of a polymer phase swollen with ethylene and CO₂, and an ethylene-CO₂ phase. The fact that no polymer dissolves in the ethylene-CO₂ phase within the experimental conditions has previously been observed for a similar polymer⁸. The swollen polymer phase, i.e. the polymer-ethylene-CO₂ system, is modeled using the Statistical Associating Fluid Theory (SAFT) eos developed by Chen and Radosz⁹. The supercritical phase, i.e. the ethylene-CO₂ system, is either modeled with the Lee-Kessler-Plöcker¹⁰ (LKP) eos or the Peng-Robinson (PR) eos.

The SAFT eos can be written in terms of Helmholtz energies:

$$a_{\text{residual}} = a_{\text{hard sphere}} + a_{\text{chain}} + a_{\text{dispersion}} (+a_{\text{association}}) \quad (4.1)$$

The association term can be omitted in our calculations due to the absence of specific interactions like hydrogen bonding. Three parameters are required for each pure component: a segment volume, v^0 , the amount of segments per molecule, m , and the segment-segment interaction energy u^0/k . To describe multicomponent systems, a binary interaction parameter, k_{ij} , is used for each pair of components. The following mixing rules are used to describe the mixture parameters:

$$v_i^0 = \frac{1}{8} \left(v_i^{0\frac{1}{3}} + v_j^{0\frac{1}{3}} \right)^3 \quad (4.2)$$

$$u_{ij} = (1 - k_{ij}) \sqrt{u_i u_j} \quad (4.3)$$

$$m = \sum_i x_i m_i \quad (4.4)$$

Chapter 4

The PR eos is one of the most commonly used cubic eos. The eos uses three parameters for the description of pure components: the critical temperature, T_c , the critical pressure, P_c , and an acentric factor, ω . The PR eos can be written as follows, in which variable a is a function of T , T_c , P_c and ω , and variable b is a function of T_c and P_c :

$$P = \frac{RT}{v - b_m} - \frac{a_m}{v^2 + 2b_m v - b_m^2} \quad (4.5)$$

An interaction parameter, k_{ij} , is used to describe mixture properties. The following mixing rules are applied for the PR eos:

$$a_m = \sum_i \sum_j x_i x_j \sqrt{a_i a_j} (1 - k_{ij}) \quad (4.6)$$

$$b_m = \sum_i x_i b_i \quad (4.7)$$

The LKP eos is equivalent to the original Lee-Kesler (LK) eos, except for the mixing rules. It uses the same pure-component parameters as the PR eos, i.e. T_c , P_c and ω . The LKP eos can be described in terms of compressibility factors in which *ref1* is a reference fluid with an acentric factor of zero and *ref2* is a fluid with a high acentric factor, i.e. n-octane. The compressibility factors of the reference fluids are a function of the reduced temperature and pressure of the mixture of interest. The fluid mixture of interest is calculated by a linear combination of the mixture acentric factor:

$$Z = Z_{ref1} + \frac{\omega_m - \omega_{ref1}}{\omega_{ref2} - \omega_{ref1}} (Z_{ref2} - Z_{ref1}) \quad (4.8)$$

To obtain the mixture parameters, T_{cm} , P_{cm} and ω_m , respectively, the following mixing rules are applied using a binary interaction parameter for the critical temperature:

$$T_{cij} = k_{ij} \sqrt{T_{ci} T_{cj}} \quad (4.9)$$

$$V_{cij} = \frac{1}{8} \left(V_{ci}^{\frac{1}{3}} + V_{cj}^{\frac{1}{3}} \right)^3 \quad (4.10)$$

$$V_{cm} = \sum_i \sum_j x_i x_j V_{cij} \quad (4.11)$$

$$T_{cm} = \frac{1}{V_{cm}^{\frac{1}{4}}} \sum_i \sum_j x_i x_j V_{cij}^{\frac{1}{4}} T_{cij} \quad (4.12)$$

$$\omega_m = \sum_i x_i \omega_i \quad (4.13)$$

$$P_{cm} = (0.2905 - 0.085\omega_m) \frac{RT_{cm}}{V_{cm}} \quad (4.14)$$

The use of the SAFT eos for the simulation of both phases results in physically inconsistent behavior, because the temperatures used are just above the critical temperature of CO₂. SAFT is known to overpredict the critical properties⁹. Both PR and LK(P) are able to describe the critical properties of pure components, although LK(P) describes the density much better, as can be seen from Figure 4.1.

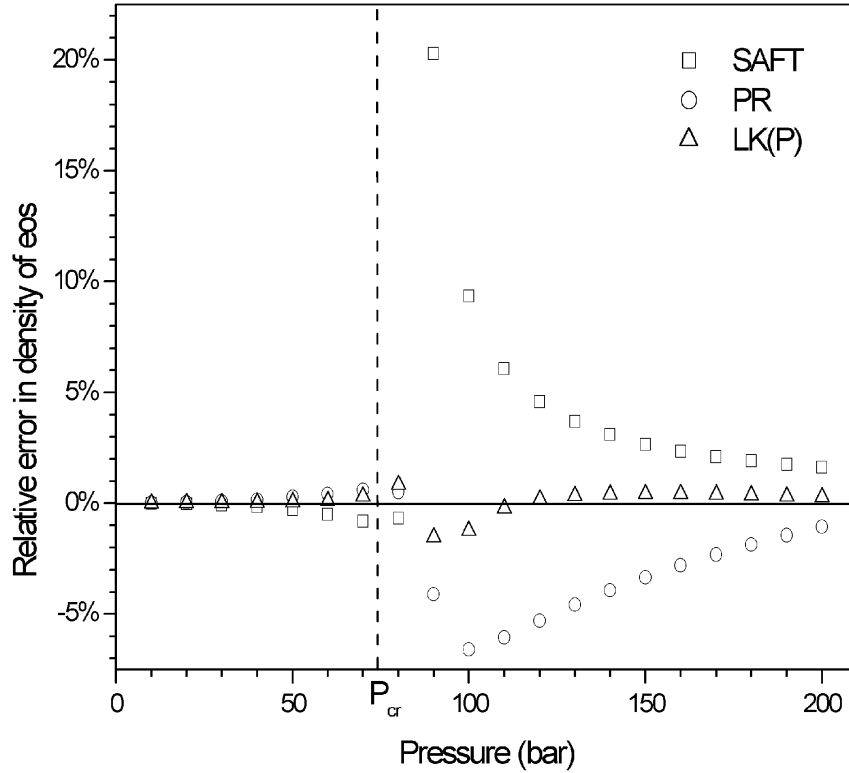


Figure 4.1. Relative error in density of pure CO₂ at 40°C calculated with SAFT, PR and LK(P).

4.3 Experimental

4.3.1 Materials

Carbon dioxide (Hoek Loos B.V., grade 4.5), ethylene (Hoek Loos B.V., grade 3.5) and n-heptane (Aldrich, 95%) were used as received. The palladium-based polymerization catalyst was synthesized according to literature procedures^{11,12}. The synthesis is schematically shown in Figure 4.2. To allow for sufficient solubility of the catalyst in scCO₂, Sodium tetrakis-(3,5-bis(trifluoromethyl)phenyl)borate (abbreviated as NaBARF) was used to synthesize the active catalyst, for which the CO₂-philic BARF-anion acts as the counter ion for the Pd complex.

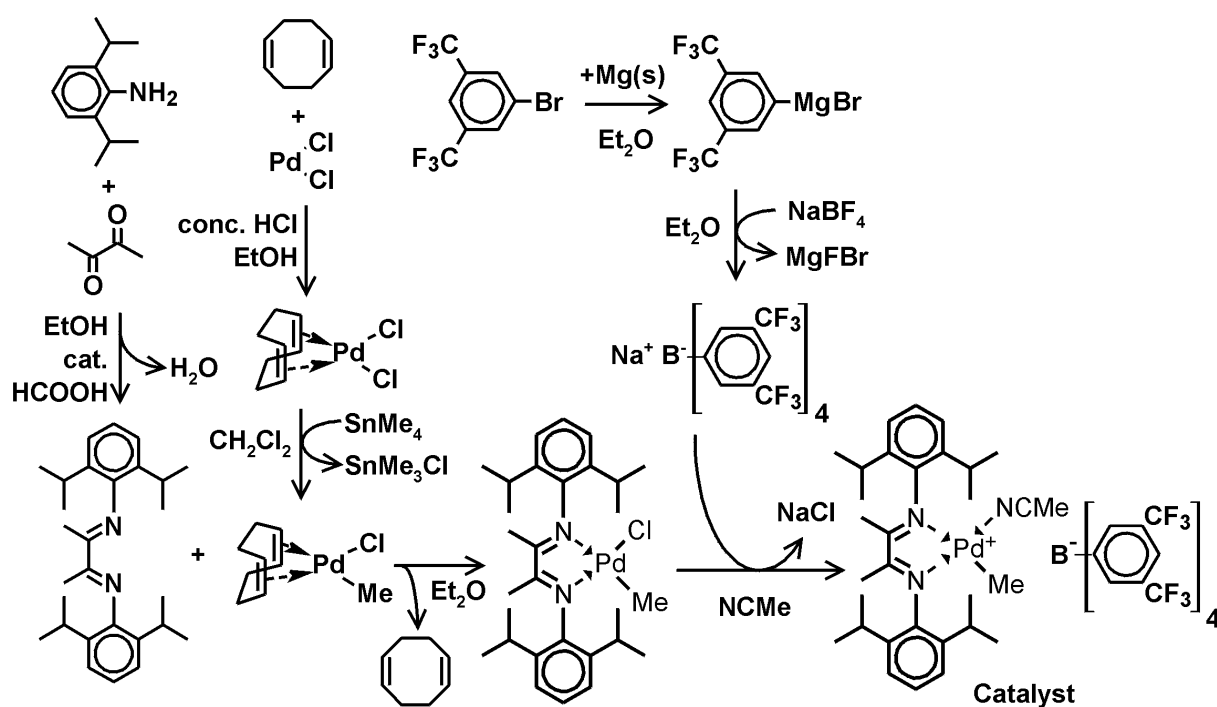


Figure 4.2. Synthesis of palladium-based catalyst used for polymerizations in scCO₂.

4.3.2 Polymerizations

The polymerizations were performed in a 536 mL high-pressure reactor, equipped with two sapphire windows, a magnetically coupled stirrer, a Pt-100, a pressure sensor and a heating jacket, see Figure 4.3. Before a polymerization experiment was started, the air in the reactor was removed by repeatedly applying vacuum and filling with 2 bar of argon (3 times). Secondly, vacuum was applied and approximately 50 bar of ethylene was added directly from

the cylinder into the reactor. Subsequently, CO₂ was added to the reactor up to 10 bars below the final polymerization pressure. The catalyst (0.02 mmol) was put in the catalyst injection port, which was placed under a vacuum to remove air. Finally, the catalyst was flushed into the reactor with 300 bar CO₂ until the desired polymerization pressure was obtained. During the polymerization the pressure and temperature were recorded.

After the reaction time, the pressure was relieved through a polymer trap and the polymer was collected by rinsing the reactor several times with heptane. The solvent was removed from the polymer in a rotary evaporator. The polymer was analyzed with gel permeation chromatography (GPC) using polystyrene standards and tetrahydrofuran (THF) eluents.

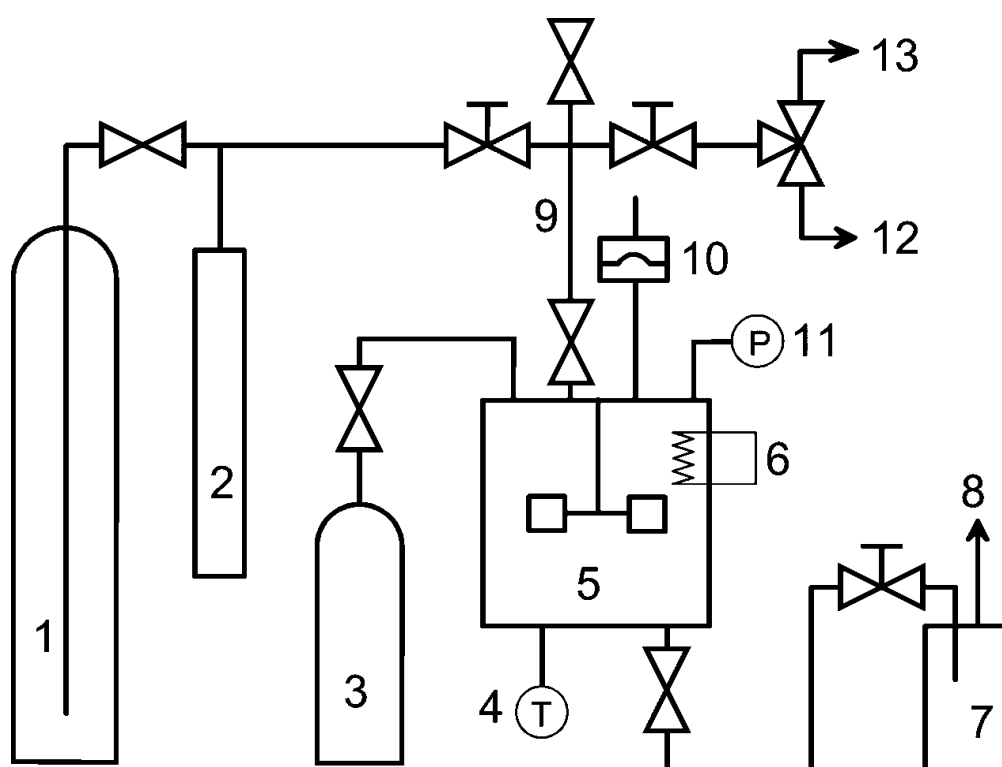


Figure 4.3. Experimental setup for ethylene polymerizations in scCO₂: (1) CO₂ cylinder, (2) syringe pump, (3) ethylene cylinder, (4) Pt-100 resistance thermometer, (5) reactor with sapphire windows and magnetically coupled stirrer, (6) heating jacket, (7) polymer trap, (8) vent, (9) catalyst injection port, (10) rupture disc, (11) pressure transducer connected to a computer, (12) argon, (13) vacuum pump.

4.3.3 Determination of reaction rate

The eos models were used to calculate the pressure in the reactor as a function of the conversion. A third-order polynome was used to correlate pressure with conversion, which in turn was applied to calculate the reaction rate. The iteration scheme is given in Figure 4.4. The programs were written in Mathematica (see Appendix 1). The pure-component parameters and the interaction parameters necessary for the eos models are given in Tables 4.1 and 4.2, respectively.

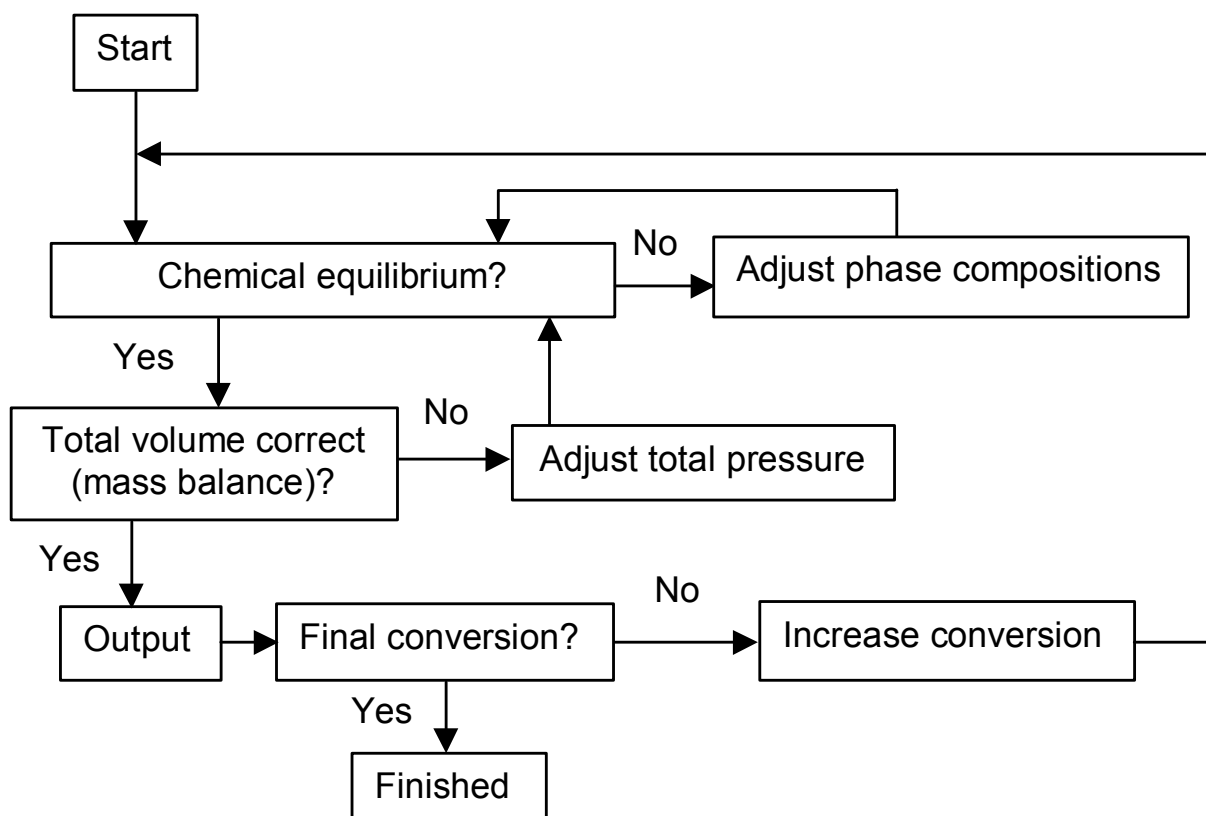


Figure 4.4. Iteration scheme for the SAFT-LKP and SAFT-PR programs.

Table 4.1. Pure-component parameters for the SAFT, LKP and PR eos.

Model	component	u^0/k (K)	v^{00} (mL/mol)	m	e/k	source
SAFT	CO ₂	216.08	13.578	1.417	40	9
	C ₂ H ₄	212.06	18.157	1.464	10	9
	polymer	469.86	21.618	0.034365 M^a)	10	8
		T_c (K)	P_c (bar)	ω		source
LKP, PR	CO ₂	304.1	73.8	0.225		13
	C ₂ H ₄	282.4	50.4	0.089		13

^{a)} The polymer molecular mass is set to 51000, as the influence of the molecular mass on the calculations is negligible.

Table 4.2. Binary interaction parameters for the SAFT, LKP and PR eos.

Model	system	Binary interaction parameter	Source
SAFT	C ₂ H ₄ - polymer	$-0.0011847 \cdot T(K) + 0.27616$	8
	C ₂ H ₄ -CO ₂	$0.000491 \cdot T(K) - 0.0669$	8
	polymer-CO ₂	$-0.001043 \cdot T(K) + 0.49125$	8
LKP	C ₂ H ₄ -CO ₂	0.957	14
PR	C ₂ H ₄ -CO ₂	0.0541	14

4.4 Results and Discussion

4.4.1 Polymerization experiments

The polymerizations of ethylene have been performed at two different temperatures and two overall pressures (approximately 100 and 200 bar). The results are summarized in Table 4.3. From Table 4.3 it can be concluded that high molecular weight polymers have been produced in all polymerization runs. An increase in reaction temperature from 40 to 50 °C results in a decrease in the number averaged polymer weight (M_n). This effect is most likely caused by an increase in chain transfer rate, which involves a dissociative displacement mechanism

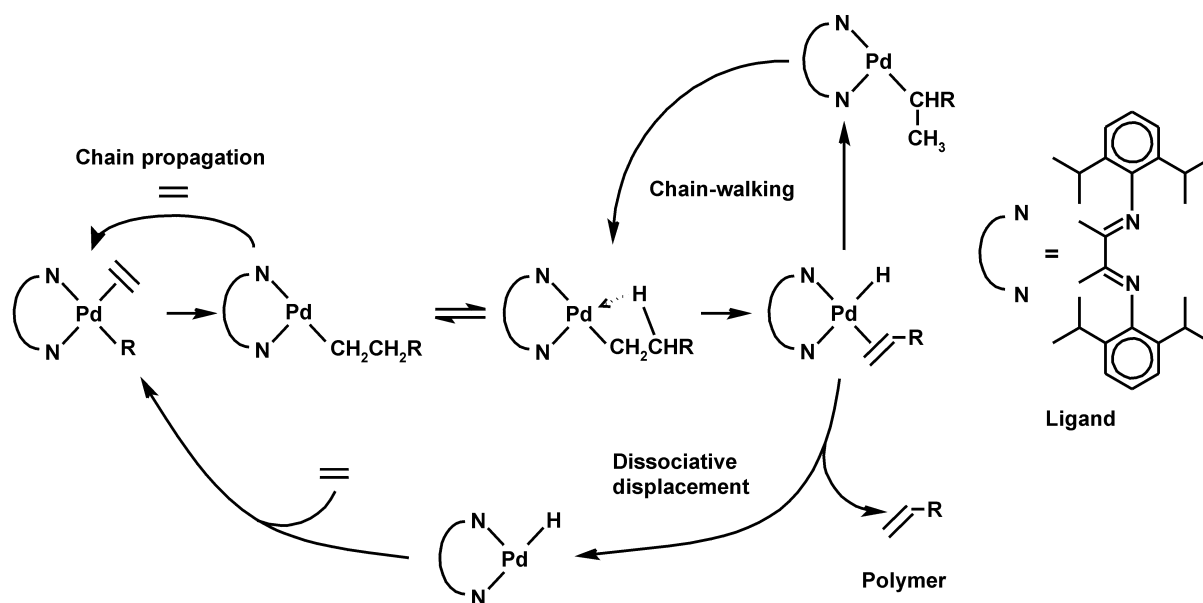


Figure 4.5. Polymerization mechanism of ethylene by the palladium based-catalyst

Table 4.3. Experimental results of ethylene polymerization.

Exp. no.	Temperature (°C)	Reaction time (hr)	Pressure (initial - final) (bar)	Initial mass of ethylene (g)	Polymer yield (g)	M _n (kg/mol)	Mw/Mn (-)
1	40	48.7	207.2 - 154.4	45.2	23.5	182	2.71
2	40	70.4	106.6 - 97.5	45.1	24.9	191	2.68
3	50	28.2	205.7 - 179.7	40.4	13.0	123	2.65
4	50	38.2	108.4 - 100.0	40.1	19.6	129	2.45
5	40	96.1	221.3 - 176.7	20.2	12.7	129	2.96

according to molecular modelling studies of Musaev et al.¹⁵. The reaction mechanism is shown in Figure 4.5.

Apparently, the overall pressure does not influence the resulting polymer, as the molecular weight distribution of the resulting polymer is similar at different pressures, see Figure 4.6. The pressure keeps decreasing even after long reaction times during all polymerization runs (28-96 hours), which shows that at least some of the catalyst remains active, see Figure 4.7. It is unlikely that the pressure decrease has been caused by small leaks, as leak tests at 40°C with pure CO₂ of 108 and 204 bar have shown that the pressure decrease due to possible small leaks is less than 0.1 and 0.4 bar, respectively, over a period of more than 65 hours.

The higher yields of the polymerization runs 1 and 2 as compared to runs 3 and 4 can be attributed to the lower reaction temperature. The lower reaction temperature causes the catalyst to remain active for a longer period of time due to a slower deactivation of the catalyst. Brookhart et al. observed a deactivation mechanism by an internal reaction of the palladium with the isopropyl groups of the ligand¹⁶, which occurs when no olefin is coordinated to the catalyst. At higher temperatures, the binding of ethylene is slightly weaker. Therefore, the catalyst will deactivate faster at higher temperatures or at lower ethylene concentrations.

Lowering the initial ethylene concentration (run 5) results in a lower M_n , a somewhat broader molecular weight distribution (M_w/M_n) and a lower yield. Because chain transfer can only occur when no olefin is coordinated to the metal center, a lower ethylene concentration lowers M_n . The increase in mass transfer limitation causes a concentration gradient of ethylene in the precipitated polymer and subsequently a broadening of the molecular weight distribution.

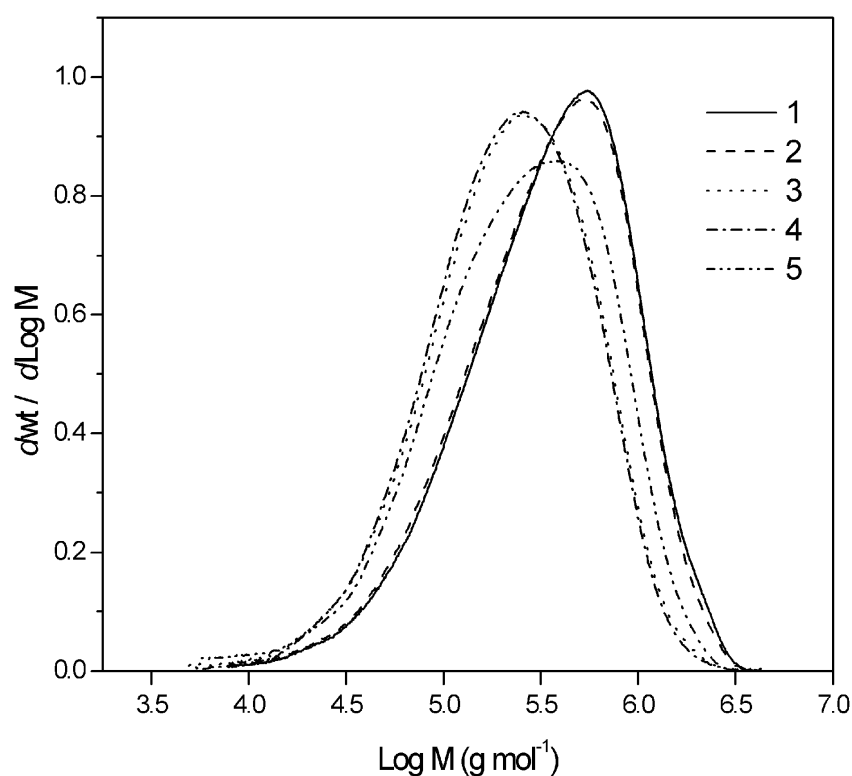


Figure 4.6. Molecular weight distributions of polymer samples of runs 1 through 5.

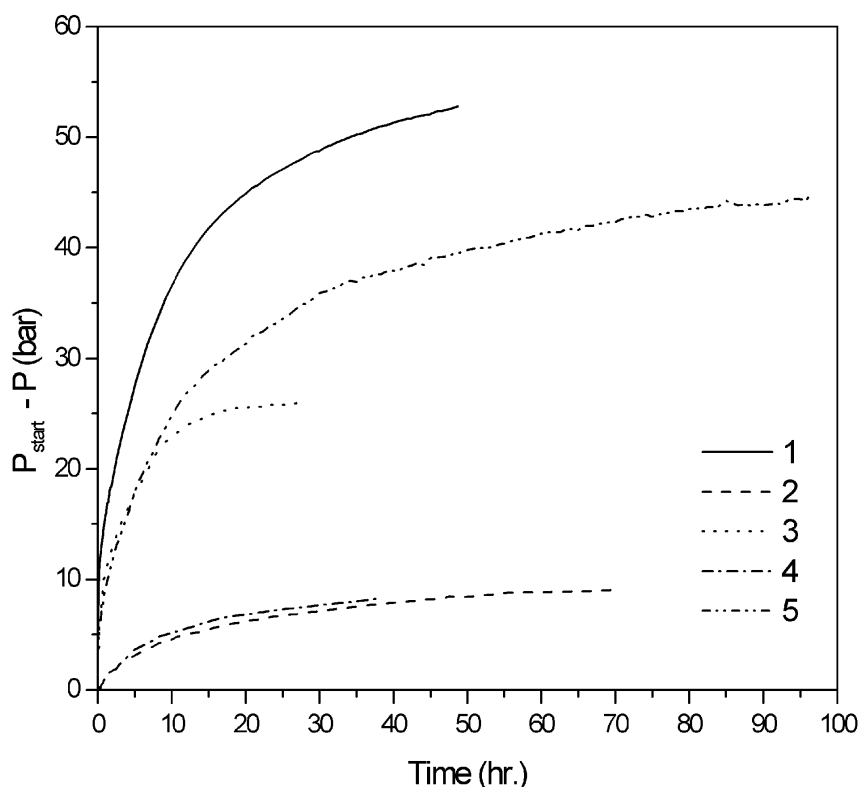


Figure 4.7. Pressure change as a function of time for polymerization runs 1 through 5.

4.4.2 Determination of reaction rate using SAFT-LKP and SAFT-PR

The measured pressure-time curves have been combined with the conversion-pressure curves calculated by either the SAFT-LKP or the SAFT-PR model to yield the conversion as a function of time. The shape of the conversion versus time curves of all polymerizations is similar. At the start of the polymerization, high conversion rates are observed which gradually decrease. As the reaction rate does not become zero, this indicates that at least some of the catalyst is still active at the end of the experiment. As the volume of the polymer phase is approximately 4 to 8 vol% according to the SAFT model, the choice for the LKP or PR eos model to describe the supercritical phase largely determines the outcome of the calculations.

Since the yield is a function of pressure decrease, the calculated yield based on the observed pressure decrease should in principle correspond with the observed yield. Similarly, the calculated pressure decrease using the observed yield should correspond with the observed pressure decrease. The discrepancies then give a good indication of the accuracy of the models. The calculations are summarized in Table 4.4. The deviations in the model calculations of run 1 and 3 (relatively high pressure) are very small for the SAFT-LKP model.

Table 4.4. Simulated results of ethylene polymerization.

Exp.	Final pressure [bar]			Polymer yield [g]		
	experiment	SAFT-LKP	SAFT-PR	experiment	SAFT-LKP	SAFT-PR
1	154.4	152.5	165.4	23.5	22.5	30.3
2	97.5	95.2	94.7	24.9	19.5	18.5
3	179.7	179.8	185.1	13.0	13.1	16.5
4	100.0	99.4	99.2	19.6	18.2	17.9
5	176.7	182.6	193.9	12.7	14.8	21.1

The SAFT-PR model, however, shows a significant deviation. This is consistent with the deviation in density as a function of pressure for pure components for the PR eos, as can be seen in Figure 4.1.

Both models show some deviation from the experiments for run 2 and 4 (relatively low pressure). This discrepancy can partly be explained by the smaller overall pressure change during the course of the polymerization, which induces the error in the calculated conversion. The discrepancy can further be explained by the calculated swelling, which is far too low. Swelling experiments with pure CO₂ of the polymer produced in run 1 show that the polymer swelling is approximately 20 and 25 vol% at 100 and 200 bar, respectively. However, the calculated swelling under these conditions using the SAFT-LKP and SAFT-PR models is less than 4 vol%. Because the difference in density between the swollen polymer phase and the supercritical phase is much higher at lower pressures, a more pronounced difference between experiment and modeling can be expected at lower pressures as sorption and swelling will have a significant influence.

As the model calculations using the SAFT-LKP approach are considered to be the most accurate, they have been used to fit a rate equation. The rate of polymerization using the palladium-based catalyst is known to be zero-order in monomer concentration:

$$r_{\text{pol}} = k_{\text{pol}} n_{\text{cat}} \quad (4.15)$$

From a mechanistic point of view, the catalyst decay is likely to be first order in catalyst:

$$r_{\text{deact}} = k_{\text{deact}} n_{\text{cat}} \quad (4.16)$$

However, a first order fit in catalyst decay results in a poor description of the polymerization rate. The fitted polymerization rate is either too low at the start of the polymerization or too low at the end, see Figure 4.8. Fitting the observed polymerization rate to equations (4.15) and (4.17), which is second order in catalyst decay, gives a much better representation:

$$r_{\text{deact}} = k_{\text{deact}} n_{\text{cat}}^2 \quad (4.17)$$

However, due to the steric hinderance of the isopropyl groups on the ligand, it is not likely that two catalyst molecules react with each other and become inactive. A more reasonable explanation is that the catalyst is starved due to mass transfer limitations in the precipitated polymer, which is related to the amount of active catalyst. Therefore, the observed rate of deactivation is higher order in catalyst than first order in catalyst.

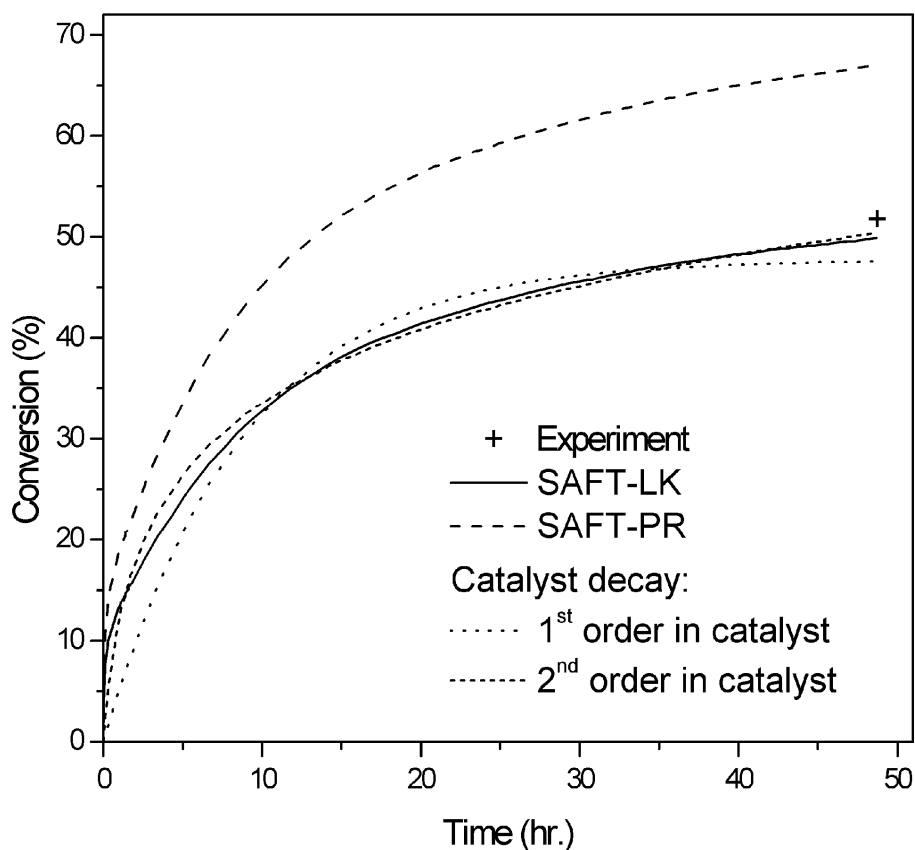


Figure 4.8. Conversion versus time curves as calculated by the SAFT-LKP and the SAFT-PR model and the experimentally observed conversion of run 1. The deactivation rate of the catalyst has been modeled as first and second order in catalyst concentration.

4.5 Conclusions

Observing the evolution of pressure during high-pressure reactions can be an effective method to determine the reaction rate. Both the SAFT-LKP and the SAFT-PR model described in this paper are able to derive a reaction rate from pressure change upon reaction in supercritical fluid systems. However, the SAFT-LKP model is more accurate than the SAFT-PR model, due to the better description of PVT behavior of the LKP eos in comparison with the PR eos. Fitting different rate equations to the observed reaction rate indicates that the polymerization suffers from catalyst deactivation by local depletion of monomer in the precipitated polymer.

4.6 Acknowledgement

The authors thank R. Duchateau for helping to prepare the catalyst, W.J. Kingma for performing the GPC measurements, M.A. Jacobs for conducting the swelling experiments and the Dutch Polymer Institute for financial support.

4.7 References

- (1) Kendall, J. L.; Canelas, D. A.; Young, J. L.; DeSimone, J. M., Polymerizations in Supercritical Carbon Dioxide. *Chem. Rev.* **1999**, *99*, 543-563.
- (2) Shaffer, K. A.; Jones, T. A.; Canelas, D. A.; DeSimone, J. M., Dispersion polymerization in carbon dioxide using siloxane-based stabilizers *Macromol.* **1996**, *29*, 2704-2706.
- (3) Lepilleur, C.; Beckman, E. J., Dispersion polymerization of methyl methacrylate in supercritical CO₂ *Macromol.*, **1997**, *30*, 745-756.
- (4) Fehrenbacher, U.; Ballauf, M., Kinetics of the Early Stage of Dispersion Polymerisation in Supercritical CO₂ As Monitored by Turbidimetry. 2. Particle formation and Locus of Polymerization. *Macromol.* **2002**, *35*, 3653-3661.
- (5) Super, M. S.; Berluche, E.; Costello, C. A.; Beckman, E., Copolymerization of 1,2-Epoxy cyclohexane and Carbon Dioxide Using Carbon Dioxide as Both Reactant and Solvent. *Macromol.* **1997**, *30*, 368-372.
- (6) Heller, D., Effective Methode zur Verfolgung von Polymerisationen gasförmiger Monomer. *Chem.-Ing.-Tech.* **1992**, *64*, 725-726.

- (7) De Vries, T. J.; Duchateau, R.; Vorstman, M. A. G.; Keurentjes, J. T. F., Polymerisation of Olefins Catalysed by a Palladium Complex in Supercritical Carbon Dioxide. *Chem. Commun.* **2000**, 263-264.
- (8) De Vries, T. J.; Somers, P. J. A.; de Loos, T. W.; Vorstman, M. A.G.; Keurentjes, J. T. F., The Phase Behavior of Poly(ethylene-co-propylene) in Ethylene and Carbon Dioxide: Experimental Results and Modeling with the SAFT EOS. *Ind. Eng. Chem. Res.* **2000**, 39, 4510-4515.
- (9) Huang, S. H.; Radosz, M., Equation of State for Small, Large, Polydisperse, and Associating Molecules: Extension to Fluid Mixtures. *Ind. Eng. Chem. Res.* **1991**, 30, 1994-2005.
- (10) Plöcker, U.; Knapp, H.; Prausnitz, J., Calculation of High-Pressure vapor-Liquid Equilibria from a Corresponding-States Correlation with Emphasis on Assymmetric Mixtures. *Ind. Eng. Chem. Process Des. Dev.* **1978**, 17(3), 324-332.
- (11) Johnson, L. K.; Killian, C. M.; Brookhart, M., New Pd(II)- and Ni(II) Based Catalysts for Polymerization of Ethylene and α -Olefins *J. Am. Chem. Soc.* **1995**, 117, 6414-6415.
- (12) Mecking, S.; Johnson, L. K.; Wang, L.; Brookhart, M. Mechanistic Studies of the Palladium-Catalyzed Copolymerization of Ethylene and α -Olefins with Methyl Acrylate *J. Am. Chem. Soc.*, **1998**, 120, 888-889.
- (13) Reid, R. C.; Prausnitz, J. M.; Poling, B. E. *The properties of gases and liquids 4th ed.*; McGraw-Hill: London, 1987.
- (14) Gmehling, J.; Onken, U.; Arlt, W. *Vapor-liquid equilibrium data collection*; DECHEMA: Frankfurt/Main, 1980.
- (15) Musaev, D. G.; Froese, R. D. J.; Morokuma, K. Molecular Orbital and IMOMM Studies of the Chain Transfer Mechanisms of the Diimine-M(II)-Catalyzed (M = Ni,Pd) Ethylene Polymerization Reaction *Organometallics* **1998**, 17, 1850.
- (16) Mecking, S.; Johnson, L. K.; Wang, L.; Brookhart, M. Mechanistic studies of the palladium-catalyzed copolymerization of ethylene and α -olefins with methyl methacrylate *J. Am. Chem. Soc.*, 1998, **120**, 888.

Chapter 5

Characterization of polyethylenes produced in supercritical carbon dioxide by a late transition metal catalyst

Abstract

The coordination polymerization of ethylene with a palladium-based catalyst is studied using scCO₂ as a reaction medium at different temperatures, pressures and ethylene concentrations. Additionally, the polymerization is performed in dichloromethane as a reference. The polymers are analyzed with gel permeation chromatography (GPC), differential scanning calorimetry (DSC) and hydrogen and carbon nuclear magnetic resonance (¹H and ¹³C NMR). The polymerizations in scCO₂ and dichloromethane result in highly branched amorphous polymers of high molecular weight and narrow molecular weight distributions. Although the polymerization in scCO₂ is a precipitation polymerization, the obtained results are similar to the polymerization in dichloromethane, which is a solution polymerization. Moreover, the polymers produced in scCO₂ show a higher degree of short chain branching (SCB), which likely originates from the non-polar environment compared to the polar dichloromethane. Within the range investigated, temperature and ethylene concentration have an effect on the molecular weight of the polymers, however, not on the SCB of the polymers. Furthermore, analysis of the ¹³C NMR spectra of the polyethylenes gives a strong indication of a new branch on branch structure, which has not been assigned before.

5.1 Introduction

Supercritical carbon dioxide (scCO₂) possesses unique properties as a reaction medium, since it is an environmentally benign, non-toxic, non-flammable and inexpensive compound. The relatively low critical temperature (31.1°C) and pressure (73.8 bar) permits the use of CO₂ above the critical temperature, which has the advantage that the behavior of CO₂ can be varied from liquid-like to gas-like. Consequently, the physical properties of the reaction medium can easily be tuned, simply by changing pressure and/or temperature, which can aid in a more efficient process design. The low viscosity of scCO₂ permits strong agitation, thus enabling high heat and mass transfer rates during reactions. Furthermore, purification of the polymer is simple, especially from residual traces of solvent, as compared to traditional solvents used in polymerization processes.

Most polymers are insoluble in scCO₂, whereas non-polar or slightly polar monomers have a very high solubility. Consequently, most polymerizations in scCO₂ initially start homogeneous and become heterogeneous very rapidly. Many polymerizations that have been performed in traditional solvents have also been performed in scCO₂¹, for example radical², carbocationic³ and transition metal catalyzed^{4,5} polymerizations. Although CO₂ is in many reactions an inert solvent, some polymerizations can not be performed in scCO₂. Traditional catalysts for olefin polymerization cannot be used in scCO₂, as the early transition metals are highly oxophilic and will react with CO₂. However, late transition metal catalysts for olefin polymerization are less oxophilic⁶.

A palladium-based catalyst has been successfully applied to polymerize olefins in scCO₂⁷. Carbon dioxide as a reaction medium does not influence the molecular weight of the produced polymers, indicating that no complexes with the catalyst are formed. The palladium-based catalyst, however, produces unique polymers when in contact with ethylene, as the polyethylenes produced by this catalyst are highly branched due to a process called chain-walking. Branches ranging from methyl to hexyl and longer as well as so-called sec-butyl-ended branches (branch structures on branches) are reported in literature⁸. This eliminates the necessity to use α -olefins to introduce short chain branching (SCB) in polyethylenes. SCB is used to modify the chemical and physical properties of the polymer, like glass transition temperature and crystallinity. In this chapter, the influence of CO₂ on the produced polymer is more thoroughly investigated by quantitative ¹H and ¹³C NMR spectroscopy, GPC and DSC

on a number of polyethylenes produced at different reaction conditions in CO₂ and in dichloromethane as a reference.

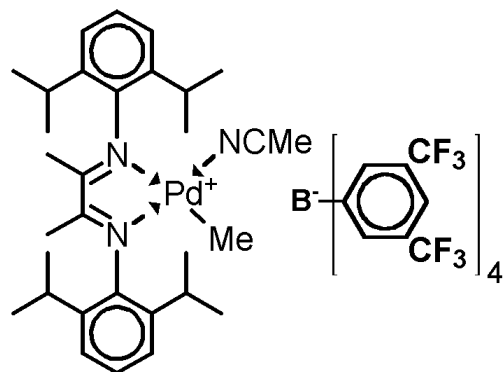


Figure 5.1. Palladium-based catalyst for polymerizations in scCO₂ and dichloromethane.

5.2 Experimental

5.2.1 Polymer synthesis

Figure 5.1 shows the palladium based catalyst used for the polymerizations⁶. The batch polymerizations were performed in a 536 mL high-pressure reactor, equipped with two sapphire windows, a magnetically coupled stirrer, a Pt-100, a pressure sensor, a rupture disc and a heating jacket. The set-up is schematically shown in Figure 5.2.

The polymerization procedure was as follows⁹: the air in the reactor was removed by applying vacuum and filling with 2 bars of argon (3 times). Secondly, vacuum was applied and approximately 50 bar of ethylene (Hoek Loos B.V., grade 3.5) was added directly from the cylinder into the reactor. Subsequently, CO₂ (Hoek Loos B.V., grade 4.5) was added to the reactor up to 10 bars below the final polymerization pressure. The catalyst was put in the catalyst injection loop, which was placed under vacuum to remove air. Finally, the catalyst was flushed into the reactor with 300 bar CO₂ until the desired polymerization pressure was obtained. During the polymerization the pressure and temperature were recorded. After the reaction, the pressure was relieved through a polymer trap and the polymer was collected by rinsing the reactor several times with heptane. The solvent was removed from the polymer in a rotary evaporator.

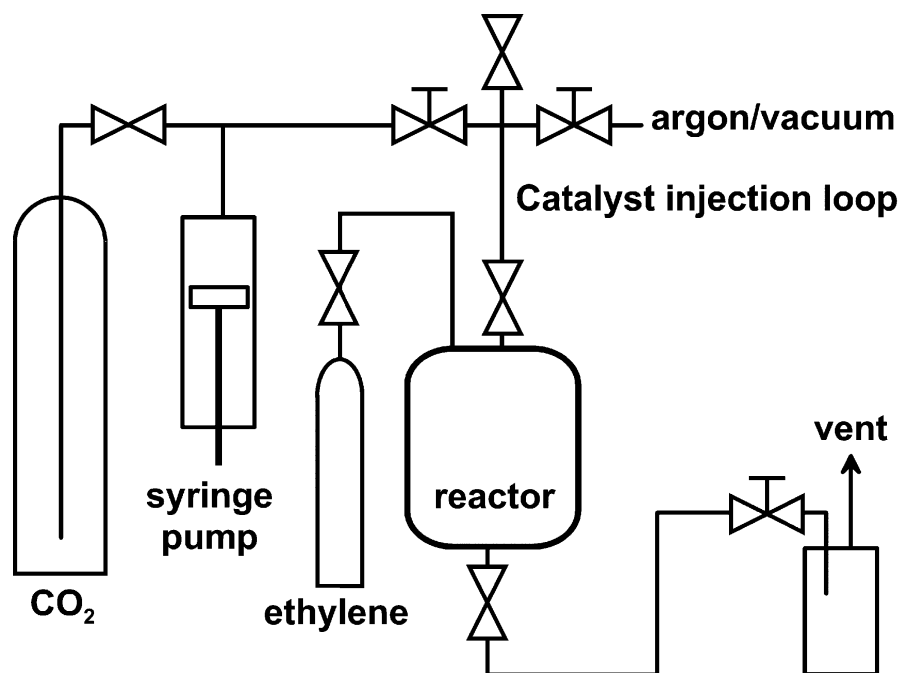


Figure 5.2. High-pressure set-up for ethylene polymerizations in scCO₂.

Polymerization in dichloromethane (AR grade, Aldrich, dried over 3Å molsieves) was carried out in a glass reactor equipped with a magnetically coupled stirrer. The following procedure was used: the reactor was filled with 50 mL dichloromethane and gas washed with ethylene by applying vacuum and filling with ethylene (3 times). The catalyst was flushed in the reactor with a head pressure of ethylene and subsequently the polymerization started. After the reaction, the solvent was removed from the polymer in a rotary evaporator.

The various polymerization conditions used are summarized in Table 5.1.

Table 5.1. Polymerization conditions of the synthesized polyethylenes

Polymer sample	1	2	3	4	5	6
Solvent	CO ₂	CH ₂ Cl ₂				
Initial pressure [bar]	207	107	206	108	221	6.9
Temperature [T]	40	40	50	50	40	40
Catalyst [10^{-6} mol L ⁻¹]	40	39	40	38	41	120
Ethylene [g L ⁻¹]	84	84	75	75	38	35 ^a

^aPolymerization in dichloromethane was carried out using a head pressure of 6.9 bar ethylene, which corresponds to an ethylene concentration of about 35 g/L⁶.

5.2.2 GPC measurements

GPC relative to polystyrene standards (Polymer Laboratories, $M = 580$ to $M = 7.1 \cdot 10^6$) was carried out at 40°C using a Waters Model 510 pump and a Waters Model 410 refractive index detector. Samples (approximately 1.5 mg polymer per mL tetrahydrofuran) were filtered over a 0.2 µm PTFE filter. Sample injections (50 µL) were done by a Waters Model WISP 712 autoinjector. The columns used were a PLgel guard column (5µm particles, 50·7.5 mm), followed by 2 PLgel mixed-C columns (5µm particles, 300·7.5 mm) in series. Tetrahydrofuran (Biosolve, stabilized with BHT) was used as an eluent at a flow rate of 1.0 mL/min. Data acquisition and processing were performed using Waters Millennium32 software.

5.2.3 DSC measurements

DSC measurements were performed on a Perkin Elmer Pyris 1 apparatus. The experiments were performed at 10 °C/min. using 11-17 mg polymer samples, which were vacuum dried in an oven at 60°C for 24 hours. The calorimetric glass transition temperatures T_g were determined using the midpoint of heat capacity change as a criterion. DSC temperature calibration was done using indium, gallium and n-dodecane as standards.

5.2.4 ¹H and ¹³C NMR characterization

Standard proton spectra of 5 wt % polymer in CDCl₃ were obtained on a 300 MHz Varian spectrometer at 25 °C and referenced to tetramethylsilane. The spectra were zero filled up to 64k data points. Baseline correction was applied to the NMR spectra before integration.

Quantitative 125 MHz ¹³C NMR experiments and standard Attached Proton Test (APT) experiments were performed on a Varian Unity Inova 500 MHz spectrometer. Measurements were performed on 10 weight percent solutions of polymer in 1,2,4-trichlorobenzene and 0.05 M Cr(acac)₃ using a 10 mm probe with a 3 mm insert. The insert contained o-dichlorobenzene-D₄ as a lock solvent. Quantitative spectra were obtained at 120°C using a 90° pulse (approx. 13 µs), a relaxation delay of 5 s, an acquisition time of 0.64 s, inverse gated decoupling and spectral width of 35 kHz. Under the selected conditions, the T_1 values of all carbons are less than 0.9 s⁸. About 5000-10000 scans were obtained per spectrum. The spectra were zero filled up to 256k data points. Carbon shifts were referenced to the main

chain carbon peak at 29.98 ppm. Baseline correction was applied to the NMR spectra before integration.

5.3 Results

5.3.1 Polymer synthesis

The polymerizations in scCO₂ start homogeneous and rapidly become heterogeneous when the polymer precipitates. At initial pressures above 200 bar, the pressure decrease is about 25 to 50 bar. At lower initial pressures, the pressure decrease is about 8 bar. The difference in pressure decrease is mainly caused by the phase behavior of the system, not by differences in conversion of ethylene. The pressure decrease in the polymerizations has successfully been modeled using the Statistical Associating Fluid Theory equation-of-state (eos) in combination with the Lee-Kesler-Plöcker eos⁹. The polymerization in dichloromethane remains homogeneous throughout the reaction.

5.3.2 GPC measurements

Table 5.2 shows that the polyethylenes produced in scCO₂ have high number average molecular weights and low polydispersities, although the polymerizations in scCO₂ are precipitation polymerizations. This indicates that mass transfer limitations are small during the polymerizations. The total pressure does not have a significant influence on the molecular weight, as the molecular weights of polymers 1 and 3 are virtually identical to polymers 2 and 4, respectively. The effect of the polymerization temperature can be resolved when polymers 1 and 2 are compared to polymers 3 and 4. The increase in polymerization temperature results in a decrease in number average molecular weight of the polyethylenes. Polymer 5 has been synthesized under identical conditions as polymer 1 except for a lower monomer concentration. The decrease in monomer concentration results in a broader molecular weight distribution and a lower number average molecular weight. The polymer synthesized in dichloromethane has a lower molecular weight and a slightly narrower molecular weight distribution when compared to the polymers produced in scCO₂ at the same temperature.

Table 5.2. Characterization of the polyethylenes with GPC, ¹H and ¹³C NMR.

Polymer sample	1	2	3	4	5	6
Mn (kg/mol) ^{a)}	182.0	191.0	123.0	129.0	129.0	159
Mw/Mn ^{a)}	2.7	2.7	2.7	2.5	3.0	2.4
Tg (°C)	-68.7	-69.1	-69.3	-68.2	-69.0	-67.4
ΔH _m (J/g)	2.5	2.2	2.4	3.4	2.3	6.6
% Crystallinity	0.9	0.8	0.8	1.2	0.8	2.3
Branches total ¹ H NMR ^{b)}	106.5	107.8	107.4	105.1	106.5	99.2
Branches total ¹³ C NMR ^{b)}	107.1	106.8	109.3	105.9	107.0	99.1
Methyl ^{b)}	36.9	36.7	37.2	36.6	35.1	32.1
- 3-methyl ended branch ^{b)}	6.8	8.2	7.7	7.4	8.1	6.0
Ethyl ^{b)}	24.3	24.2	24.7	23.9	24.8	21.7
Propyl ^{b)}	2.3	3.2	2.8	2.8	2.5	2.2
Butyl ^{b)}	11.4	10.6	11.9	11.4	13.0	10.5
- 5-methyl ended branch ^{b)}	4.5	3.1	3.0	3.0	3.4	2.2
Pentyl ^{b)}	4.0	8.6	3.9	3.8	2.8	3.0
Hexyl+ ^{b)}	28.1	23.5	28.8	27.5	28.8	29.6

^{a)} Against polystyrene standards. ^{b)} Branches per 1000 C

5.3.3 DSC measurements

Figure 5.3 shows the glass transition temperatures of the polyethylenes formed. The transitions are equally broad, however, the polyethylenes synthesized in *scCO*₂ all have a slightly lower Tg than the polyethylene produced in dichloromethane. Although the polyethylenes are highly amorphous, a small enthalpy of melting can still be observed in the range -50 to -10 °C, see Figure 5.4. This shows that the polyethylenes produced in *scCO*₂ are even less crystalline than the polyethylene produced in dichloromethane. Compared to 100% crystalline polyethylene, which has a melting enthalpy of 294 J/g, the polyethylenes produced in *scCO*₂ and dichloromethane have a crystallinity of about 1% and 2%, respectively. Although crystallinities of highly branched polyethylenes are likely to be higher than calculated from the value for 100% crystalline polyethylene due to poor quality of the polymer crystals in branched polyethylene, the relative difference between the polyethylenes produced in *scCO*₂ and dichloromethane remains the same. The melting enthalpy of 100% crystalline polyethylene can be used to determine the crystallinity sufficiently accurate, which

is supported by X-ray diffraction and DSC measurements on a series of branched polyethylenes by Mirabella and Bafna¹⁰.

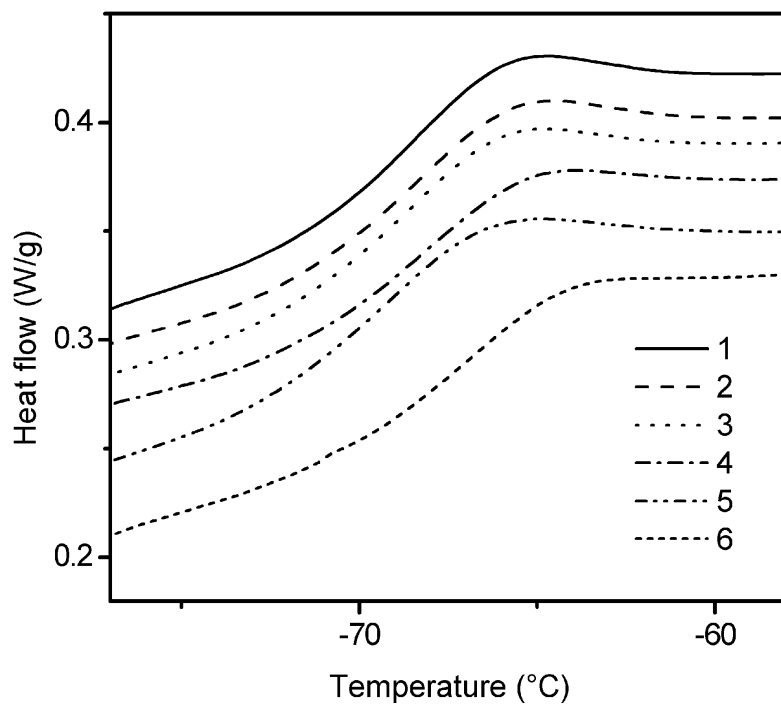


Figure 5.3. Glass transitions of the formed polymers; 1 through 5 are synthesized in scCO_2 , 6 is synthesized in dichloromethane.

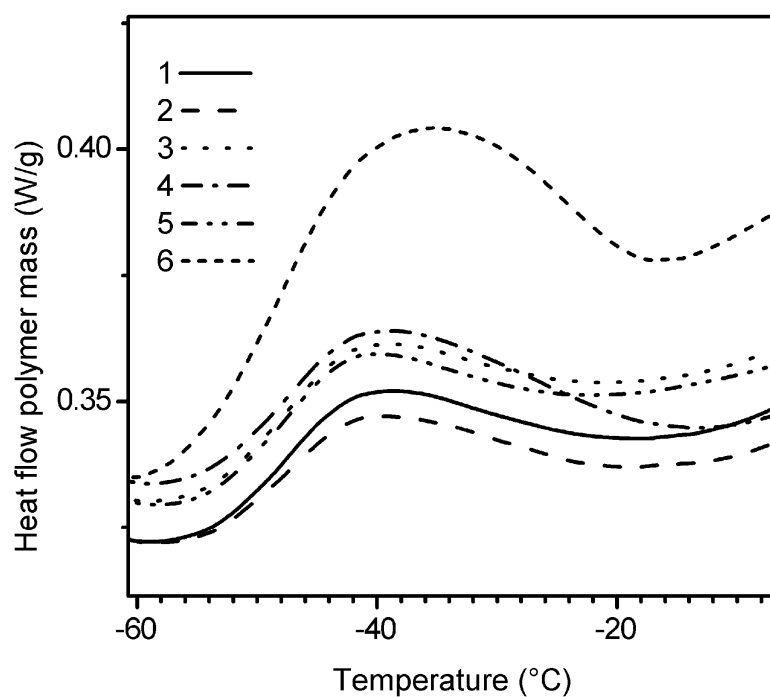


Figure 5.4. Melting range of the formed polymers; 1 through 5 are synthesized in scCO_2 , 6 is synthesized in dichloromethane.

5.3.4 1H and ^{13}C NMR characterization

Figure 5.5 shows a typical 1H NMR spectrum of the polymers produced either in $scCO_2$ or in dichloromethane. The peaks in the range from 0.76 to 0.94 ppm reflect the large amount of CH_3 groups, which indicate that the polymer is highly branched. Although the polyethylenes seem to dissolve completely in $CDCl_3$, phase segregation occurs after a few hours, rendering $CDCl_3$ unsuitable for reliable quantitative ^{13}C NMR measurements.

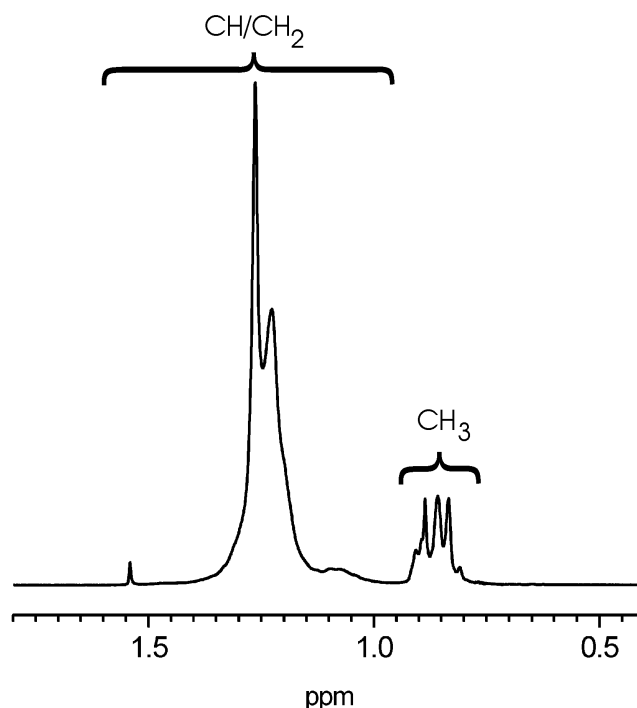


Figure 5.5. Typical 1H NMR spectrum of the polyethylenes produced by the palladium based catalyst. Spectrum is a 300 MHz 1H NMR spectrum of polymer 3 (produced at 50°C in $scCO_2$, 206 bar initial pressure) measured in $CDCl_3$ at 25°C.

Figure 5.6 shows the ^{13}C NMR spectrum of the polymer sample 4 produced in $scCO_2$ at 50 °C, 108 bar total pressure and 74.8 g/L ethylene. The spectrum shows that the polymers produced by the palladium-based catalyst are indeed highly branched. The peaks resulting from resonances of carbons belonging to methyl, ethyl, butyl, pentyl, branches longer than pentyl (hexyl⁺) and branches belonging to 3-methyl-butyl⁺-ended branches have been assigned according to literature^{8,11,12,13}. Table 5.2 shows the number of branches per 1000 carbon atoms of the polyethylenes produced in $scCO_2$ and dichloromethane. The number of branches determined by 1H NMR in $CDCl_3$ and ^{13}C NMR in TCB is very similar, which indicates that $CDCl_3$ can be used to accurately determine the number of branches. The type

and amount of branches present in the polyethylenes produced in scCO₂ is not influenced by the total pressure or the temperature. The solvent, however, appears to have a small influence on the total branch content of the polyethylenes. The total amount of branches in the polyethylene produced in scCO₂ is slightly higher. This increase in total branch content can not be attributed to a certain type or length of branch, but is rather a general increase in the amount of all branches.

5.4 Discussion

The DSC experiments show that the polyethylenes produced in scCO₂ are more amorphous than the polyethylenes synthesized in dichloromethane, which is likely to originate from the slightly higher branch content as measured with ¹H and ¹³C NMR spectroscopy. A study by Mecking et al.¹⁴ using a similar palladium-diimine catalyst has shown that branching is strongly dependent on the manner in which the polymerization is carried out. A branch content of 65, 66 and 105 branches per 1000 C atoms has been measured in water, gas phase and dichloromethane, respectively. It was concluded that the mobility of the growing polymer chain is reduced in the precipitation polymerization in the water and the gas phase, which leads to a decrease in the chain-walking process. Apparently, when the polymerizations are performed in scCO₂, the CO₂ is able to plasticize the precipitated polymer to such an extent that chain-walking is still possible.

The higher branch content measured for the polymers synthesized in CO₂ compared to the polymers synthesized in dichloromethane is not yet clear. The difference is not likely to originate from the high hydrostatic pressure of CO₂, because the polymers produced at different CO₂ pressures are identical in branch content. Also, within the investigated range, the concentration of ethylene does not change the branch content. Cotts et al.⁸ have performed polymerizations in chlorobenzene at ethylene pressures ranging from 0.1 up to 35 bar. It was shown that the SCB was only slightly decreased at higher ethylene pressures, from 99 down to 93 branches per 1000 carbon atoms. A higher branch content would be expected, if the hydrostatic pressure or the ethylene concentration is the cause of the higher branch content in scCO₂. Finally, the temperature only affects the molecular weight and not the branching of the polymers. Therefore, the observation that the polyethylenes produced in scCO₂ have a higher branch content likely originates from the strong non-polar environment compared to the relatively polar dichloromethane. In view of the fact that chain-walking is much faster than

insertion of monomer, a plausible explanation is that in $scCO_2$ insertion of ethylene in secondary carbons attached to the metal center is favoured over insertion in primary carbons, resulting in more branching. Since a secondary carbon attached to the metal center is more electron donating than a primary carbon, the former is thermodynamically favoured in the non-polar $scCO_2$.

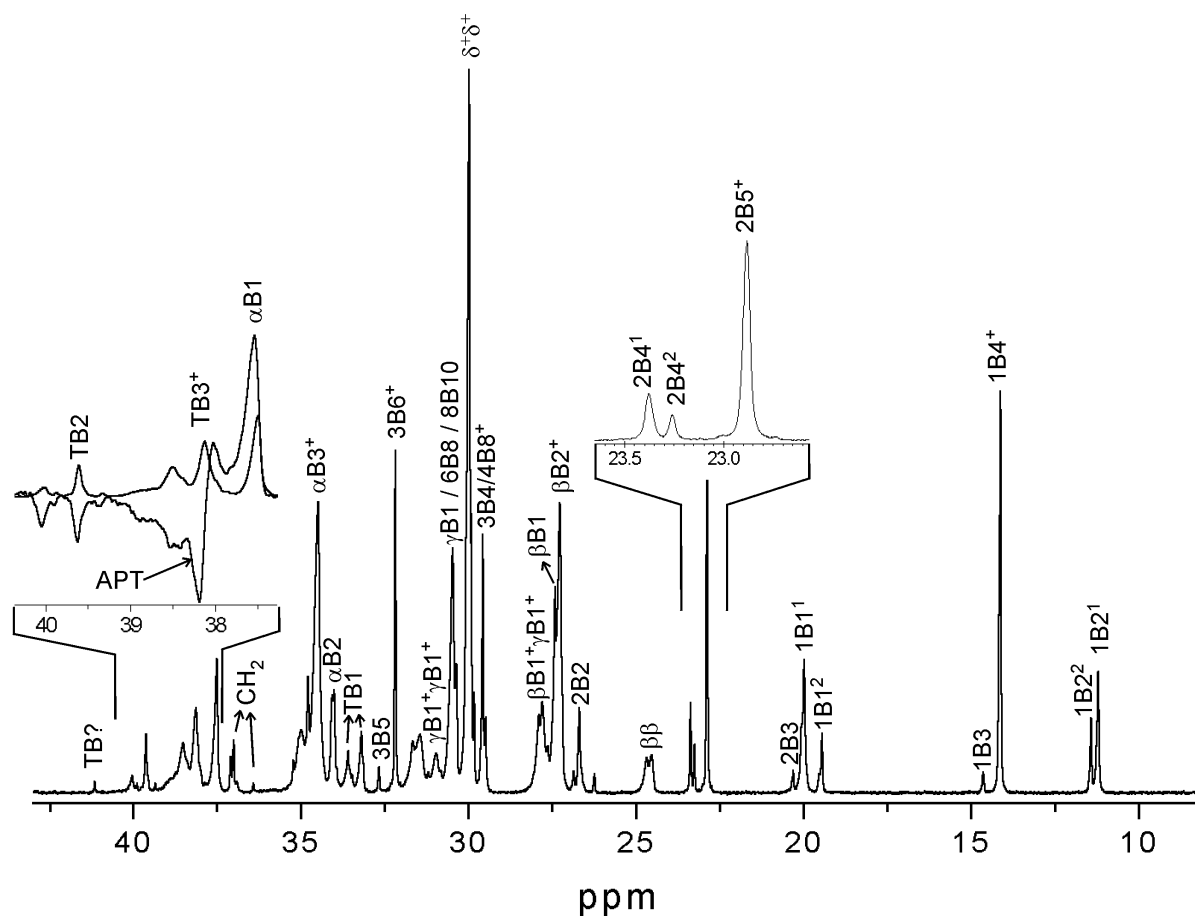


Figure 5.6. Typical ^{13}C NMR spectrum in 1,2,4-trichlorobenzene of polyethylenes produced by the palladium based catalyst. The spectrum is a 500 MHz ^{13}C NMR spectrum of sample 4 (produced at $50^\circ C$ in $scCO_2$, 108 bar initial pressure) measured at $120^\circ C$. Label xBy in case x is a number: x gives the position of the carbon in a branch of length y, in case x is a Greek symbol: carbon in the main chain with 1, 2, 3 or 4 carbons from a branch, respectively denoted as α , β , γ , δ . Positive peaks in the APT insert (attached proton test) mean CH_2 groups, negative peaks mean CH or CH_3 groups.

There is a strong indication that a new branch on branch structure is identified, see Figure 5.7. According to the literature, the 2B4 peak occurs at 23.37 ppm. Near that shift an additional resonance can be observed at 23.26 ppm, which in all ^{13}C NMR spectra is equal in size to the $1\text{B}4^+$ minus the $2\text{B}5^+$ peak (total amount of 'butyl' branches). The shift difference can not be explained by configurational differences of a 2B4 peak. Therefore, the peak must originate from a different structure. The most likely structure is a 5-methyl-ended branch, because the 5-ethyl-ended branch is very likely to give a similar shift as an ordinary butyl branch, as it has the same type of carbons up to 4 carbons from the carbon in question. When the shifts are calculated using the modified Grant and Paul parameters¹¹ a similar trend is observed, although these parameters have been fitted to poly(ethylene-co- α -olefin)s, which do not contain structures like the 5-methyl-ended branch. For a normal butyl branch and a 5-methyl-ended branch, a shift is calculated of 23.11 and 23.05 ppm, respectively.

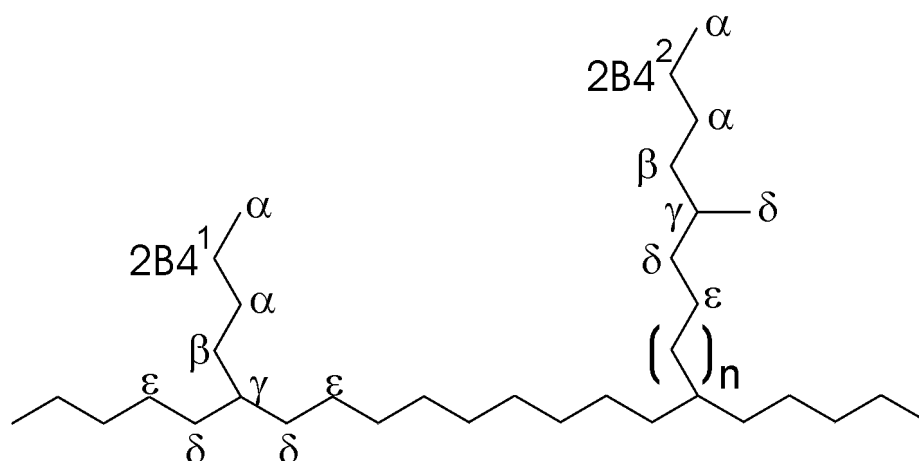


Figure 5.7. Ordinary 2B4 branch and branch on branch structure.

In conclusion, precipitation polymerizations of ethylene can effectively be carried out in scCO_2 . Due to the plasticizing effect of scCO_2 , highly branched polyethylenes can be produced, which have an even higher branch content than polyethylenes produced in dichloromethane.

5.5 Acknowledgment

We thank Marcel van Genderen for assistance with the ¹³C-NMR measurements, Wieb Kingma for performing the GPC measurements and Henny Bruinewoud for the help with the DSC measurements.

5.6 References

- (1) Kendall, J. L.; Canelas, D. A.; Young, J. F.; DeSimone, J. M. *Chem. Rev.* **1999**, *99*, 543.
- (2) Shaffer, K.A.; Jones, T.A.; Canelas, D.A.; DeSimone, J.M. *Macromolecules* **1996**, *29*, 2704.
- (3) Pernecker, T. and Kennedy, J. P. *Polymer Bulletin* **1994**, *32*, 537.
- (4) Super, M.S.; Berluce, E.; Costello, C. A.; Beckman, E. *Macromolecules* **1997**, *30*, 368.
- (5) Hori, H.; Six, C.; Leitner, W. *Macromolecules* **1999**, *32*, 3178.
- (6) Mecking, S.; Johnson, L. K.; Wang, L.; Brookhart, M., *J. Am. Chem. Soc.*, **1998**, *120*, 888.
- (7) De Vries, T. J.; Duchateau, R.; Vorstman, M. A. G.; Keurentjes, J. T. F. *Chem. Commun.* **2000**, 263.
- (8) Cotts, P.M.; Guan, Z.; McCord, E.; McLain, S. *Macromolecules* **2000**, *33*, 6945.
- (9) De Vries, T. J.; Kemmere, M. F.; Keurentjes, J. T. F, submitted.
- (10) Mirabella, F. M.; Bafna, A. *Pol. Sci. B Pol. Phys* **2002**, *40*, 1637.
- (11) Randall, J.C. *J. Polym. Sci., Polym. Phys. Ed.* **1975**, *13*, 901.
- (12) Liu, W.; Ray III, D.G.; Rinaldi, P.L. *Macromolecules* **1999**, *32*, 3817.
- (13) Randall, J.C. *J. Macromol. Sci., Rev. Macromol. Chem. Phys.* **1989**, *C29*, 201.
- (14) Held, A.; Mecking, S. *Chem. Eur. J.* **2000**, *6*, 4623.

Chapter 6

Late-transition-metal catalyzed copolymerization of ethylene and methyl acrylate in compressed carbon dioxide

Abstract

Copolymerizations of methyl acrylate and ethylene using a palladium-based catalyst have successfully been carried out in compressed carbon dioxide at different monomer concentrations and monomer ratios. The incorporation of methyl acrylate and the molecular weight of the polymers were compared to literature values of polymerizations conducted in dichloromethane. In comparison with dichloromethane, similar molecular weights can be obtained. The incorporation of methyl acrylate in the copolymer is higher in compressed CO₂, which can be attributed to a higher methyl acrylate concentration near the catalyst and/or to an energetically more favorable catalyst-methyl acrylate complex as compared to a catalyst-ethylene complex.

6.1 Introduction

Carbon dioxide (CO₂) possesses unique properties as a reaction medium, since it is an environmentally benign, non-toxic, non-flammable and inexpensive compound. The relatively low critical temperature (31.1 °C) and pressure (73.8 bar) permits the use of CO₂ above the critical temperature, which has the advantage that the behavior of CO₂ can easily be varied from liquid-like to gas-like. CO₂ is a good solvent for small molecules both in the liquid and supercritical state. However, most polymers are not soluble in liquid or supercritical CO₂¹, which makes CO₂ a suitable solvent for dispersion and precipitation polymerizations². The low viscosity of compressed CO₂ permits strong agitation, thus enabling high heat and mass transfer rates during reaction. Furthermore, vinyl monomers are toxic and are difficult to remove from the polymer. CO₂ can also act as an efficient extraction agent³, allowing for simple purification of the polymer as compared to the traditional solvents used in polymerization processes.

Conventional catalysts for poly(olefin) production are based on early-transition-state metals, which are highly oxophilic and therefore less suitable for (co)polymerization of polar monomers. Late-transition-state metal complexes are less oxophilic and have a high tolerance for heteroatom functionality, which enables copolymerization of polar monomers^{4,5,6} and polymerization in scCO₂⁷. In this Chapter, the copolymerization of ethylene with methyl acrylate (MA) is investigated in compressed CO₂.

6.2 Experimental section

6.2.1 Materials

Methyl acrylate (MA) was obtained from Merck and was dried over 3 Å molsieves. Before use, MA was distilled under an Argon atmosphere to remove the inhibitor hydroquinone monomethylether. 2,6-di-*tert*-butyl-4-methylphenol (Aldrich), abbreviated as BHT, was added to inhibit radical polymerization⁸. CO₂ (Hoek Loos B.V., grade 4.5) and ethylene (Hoek Loos B.V., grade 3.5) were used as received.

6.2.2 Polymerization in compressed CO₂

Figure 6.1 shows the palladium based catalyst precursors⁵ used for the copolymerizations. The batch polymerizations with MA were performed in a 536 mL high-pressure reactor, equipped with two sapphire windows, a magnetically coupled stirrer, a Pt-100, a pressure sensor, a rupture disc and a heating jacket. The set-up is schematically shown in Figure 6.2. The polymerization procedure was as follows: the air in the reactor was removed by applying vacuum and filling with argon at 2 bar (3 times). Secondly, vacuum was applied and ethylene was added directly from the cylinder into the reactor. Subsequently, the desired amount of MA was pumped into the reactor using a HPLC pump. CO₂ was added to the reactor up to approximately 150 bars. The catalyst was put in the catalyst injection loop, which was placed under vacuum to remove air. Finally, the catalyst injection loop was flushed three times with 300 bar CO₂. After the reaction, the pressure was relieved through a polymer/monomer trap and the polymer was collected by rinsing the reactor several times with heptane. The polymer solution was evaporated in a rotary evaporator.

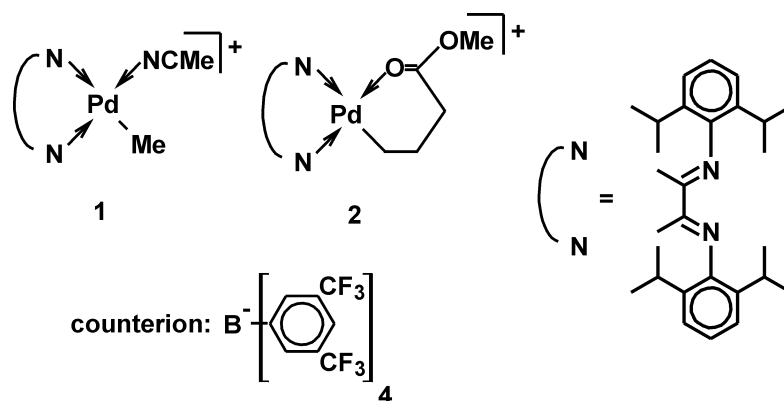


Figure 6.1. Structure of diimine palladium catalyst precursors used in this work (1) and in literature^{5,8} (1,2) to copolymerize MA and ethylene.

Due to the high critical temperature of MA, the critical temperature of the mixture is approximately 50 °C, which is substantially higher than the critical temperature of pure CO₂. Therefore, the polymerization temperature has to be set above or below 50 °C to avoid the unstable critical point. Because temperatures above 50 °C induce rapid catalyst deactivation, the polymerization temperature of choice was 25 °C.

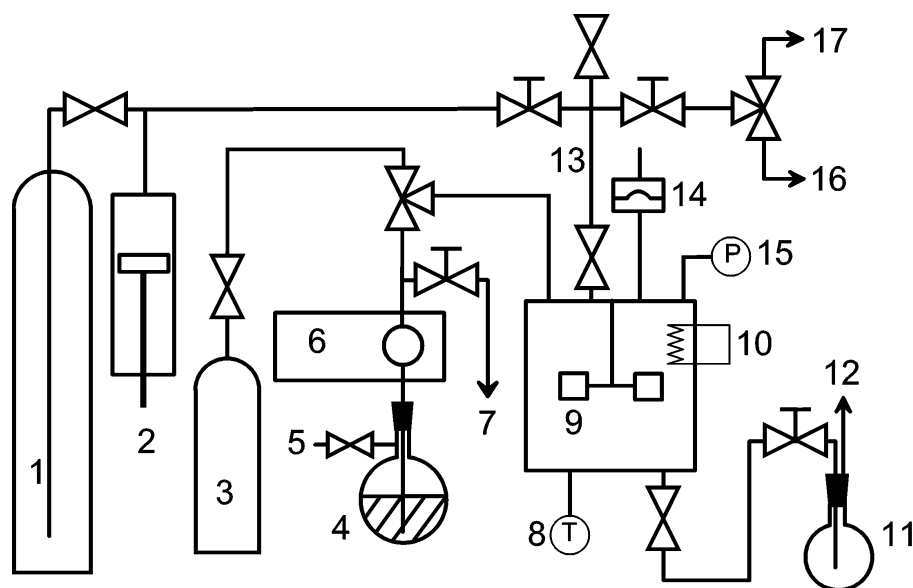


Figure 6.2. High pressure reactor set-up for copolymerizations in compressed CO₂. (1) CO₂ cylinder, (2) syringe pump, (3) ethylene cylinder, (4) MA supply, (5) argon 1.5 bar, (6) HPLC pump, (7) MA waste, (8) Pt-100, (9) HP reactor with magnetically coupled stirrer, (10) heating jacket, (11) MA/polymer trap (0 °C), (12) vent, (13) catalyst injection loop, (14) rupture disc, (15) pressure sensor, (16) vacuum, (17) argon.

6.2.3 Polymer characterization

¹H NMR was used to determine the comonomer incorporation. Measurements were performed on a 300 MHz Varian spectrometer at 25 °C with 5 weight percent polymer solutions in CDCl₃ with TMS as an internal reference. The molecular weight distributions were determined using gel permeation chromatography (GPC). GPC was measured relative to polystyrene standards (Polymer Laboratories, M = 580 to M = 7.1·10⁶) at 40 °C using a Waters Model 510 pump and a Waters Model 410 refractive index detector. Samples (approximately 1.5 mg polymer per mL tetrahydrofuran) were filtered over a 0.2 μm PTFE filter. Injections (50 μL) were done by a Waters Model WISP 712 autoinjector. The columns used were a PLgel guard column (5 μm particles, 50·7.5 mm), followed by 2 PLgel mixed-C columns (5 μm particles, 300·7.5 mm) in series. Tetrahydrofuran (Biosolve, stabilized with BHT) was used as an eluent at a flow rate of 1.0 mL/min. Data acquisition and processing were performed using Waters Millennium32 software.

6.3 Results and discussion

The copolymerizations of MA and ethylene in compressed CO₂ are initially homogeneous and become heterogeneous when polymer is formed. Figure 6.3 shows a typical ¹H NMR spectrum of a copolymer of MA and ethylene synthesized in scCO₂. The integrated areas of the peaks designated as **a** and **b** are approximately equal in size and are approximately two-third of the integrated area of peak **c**. This shows that after insertion of MA, chain-walking occurs resulting in functional groups primarily located at the end of a branch, which has also been observed in polymerizations in dichloromethane with the same catalyst⁵. The results of the copolymerizations of MA and ethylene are summarized in Table 6.1.

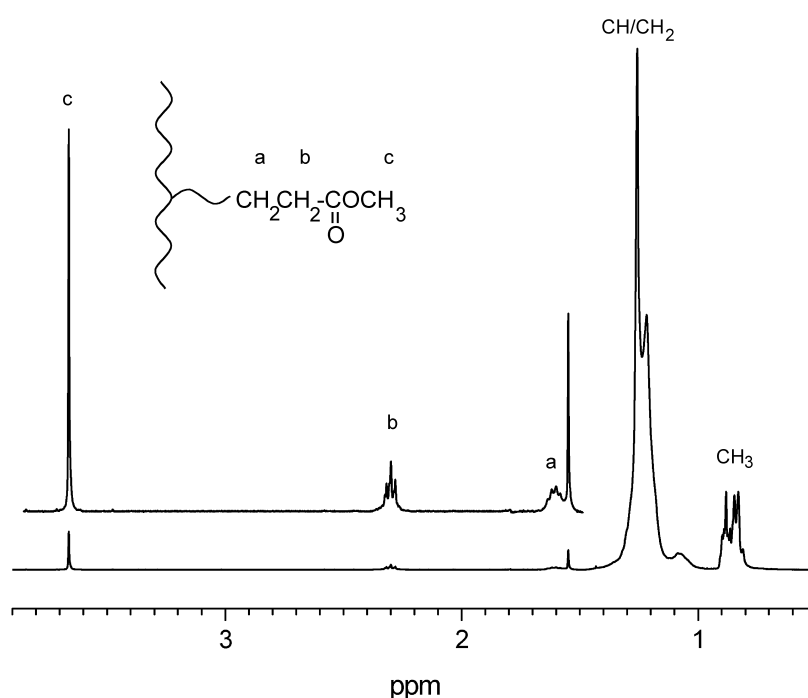


Figure 6.3. 300 MHz ¹H NMR spectrum of the poly(ethylene-co-methyl acrylate) measured in CDCl₃ at 25 °C produced by the palladium based catalyst in experiment 3 in compressed CO₂.

In dichloromethane it has been shown that the incorporation of MA is directly proportional to the concentration of MA in solution at a head pressure of 2 bar ethylene⁵. Figure 6.4 shows that the incorporation of MA is also directly proportional to the ratio of monomer concentrations of MA and ethylene in solution. The difference in MA incorporation in dichloromethane between the two literature sources can be attributed to the use of the BHT inhibitor.

Table 6.1. Results of copolymerizations of ethylene and methyl acrylate in compressed carbon dioxide.

Exp. ^a	MA (mol/L)	Ethylene (mol/L)	p ^b (bar)	M _n ^c (kg/mol)	M _w /M _n	Branches (CH ₃ /1000C)	inc. MA ^d (mol%)	TON ^e MA	TON ethylene
1	1.82	1.94	221	162	1.9	98	1.3	127	9448
2	2.67	0.88	224	51	2.0	100	3.9	117	2895
3	2.05	0.68	184	46	1.7	102	4.4	64	1404

^aReaction conditions: 25 °C, 0.05 mmol catalyst/L, 1 mmol/L BHT, reaction time: 168 hours.

^bInitial total pressure. ^cAgainst polystyrene standards. ^dAmount of MA incorporated in the copolymer. ^eTurnover number, mol monomer per mol catalyst.

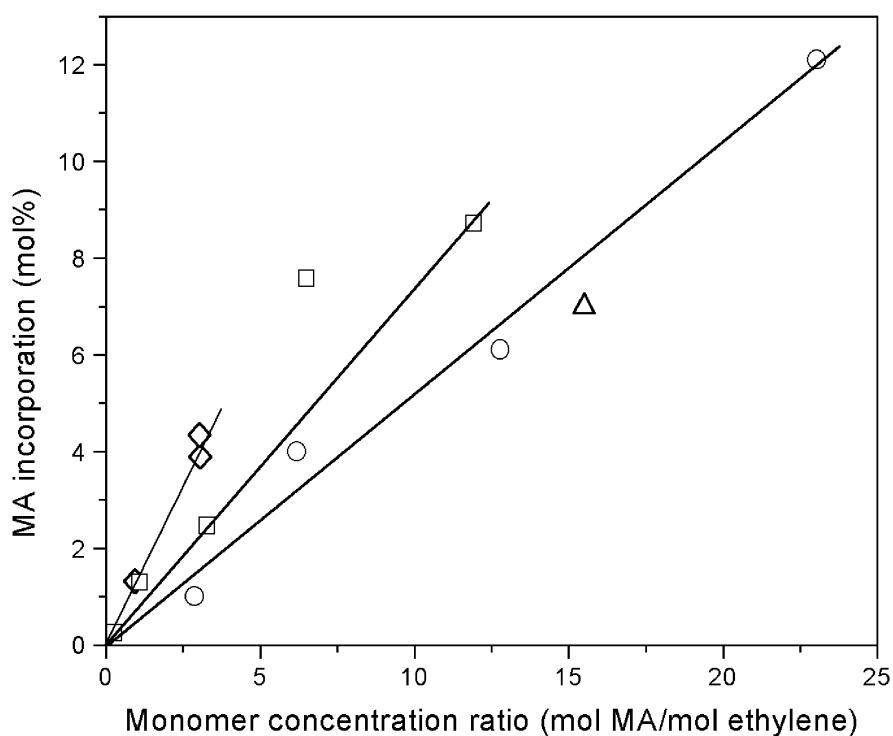


Figure 6.4. Incorporation of methyl acrylate in copolymer as a function of concentration-ratio of methyl acrylate and ethylene. (◇) CO₂ at 25 °C using catalyst precursor 1; (○⁵, □⁸) literature values in dichloromethane at 35 °C using catalyst precursor 2; (Δ⁵) literature value in dichloromethane at 25 °C using catalyst precursor 1. Lines are drawn for visual aid.

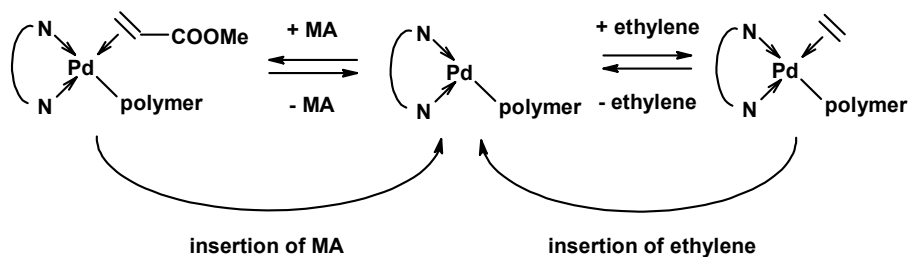


Figure 6.5. Mechanistic description of growth of the copolymer by insertion of MA and ethylene.

It was reported that the inhibitor effectively suppresses the formation of MA-homopolymer, which decreases the catalyst activity and incorporation of MA into the polymer⁸. In comparison with copolymerizations performed in dichloromethane, the incorporation of MA into the copolymer is approximately twice as large in CO₂ at the same monomer ratio. Therefore, less MA is needed for similar incorporation of MA in the copolymer. The rate determining step in the polymerization is the insertion of the monomers. Therefore, the incorporation of MA and ethylene is determined by the ratio of the catalyst-ethylene complex and catalyst-MA complex, see Figure 6.5. Apparently, the polymerization temperature does not seem to influence the incorporation of MA in the polymer, because the polymerization performed by Brookhart et al.⁵ at 25 °C follows the same trend as the polymerizations at 35 °C. It could be anticipated that the high static pressure in CO₂ influences the polymerization. However, the negative activation volumes of the complexation of the monomers with the catalyst are likely to be even more negative for ethylene than for MA. This would result in a lower MA incorporation at a higher pressure, while the opposite is observed experimentally.

The difference in solvent properties can affect the chemical potential of the catalyst complexes and monomers. The latter effect is likely to be small due to the absence of strong interactions between MA, CO₂ and ethylene. A higher incorporation of MA in the copolymer in CO₂ can be caused by an energetically more favorable catalyst-MA complex compared to the catalyst-ethylene complex. Another effect of the non-polar CO₂ is that the local concentration of the polar MA is likely to be higher around the catalyst than in the bulk to stabilize the electrical charge of the cationic palladium complex and the counterion in CO₂. In dichloromethane, these charges are mostly stabilized by the polar dichloromethane. This higher local concentration of MA could explain the higher incorporation of MA into the polymer.

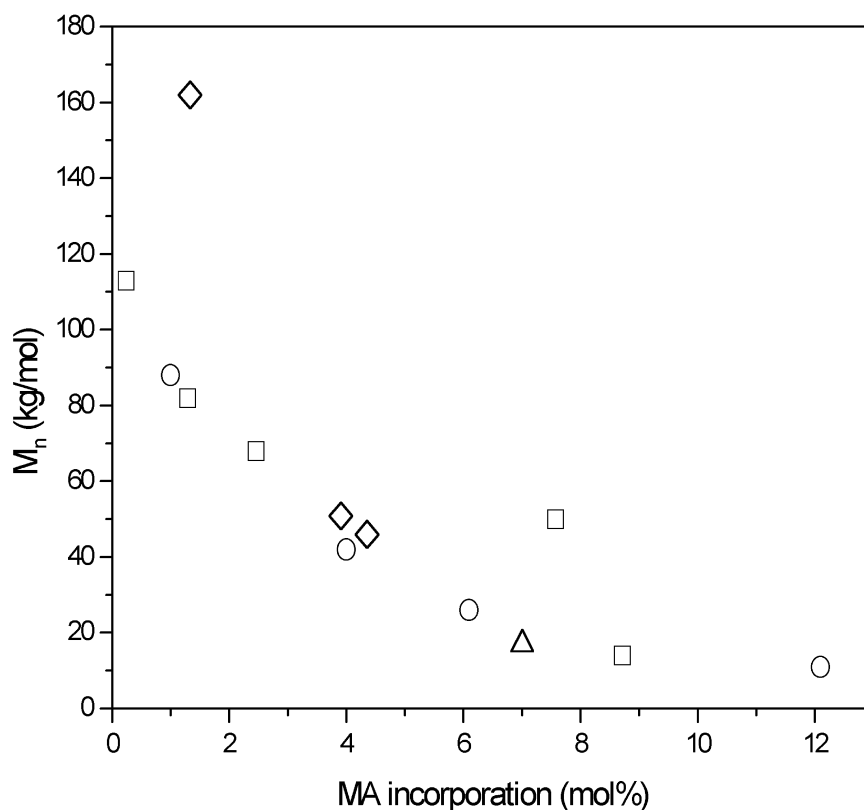


Figure 6.6. Number average molecular weight of copolymer as a function of methyl acrylate incorporation. (◇) CO_2 at 25 °C using catalyst precursor 1; (○⁵, □⁸) literature values in dichloromethane at 35 °C using catalyst precursor 2. (△⁵) literature value in dichloromethane at 25 °C using catalyst precursor 1.

In Figure 6.6 the number-averaged molecular weight, M_n , is given as a function of the incorporation of MA in the polymer. The experiments show a decrease in M_n as the MA incorporation increases. Both the polymerizations in CO_2 and dichloromethane follow the same trend, indicating that the chain-transfer due to inserted MA^5 is similar in both reaction media.

In conclusion, copolymerizations of MA and ethylene can effectively be carried out in compressed CO_2 . In comparison with dichloromethane, similar molecular weights can be obtained. The incorporation of MA in the copolymer at the same monomer ratio is approximately twice as large in compressed CO_2 , which can be attributed to a higher MA concentration near the catalyst and/or to an energetically more favorable catalyst-MA complex compared to the catalyst-ethylene complex.

6.4 References

- (1) O'Neill, M. L.; Cao, Q.; Fang, M.; Johnston, K. P.; Wilkinson, S. P.; Smith, C. D.; Kerschner, J. L.; Jureller, S. H. *Ind. Eng. Chem. Res.* **1998**, *37*, 3067.
- (2) Kendall, J. L.; Canelas, D. A.; Young, J. F.; DeSimone, J. M. *Chem. Rev.* **1999**, *99*, 543.
- (3) Kemmere, M. F.; Cleven, M.; Schilt, M. A.; Keurentjes, J. T. F. *Chem. Eng. Sci.* **2002**, *57*, 3929.
- (4) Klabunde, U.; Ittel, S.D. *J. Mol. Cat.* **1987**, *41*, 123.
- (5) Mecking, S.; Johnson, L. K.; Wang, L.; Brookhart, M. *J. Am. Chem. Soc.* **1998**, *120*, 888.
- (6) Younkin, T. R.; Conner, E. F.; Henderson, J. I.; Friedrich, S. K.; Grubbs, R. H.; Bansleben, D. A. *Science* **2001**, *287*, 460.
- (7) De Vries, T. J.; Duchateau, R.; Vorstman, M. A. G.; Keurentjes, J. T. F. *Chem. Commun.* **2000**, 263.
- (8) Heinemann, J.; Mülhaupt, R.; Brinkmann, P.; Luinstra, G. *Macromol. Chem. Phys.* **1999**, *200*, 384.

Chapter 7

Prospects and issues for transition-metal catalyzed polymerizations in scCO₂

Abstract

In this thesis, a number of issues regarding the late-transition-state metal catalyzed olefin polymerizations in scCO₂ have been discussed. Nevertheless, some issues have to be resolved or investigated in more detail before a viable process can be designed. Catalyst activity and solubility still need improvement. Some aspects of the phase behavior and rheological properties of the often heterogeneous polymer-monomer-CO₂ mixtures are not completely clear, and mass and heat transport phenomena in these mixtures are complex. These issues are discussed in this chapter. Furthermore, a preliminary concept for a future process design is presented.

7.1 Catalytic polymerizations in scCO₂

The previous chapters have shown that late-transition-state metals can be active in olefin polymerization in scCO₂. With a palladium-based catalyst, highly branched polymers with similar molecular weights and molecular weight distributions have been obtained both in scCO₂ and in reference experiments in organic solvents. However, small differences in the microstructure of the polymers were observed. Detailed characterization of the polymers showed a slight increase in the number of branches per 1000 carbons in scCO₂. This likely originates from the non-polar environment in scCO₂ compared to the polar dichloromethane.

The research on catalysts based on late-transition-state metals has increased remarkably in the last decade. The objective of many researchers is to design catalysts which are able to copolymerize α -olefins with comonomers bearing heteroatom functional groups and which are less prone to deactivation by impurities. These developments often lead to catalysts that can also be used in scCO₂. Unfortunately, the activity of these catalysts is still much lower than the traditional early-transition-state metal catalysts used for the polymerization of olefins. Since research on catalysts based on late-transition-state metals has just started, it can be expected that the activity and stability of these catalysts will improve significantly in the future.

The phase behavior of the polyolefins and the catalyst in scCO₂ has been discussed in detail in the previous chapters. The catalyst used is only soluble in scCO₂ to a limited extent and the solubility is greatly influenced by CO₂-density and temperature. Methods to increase the limited catalyst solubility in scCO₂ or even to avoid this issue are discussed in section 7.2 and examples are described in sections 7.3 and 7.4. It has been shown that the polyolefins are not soluble, yet appear to become highly plasticized by CO₂. For a future process design, the extent of sorption and swelling and the rheological properties of the swollen polymers have to be known. The swelling experiments briefly mentioned in Chapter 4, as well as the modeling thereof, are discussed in section 7.5. Section 7.6 discusses mass and heat transport phenomena occurring in the heterogeneous polymerizations in scCO₂.

Views on the design of polymerization equipment suitable for performing polymerizations in scCO₂ are given in section 7.7. A process concept of a polymerization reactor is also discussed.

7.2 Solubility of polymerization catalysts in $scCO_2$

The palladium-diimine catalyst used in this thesis is soluble in $scCO_2$. However, the solubility is rather limited because of the ionic character of the catalyst. In general, the intrinsic activity of a catalyst is higher when the catalyst is dissolved or highly dispersed. To increase the solubility, the catalyst can be made more CO_2 -philic by lowering the self-cohesion of the catalyst. Perfluorinated alkane tails are mostly used for this purpose¹⁻⁴. However, poly(propylene-oxide) tails are expected to work just as well and are much cheaper. A route to synthesize a modified diimine ligand is proposed in Figure 7.1.

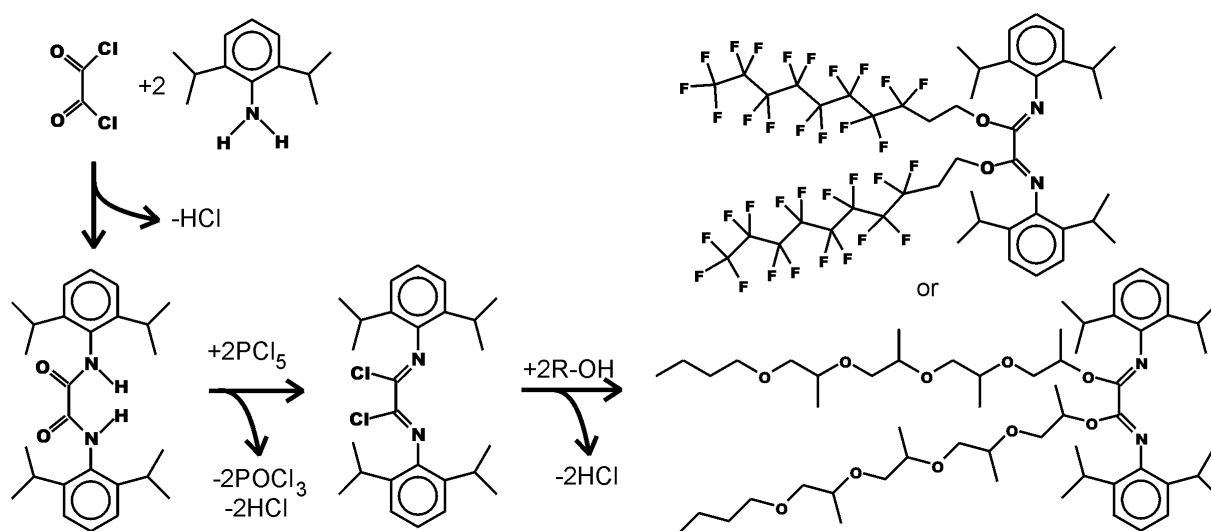


Figure 7.1. Synthetic route to a modified diimine ligand with poly(propylene-oxide) or perfluoroalkane tails to enhance solubility in $scCO_2$.

The low solubility in $scCO_2$ due to the electric charge on the catalyst can be avoided when neutral catalysts are used. Section 7.3 describes preliminary experiments of a new neutral palladium-based catalyst for the polymerization of ethylene and norbornene in dichloromethane and $scCO_2$.

The solubility of the catalyst is not important when the catalyst can be highly dispersed on a support. In section 7.4 preliminary experiments in different solvents of the ring opening metathesis polymerization of norbornene are discussed using a supported catalyst.

7.3 Polymerization of ethylene and norbornene by a neutral palladium-based polymerization catalyst in compressed carbon dioxide

7.3.1 Materials and methods

Materials Diisopropylaniline (synthesis grade, Merck), 2-hydroxy-5-nitrobenzaldehyde (Aldrich), formic acid (Merck), ethanol (Absolute, Merck) and sodium hydride (60% in mineral oil, Aldrich) were used as received. CODPdMeCl was synthesized according to literature procedures⁵. Tetrahydrofuran (THF) was obtained from Merck (extra pure), Dichloromethane, pentane and acetonitrile were obtained from Riedel-de Haën and were dried over 3 Å molsieves. Norbornene (Aldrich) and ethylene (Hoek Loos, grade 3.5) were used as received.

Synthesis of the catalyst Figure 7.2 schematically shows the synthesis of the neutral palladium-based catalyst. The ligand was prepared using a similar synthetic route as described by Wang et. al.⁶ 7.5 mL diisopropylaniline (39.8 mmol) and 5.29 g 2-hydroxy-5-nitrobenzaldehyde (31.5 mmol) were dissolved in 30 mL ethanol. 1.4 mL formic acid was added as a catalyst and the reaction was stirred for 2½ days at room temperature. The yellow precipitated product was filtered, washed with 3x10 mL ethanol and dried in vacuum (8.9 g, 87%). 300 MHz ¹H NMR spectrum of 2-[(2,6-Diisopropyl-phenylimino)-methyl]-4-nitrophenol in CDCl₃: δ 8.39-8.29 (m,3H), δ 7.23 (s,3H), 7.11 (d,1H), δ 2.92 (septett,4H), δ 1.20 (d,12H).

The novel catalyst complex was obtained as follows: 0.123 g NaH (60% in mineral oil) was washed with pentane. 0.3345 g ligand and 10 mL THF was added and the mixture was stirred for 1 hour at room temperature. The mixture was left to settle out and the clean liquid was siphoned off and vacuum dried to obtain the sodium salt of the ligand (0.233 g, 65%). CODPdMeCl (0.178 g) and 10 mL acetonitrile were added to the sodium salt of the ligand and stirred overnight. The mixture was filtered and the clear liquid vacuum dried to obtain a yellow powder. ¹H NMR indicated that more than one equivalent of acetonitrile was present. Prolonged vacuum drying for 3 days gave a yellow-orange powder. 300 MHz ¹H NMR spectrum in CDCl₃: δ 8.17-8.14 (2H), δ 7.80 (s,1H), 7.27-7.17 (m,1H), δ 3.31 (septett,4H), δ 1.29 (d,6H), δ 1.09 (d,6H), δ 0.08 (s,3H).

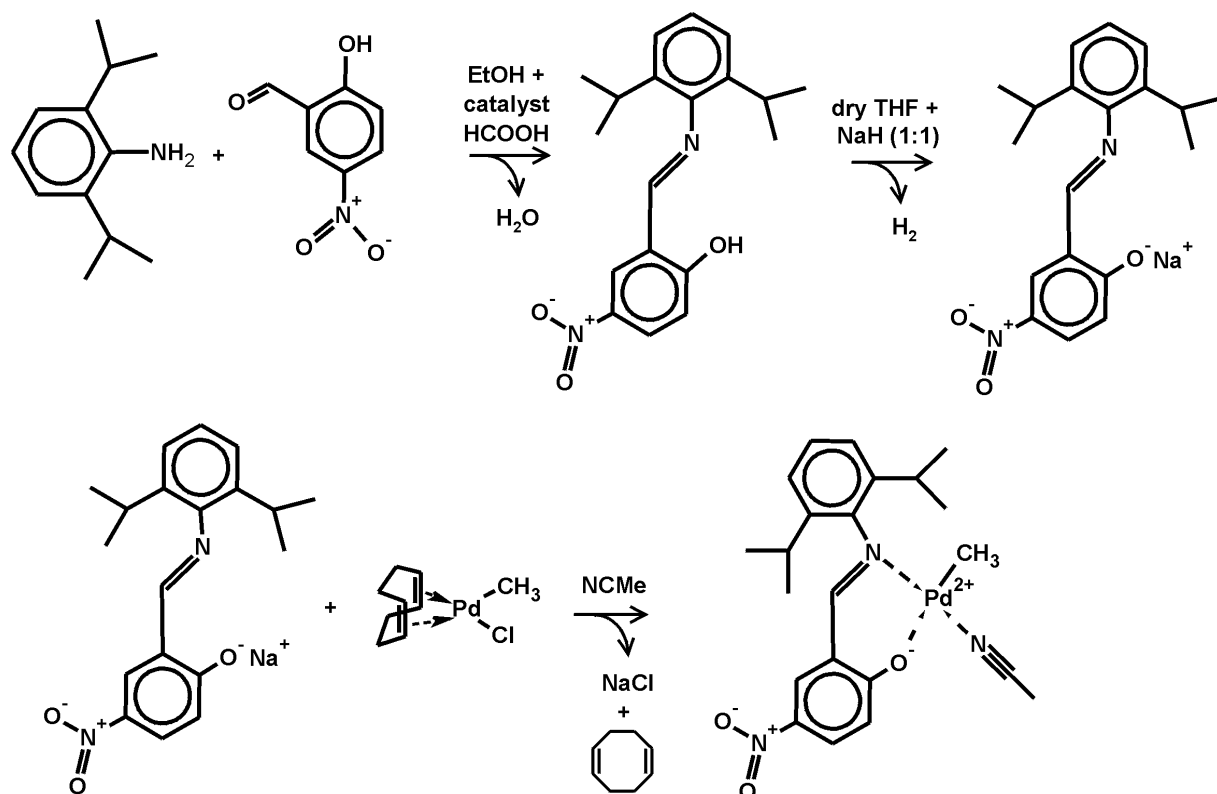


Figure 7.2. Synthesis of a neutral salicylaldiminato palladium (II) complex.

Polymerizations Polymerizations in dichloromethane were performed as follows: the glass reactor was dried in an oven. Norbornene, dichloromethane and a stirring bar were added under a positive flow of argon and the mixture was degassed. The catalyst was added under a positive flow of ethylene or argon. Polymerization in CO_2 was performed as follows: a dry high-pressure reactor equipped with a heating jacket, a temperature and pressure sensor was filled with norbornene and with a stirring bar. The air was removed by applying vacuum. CO_2 was added up to 100 bar using a syringe pump. The catalyst was flushed in the reactor with CO_2 using a loop.

7.3.2 Results and discussion

Both homo and co-polymerizations of norbornene and ethylene with this neutral palladium catalyst have successfully been performed in dichloromethane and compressed CO_2 . Homopolymerization of ethylene in dichloromethane results in a viscous liquid. Because of the low molecular weight of the oligomer, a sample of the content of the reactor was analyzed with 1H NMR to determine the yield. The 1H NMR of the vacuum-dried oligomer showed a branch content of approximately 250 methyls per 1000 CH_2 . The ^{13}C NMR spectrum of the

vacuum dried oligomer showed that the oligomer contained methyl, ethyl, propyl, butyl and longer branches, see Figure 7.3. The results of the polymerizations are summarized in Table 7.1.

The homopolymerization of norbornene (entry 2) results in a yellowish powder that does not dissolve in any common solvent, not even in trichlorobenzene at 125 °C. The type of homopolymerization of norbornene is probably addition polymerization, see Figure 7.4. When ethylene and norbornene are in the reaction mixture (entry 3 and 4), a tough glassy polymer is obtained. This polymer cannot be a homopolymer of ethylene, because this would suggest a high molecular weight polyethylene with very low branching. This would be inconsistent with the viscous liquid-like polyethylene obtained in entry 1. Furthermore, the polymers could be softened by dichloromethane, which is not possible with the homopolymer of norbornene (entry 2). Therefore, the obtained material is most likely a copolymer of ethylene and norbornene.

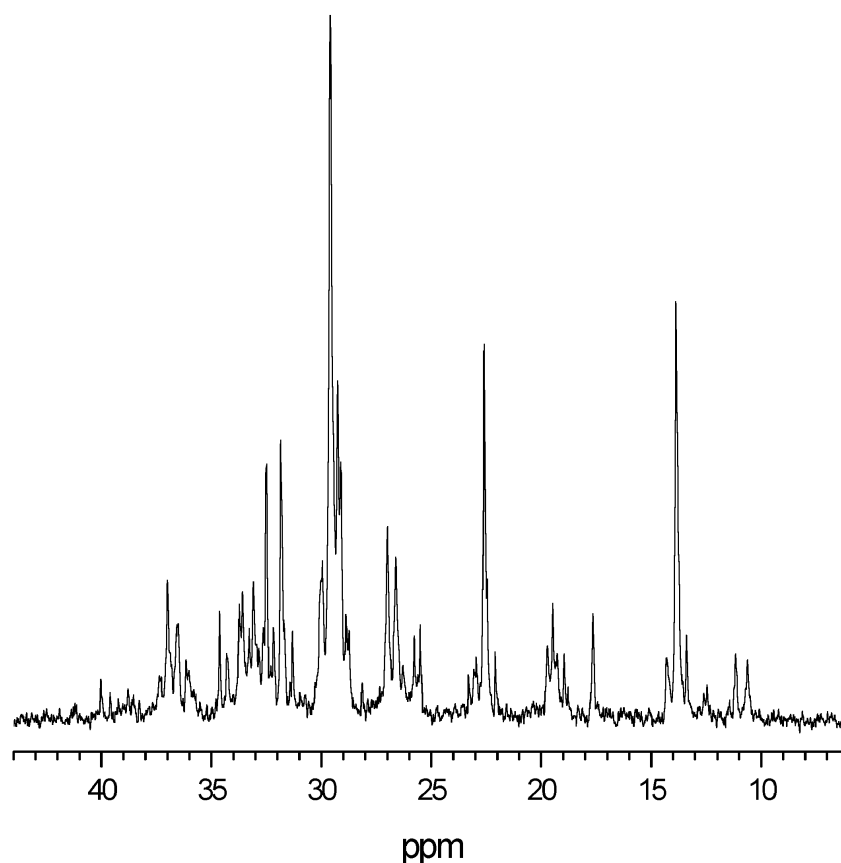


Figure 7.3. ¹³C NMR spectrum of polyethylene produced by the neutral palladium catalyst (entry 1 in Table 7.1). The spectrum is a 400 MHz ¹³C NMR spectrum measured in CDCl₃ at 25 °C.

7.4 Ring opening metathesis polymerization of norbornene using a supported methyltrioxorhenium catalyst in supercritical carbon dioxide⁷

7.4.1 Materials and methods

Methyltrioxorhenium (MTO) was obtained from Strem Chemicals and was used as received. $\text{SiO}_2 \cdot \text{Al}_2\text{O}_3$ (Akzo Nobel, 25 wt% alumina) was calcinated in an oven for 3 hours under oxygen, followed by 3 hours under nitrogen at 500 °C and was stored under argon. Dichloromethane (Riedel-deHaën), chlorobenzene (Aldrich, ACS Reagent) and perfluorodecaline (Fluorochem) were dried with 3Å molsieves and were stored under argon. Norbornene (Aldrich) was used as received. The supported catalyst was synthesized using the following procedure: a solution of 0.0250 g MTO in 2 mL dichloromethane was added to a suspension of 1.829 g $\text{SiO}_2 \cdot \text{Al}_2\text{O}_3$ in 30 mL dichloromethane. After stirring for 10 minutes the solvent was evaporated under vacuum. Figure 7.5 shows the catalyst synthesis and the presumed structure of the active metathesis catalyst⁸.

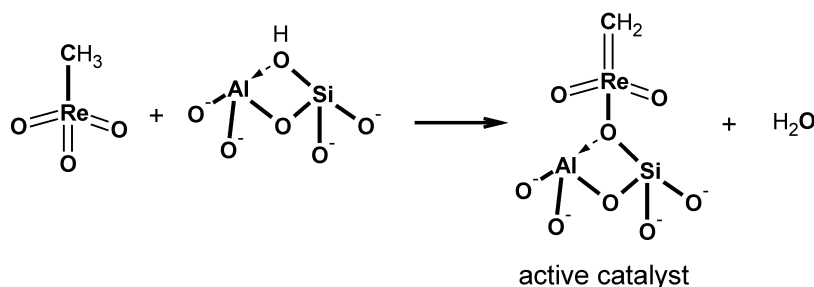


Figure 7.5. Synthesis and presumed structure of the active metathesis catalyst.

Polymerizations in organic solvents were performed as follows: a 100 mL glass reactor with magnetic stirring bar was filled with 50 mL perfluorodecaline or chlorobenzene and heated to 50 °C in a water bath. Subsequently, norbornene was added to the reactor. After the norbornene was dissolved, the supported MTO was added to the reactor. The reaction was quenched by addition of methanol.

The polymerization in scCO_2 was performed in an 80 mL high-pressure reactor equipped with a magnetic stirring bar, a pressure and temperature sensor and a heating jacket. The reactor was heated up to 50 °C. Norbornene was added, followed by CO_2 up to a pressure of 120 bar.

The catalyst was added to the reactor using a loop filled with the catalyst, which was used to flush the catalyst into the reactor with 300 bars of CO₂.

7.4.2 Results and discussion

The effect of different solvents on the ring opening metathesis polymerization (ROMP) of norbornene has been investigated. Perfluorodecaline is used as an analog for polymerization in scCO₂, since norbornene is soluble in both solvents, while the polymer is not soluble in perfluorodecaline nor in scCO₂. Polynorbornene is also not very soluble in chlorobenzene, however, a viscous gel is formed during polymerization. Polymerizations conducted in perfluorodecaline result in small floating agglomerated polymer particles. One chunk of rubberlike polymer has been obtained in the polymerization in CO₂. The results of the polymerizations are summarized in Table 7.2.

Table 7.2. Results of ring opening metathesis polymerization in different solvents.

solvent ^a	norbornene (mol/L)	TON ^b	Mn ^c (kg/mol)	Mw/Mn	Tg (°C)	cis:trans ^d (%:%)
perfluorodecaline	1.1	133	62	4.8	18	77:23
CO ₂	1.8	189	40	3.3	10	84:16
chlorobenzene	1.8	1184	100	3.7	36	78:22 ^e

^aReaction conditions: 50 °C; initial pressure in CO₂ was 150 bar. ^bTurnover number: mol norbornene/mol MTO. ^cSEC-DV in trichlorobenzene at 150 °C, universal calibration.

^dDetermined by ¹H NMR. ^ePolynorbornene is only partially dissolved.

Broad molecular weight distributions are observed in all media. The number average molecular weight and turnover numbers are much lower in scCO₂ and in perfluorodecaline than in chlorobenzene. This can be caused by the low plasticization by scCO₂ and perfluorodecaline of the tough rubberlike polynorbornene as compared to the significant plasticization by chlorobenzene. The lack of plasticization in scCO₂ and perfluorodecaline could sterically hinder polymer formation. Mass transfer limitation of norbornene through the polymer to the catalyst could also play a role. Similar cis/trans ratios are observed for all polymers, which indicates that there is no solvent effect on the polymerization mechanism.

Scanning electron microscopy (SEM) has been used to observe the structure of the polymers deposited on the supported catalyst after polymerization. Figure 7.6 shows the SEM photographs. The supported catalyst used in the polymerization in chlorobenzene is covered with a thick coating of polynorbornene (Figure 7.6b) and the original structure of the support is hardly visible (Figure 7.6a). A thin layer of polynorbornene is deposited on the catalyst support in perfluorodecaline and $scCO_2$, Figures 7.6c and d, respectively. However, the particles produced in $scCO_2$ appear to be more agglomerated than the particles produced in perfluorodecaline. This can be attributed to a small plasticizing effect by $scCO_2$ or the lower T_g of the polymer produced in $scCO_2$, which also explains the higher turnover number in $scCO_2$ compared to perfluorodecaline.

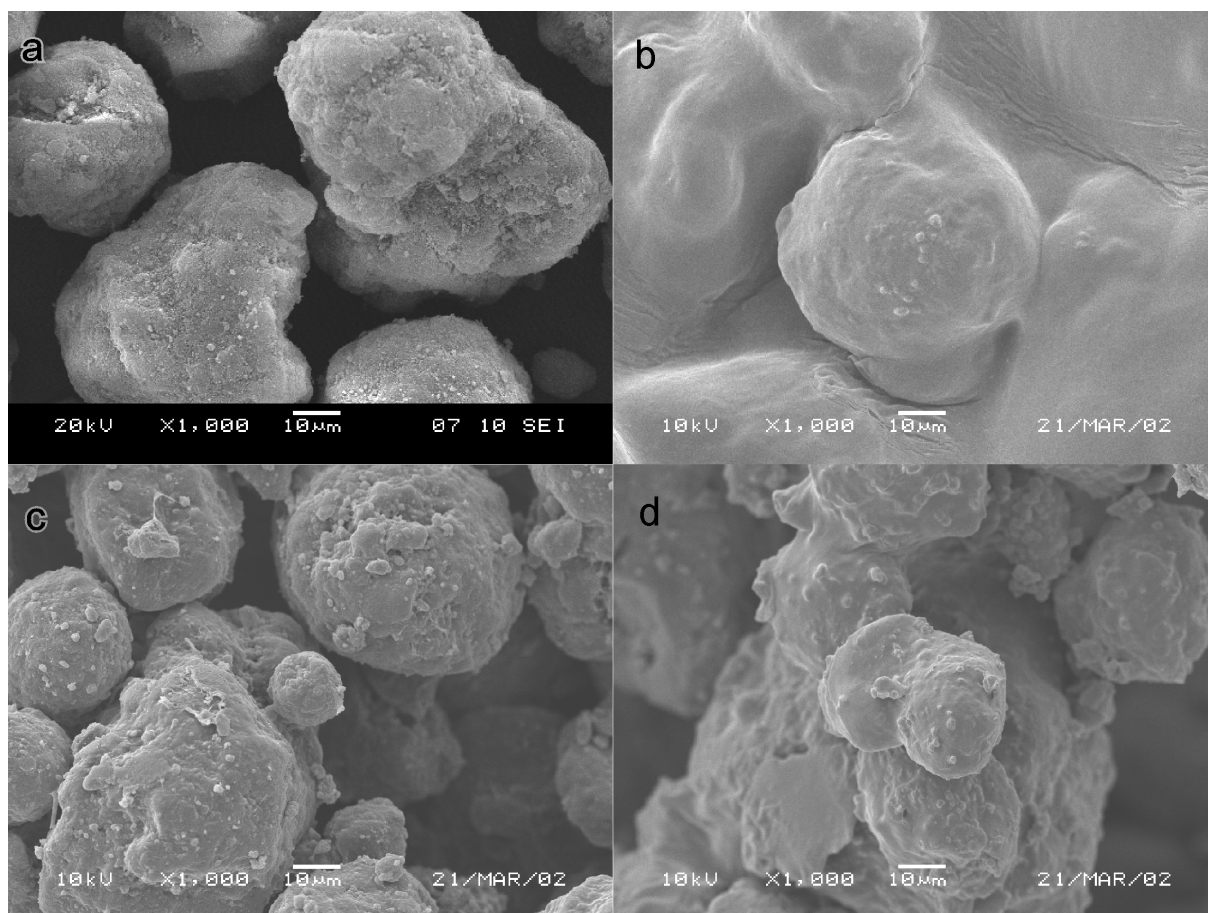


Figure 7.6. Scanning electron microscopy photograph of $SiO_2 \cdot Al_2O_3$ support and supported catalyst after polymerization. (a) support, (b) polymerization in chlorobenzene, (c) polymerization in perfluorodecaline, (d) polymerization in CO_2 .

7.5 Measurement and modelling of polymer swelling

7.5.1 Materials and methods

Highly branched polyethylene produced in $scCO_2$ was used for the swelling measurements. Details on the polymer structure are given in Table 5.2 (polymer 1). Figure 7.7 shows the experimental high-pressure set-up for the swelling experiments. The glass cylinder with a diameter of 10 mm was filled with approximately 1 mL of polymer. The polymer was equilibrated at ambient pressure at the temperature of the measurement. CO_2 was added from low to high pressure, measuring the volume change at equilibrium at each pressure, which generally took 3 to 4 hours. The volume change was measured using a cathetometer.

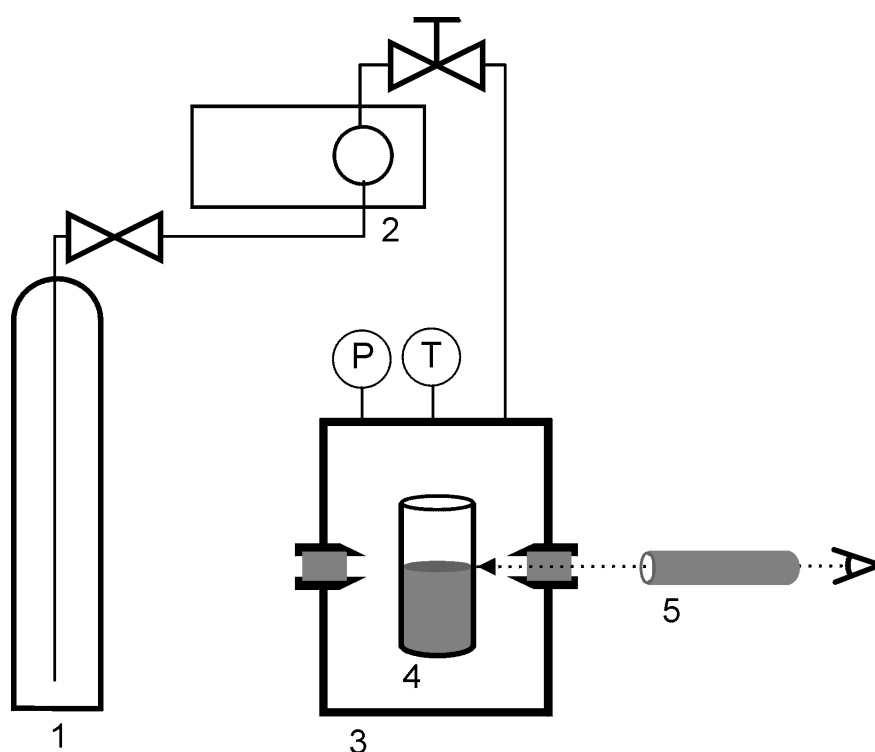


Figure 7.7. High pressure set-up for swelling measurements. (1) CO_2 cylinder, (2) HPLC pump with cooled pump head, (3) high-pressure view cell with two sapphire windows, heating jacket, temperature and pressure sensor, (4) open glass cylinder filled with polymer, (5) cathetometer.

The modeling was performed using the statistical associating fluid theory (SAFT) equation-of-state (eos) and the hybrid SAFT-Lee Kesler Plöcker (LKP) model (see Chapter 4 for details on the models). In the hybrid SAFT-LKP model, the SAFT eos describes the polymer

phase and the LKP eos describes the gas phase. The models assume that the polymer is insoluble in the gas phase. The pure component parameters of the polymer, ethylene and CO₂ are given in Table 4.2. Binary interaction parameters were used as determined in Chapter 2, unless noted otherwise. The programs were written in Mathematica 4.2 (see Appendix 2). The use of SAFT or SAFT-LK to correlate or predict the sorption and swelling of polymers has not been described in the literature before.

7.5.2 Results and discussion

Figure 7.8a shows the experimentally observed swelling of the highly branched polyethylene in scCO₂ and the modeling using the SAFT eos and the hybrid SAFT-LKP model. The SAFT eos gives a slightly better correlation with the experimental results than the hybrid SAFT-LKP model. Both models need adjustment of the binary interaction parameter, k_{ij} . The k_{ij} that follows from the cloud-point measurements ($k_{ij} = 0.154$ at 50 °C, see Chapter 2) results in a much lower swelling, approximately 4 vol% at 200 bar.

Although the SAFT eos describes the experimental swelling more accurately, the SAFT eos gives an inadequate description of scCO₂ near the critical point. The critical temperature and pressure of CO₂ according to the SAFT eos are 47.6 °C and 92.5 bar, respectively, which strongly deviates from the actual critical temperature and pressure of CO₂, 31.1 °C and 73.8 bar, respectively. As a result, different k_{ij} s for the interaction between polymer and CO₂ are obtained. Overprediction of critical temperatures and pressures of pure components is a general error in all analytic eos, which limits the usefulness of these eos models near the critical point. A prediction of the polymer swelling by the SAFT eos in the temperature range between 31.1 and 47.6 °C would result in three-phase behavior instead of the observed two-phase behavior.

The sorption of CO₂ in the polymer has been predicted using the fitted k_{ij} determined in the swelling experiments. Figure 7.8b shows the sorption of CO₂ in the polymer for the two models as a function of pressure. The differences between the model predictions of the sorption are also small. Therefore, both models are equally suitable for correlation of polymer sorption and swelling. However, the SAFT eos should be used with caution for gaseous components at temperatures between the critical temperature and the critical temperature predicted by SAFT eos as the results might be physically incorrect.

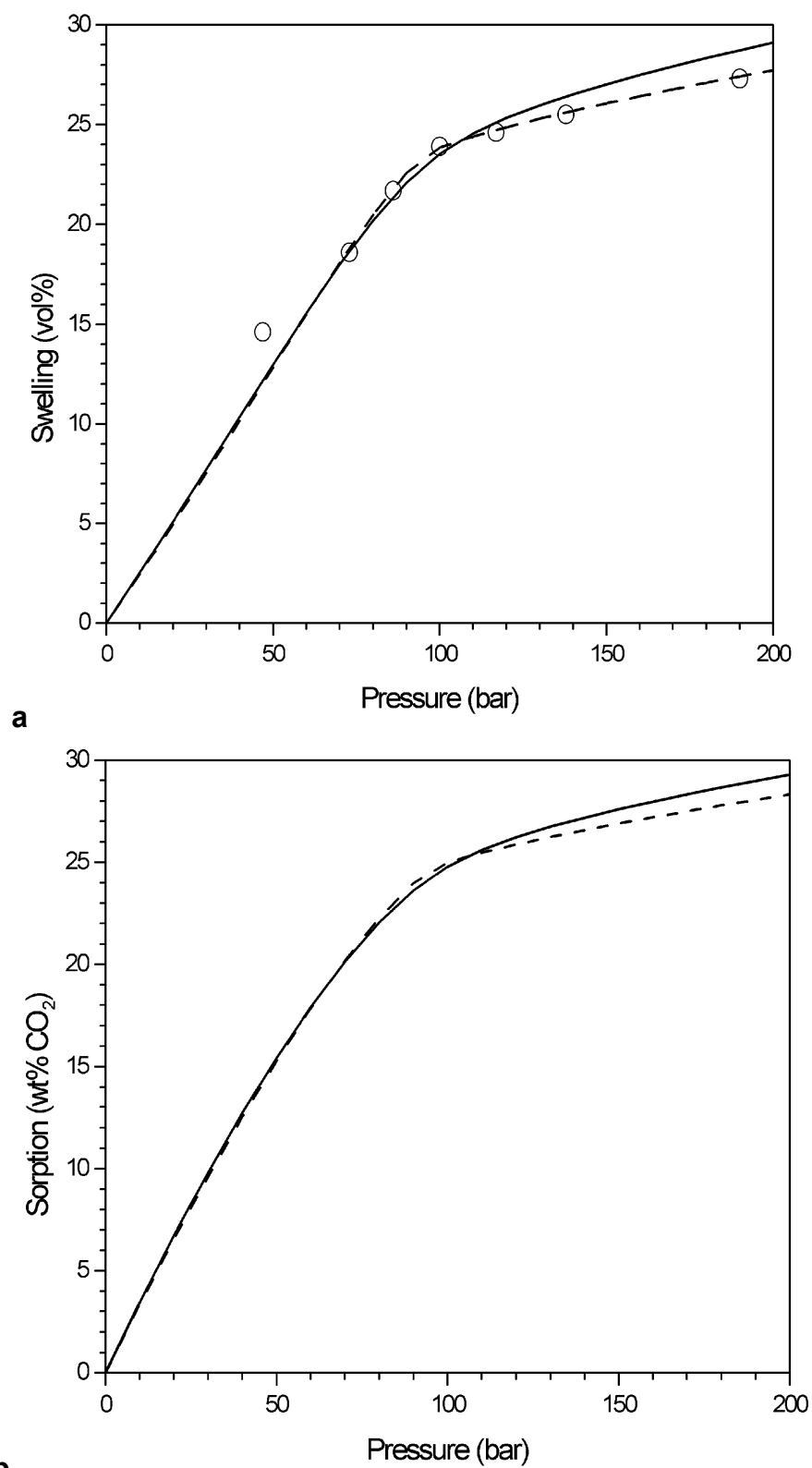


Figure 7.8. (a) Swelling and (b) sorption of highly branched polyethylene by $scCO_2$ at 50 °C. The polyethylene is produced by a diimine palladium catalyst in $scCO_2$ (entry 1 in Table 5.2). (o) swelling measurements, (dashed line) SAFT modeling; $k_{ij} = 0.046$, (solid line) SAFT-LKP modeling; $k_{ij} = 0.056$.

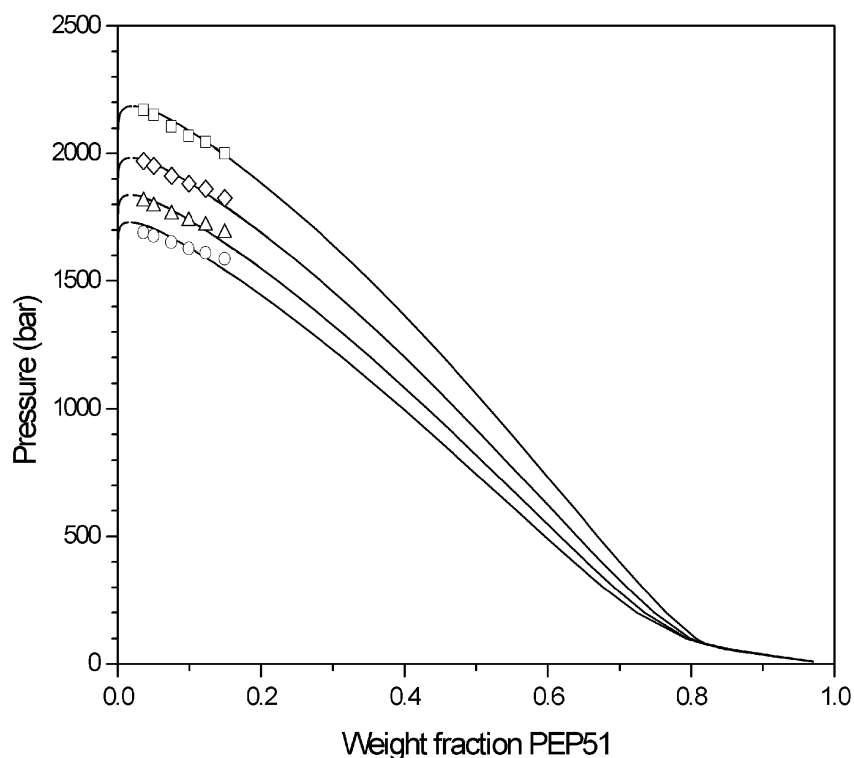


Figure 7.9. Cloud-point measurements (symbols) and SAFT modeling (solid line) of the system PEP51-ethylene as a function of polymer weight fraction. (○) 40 °C, (△) 50 °C, (◇) 60 °C, (□) 70 °C.

Figure 7.9 shows for different temperatures the cloud points of a poly(ethylene-*co*-propylene) (PEP51) in ethylene (Chapter 2) and the cloud-point curve calculated with the SAFT eos. By extrapolating the cloud-point curve to lower pressures, the sorption and swelling of the polymer can be predicted over a broader range.

The predicted sorption and swelling curves by the SAFT eos as a function of ethylene pressure are shown in Figure 7.10. The SAFT eos and the hybrid SAFT-LK model predictions give very similar results, since the critical temperature of ethylene is 9.2 °C and the predictions have been performed above 40 °C.

Moore and Wanke⁹ measured the sorption and swelling by ethylene of a number of branched polyethylenes. The measured sorption is approximately half the sorption level predicted for PEP51. It should be noted, however, that the crystallinities of the pure polyethylenes ranged from 18.5 to 70%, whereas the poly(ethylene-*co*-propylene) is highly amorphous. This crystallinity strongly reduces sorption and swelling.

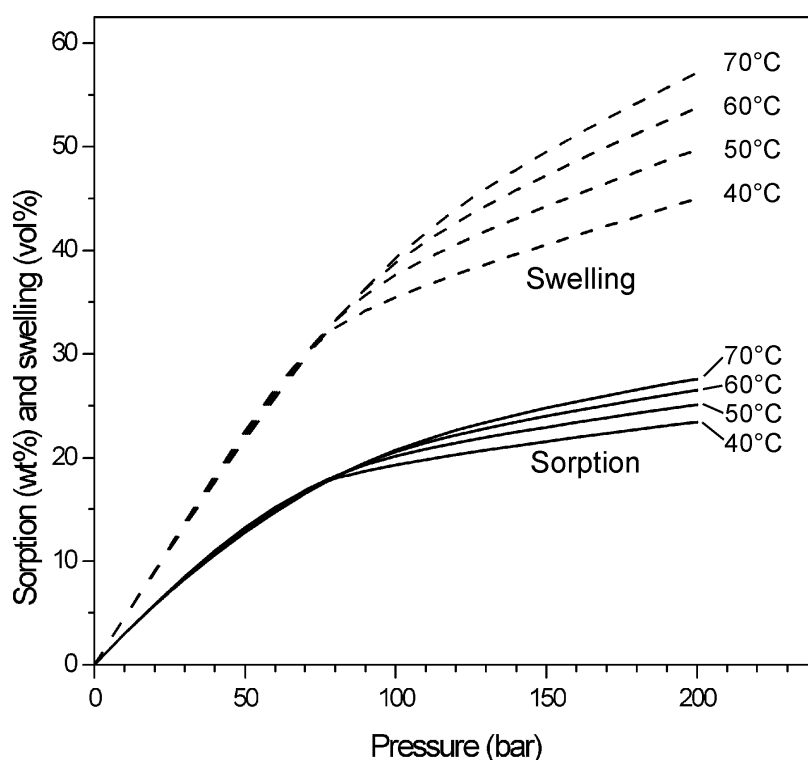


Figure 7.10. Sorption and swelling of PEP51 by ethylene predicted with SAFT using a binary interaction parameter derived from cloud-point measurements.

7.6 Mass and heat transfer in $scCO_2$

Supercritical CO_2 is often associated with high mass and heat transfer. It is certainly true that diffusion coefficients are 5 to 10 times larger than in most common solvents, however, they are by far not as high as diffusion coefficients in the gas phase, which are still orders of magnitudes higher. Binary diffusion coefficients of various substances in $scCO_2$ have already been determined as a function of CO_2 density¹⁰.

Mass and heat transfer in supercritical fluids are different from mass and heat transfer in ordinary fluids, therefore, different mass and heat transfer correlations have to be used. An important factor is the large density change upon a small temperature change. Buoyancy effects are found to be significant for flow of $scCO_2$ in tubes at Reynolds numbers as large as 10^5 . Therefore, the choice of the flow orientation (up, down or horizontal) will have a large impact on mass and heat transfer¹¹.

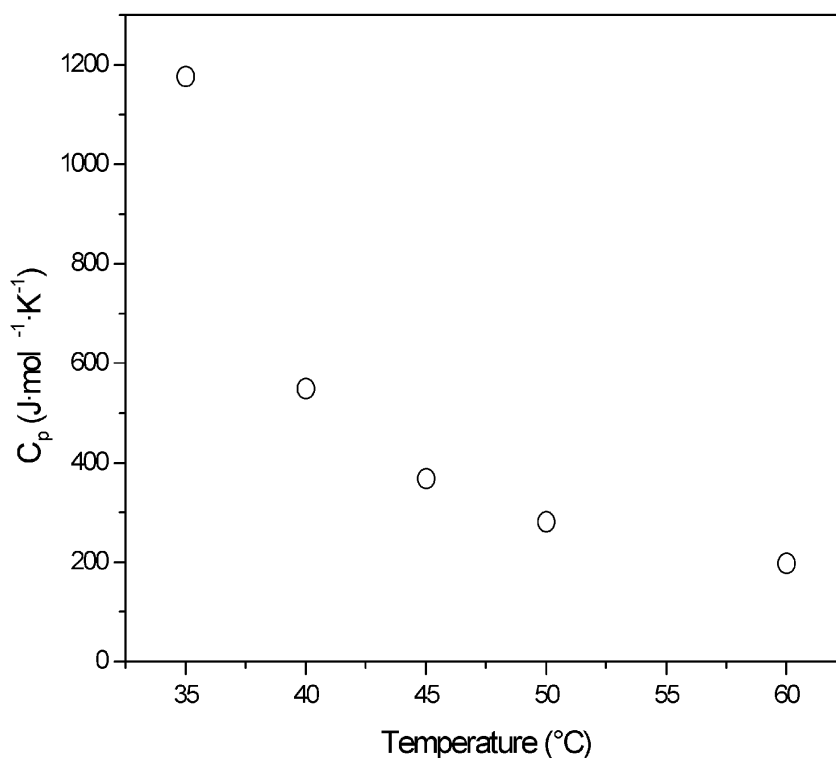


Figure 7.11. Heat capacity at constant pressure of scCO₂ as function of temperature on the pseudocritical line¹⁶.

Furthermore, along the pseudocritical line (the extrapolated vapour-liquid equilibrium curve into the supercritical region), the density changes are large with small changes in temperature. This results in a relatively large heat capacity at constant pressure, C_p . Figure 7.11 shows C_p as a function of temperature at pseudocritical pressures. The heat capacity at constant volume, C_v , is much lower, about 40 to 50 J·mol⁻¹·K⁻¹. However, any local formation of heat in a supercritical fluid, especially along the pseudocritical line, is largely dissipated due to a fast local expansion of the fluid. The expanding fluid compresses the surrounding fluid, which in turn is heated due to the work (also called piston effect¹²⁻¹⁵). Therefore, C_p locally determines the heat capacity of a supercritical fluid even at constant total volume. Consequently, in precipitation polymerizations, heat transfer limitations will mainly occur in the precipitated polymer and through the reactor wall.

A key issue that remains in heterogeneous polymerizations, however, is the mass and heat transport in the polymer phase in combination with the hydrodynamics of the polymer phase

in the supercritical fluid. ScCO₂ is known to act as an extremely effective plasticizer for polymers. Viscosities can be greatly reduced and glass transition temperatures can be lowered by tens of degrees. Different research groups measured and modeled the viscosity reduction by CO₂¹⁷⁻²⁰. For example, low-density polyethylene at 200 °C shows a viscosity reduction of nearly 75% at only 4 wt% CO₂²⁰. This implies that, although polymerizations in scCO₂ will generally be heterogeneous, the polymers become highly plasticized and coagulate more easily. Furthermore, the plasticization may facilitate diffusion of monomers into the polymer phase.

7.7 Concept for a process design

To this date, the most promising catalysts capable of (co)polymerizing olefins in scCO₂ are based on nickel and palladium. Typically, these catalysts have lifetimes longer than one hour. Therefore, the type of reactor should permit long residence times. In addition, the high stability of some of the late-transition-metal polymerization catalysts enables the recycling of the catalyst²¹.

Due to the high pressures involved, a reactor of low diameter is preferred over large vessels, because of the required wall thickness. Large vessels will need very thick walls, which will be more expensive and inefficient for removal of reaction heat. Another consideration is that the polymer is highly plasticized by CO₂, however, not soluble in scCO₂. Therefore, the polymerization is heterogeneous.

Considering these restrictions, the process concept for the catalytic polymerization of olefins in scCO₂ most likely includes a loop reactor shown in Figure 7.12, as described for the slurry polymerization of ethylene in supercritical propane²². In this type of reactor, the residence time can be adjusted to sufficiently long values to obtain a reasonable conversion. Extending the concept to several loop reactors in series allows for setting the right conditions in each reactor for fine tuning the properties of the polymer produced. This allows for the addition of different monomers or monomer ratios at different locations in the system. In principle, this type of equipment also allows for forced convection, thus providing an efficient means to avoid heat and mass transfer limitations.

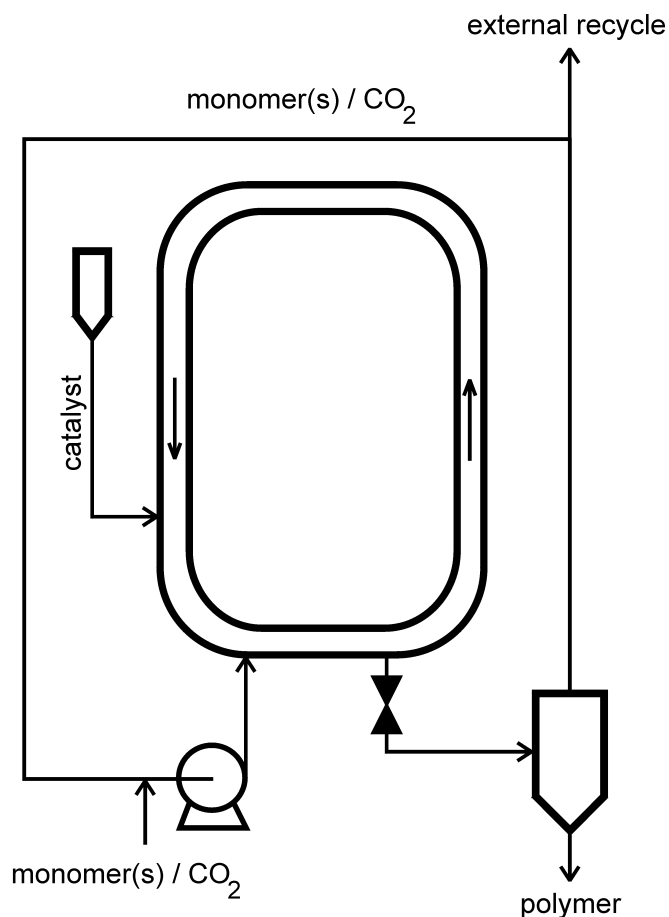


Figure 7.12. Process concept for catalytic (co)polymerization of olefins in (sc)CO₂ using a loop reactor design.

7.8 Concluding remarks

In this thesis the potential of late-transition-state metal catalysts to synthesize polymers in scCO₂ has been demonstrated. One of the most interesting aspects of the catalysts used is their ability to copolymerize ethylene and α -olefins with polar monomers and their inertness towards impurities. This would allow for a relatively straightforward production of this type of polymers in scCO₂. Although the activity of these catalysts is still somewhat low for commercial use, it can be expected that this will improve significantly in the near future, which will enable the development of clean polymerization processes based on scCO₂.

7.9 References

- (1) Kainz, S.; Koch, D.; Baumann, W.; Leitner, W. *Angew. Chem.* **1997**, *109*, 1699.
- (2) Palo, D. R.; Erkey, C. *Ind. Eng. Chem. Res.* **1998**, *37*, 4203.
- (3) Super, M. S.; Berluche, E.; Costello, C. A.; Beckman, E. *Macromolecules* **1997**, *30*, 368.
- (4) Hori, H.; Six, C.; Leitner, W. *Macromolecules* **1999**, *32*, 3178.
- (5) Rulke, R. E.; Ernsting, J. M.; Spek, A. L.; Elsevier, C. J.; van Leeuwen, P. W. N. M.; Vrieze, K. *Inorg. Chem.* **1993**, *32*, 5769.
- (6) Wang, C.; Friedrich, S.; Younkin, T. R.; Li, R. T.; Grubbs, R. H.; Bansleben, D. A.; Day, M. W. *Organometallics* **1998**, *17*, 3149.
- (7) Van den Broeke, L. J. P.; Goetheer, E. L. V.; De Vries, T. J.; Keurentjes, J. T. F., *Abstracts of Papers, 223rd ACS National Meeting* **2002**, April 7-11, Orlando, USA.
- (8) Morris, L. J.; Downs, A. J.; Greene, T. M. *Organometallics* **2001**, *20*, 2344.
- (9) Moore, S. J.; Wanke, S. E. *Chem. Eng. Sci.* **2001**, *56*, 4121.
- (10) Suarez, J. J.; Medina, I.; Bueno, J.L. *Fluid Phase Equilibria* **1998**, *153*, 167.
- (11) Liao, S. M.; Zhao, T. S. *Int. J. Heat and Mass Transfer* **2002**, *45*, 5025.
- (12) Zappoli, B.; Bailly, D.; Garrabos, Y.; Le Neindre, B.; Guenoun, P.; Beysens, D. *Phys. Rev. A* **1990**, *41*, 2264.
- (13) Boukari, H.; Shaumeyer, J. N.; Briggs, M. E.; Gammon, R. W. *Phys. Rev. A* **1990**, *41*, 2260.
- (14) Onuki, A.; Hao, H.; Ferrell, R. A. *Phys. Rev. A* **1990**, *41*, 2256.
- (15) Carles, P. *Proc. of 7th ISASF meeting on supercrit. fluids* **2000**, 881, Antibes, France.
- (16) Bush, D. *Equation of state for Windows 95 version 1.0.14*, Georgia Institute of Technology, **1994**.
- (17) Mertsch, R.; Wolf, B. A. *Macromolecules* **1994**, *27*, 3289.
- (18) Kwag, C.; Manke, C. W.; Gulari, E. J. *Pol. Sci. B Pol. Phys.*, **1999**, *37*, 2771.
- (19) Royer, J. R.; Gay, Y. J.; Desimone, J. M. Khan, S. A. *Pol. Sci. B Pol. Phys.*, **2000**, *38*, 3168.
- (20) Royer, J. R.; Desimone, J. M. Khan, S. A. *Pol. Sci. B Pol. Phys.*, **2001**, *39*, 3055.
- (21) Verspui, G.; Schanssema, F.; Sheldon, R. A. *Angew. Chem. Int. Ed.* **2000**, *39*, 804.
- (22) Ahvenainen, A.; Sarantila, K.; Andtsjo, H. *WO patent 92/12181*, **1992**.

Appendix 1: Programs to calculate overall pressure as function of conversion in batch precipitation polymerizations

```
(*Mathematica 4.1 notebook file;
SAFT-LKP model – simulation of polymerisation run 1;
assumption: polymer insoluble in supercritical phase*)
Off[Remove::"rmnsm"];
Remove["Global`*"];
Off[General::"spell1"];
Off[General::"spell"];
(*Output directory & filename:*)
SetDirectory["C:\windows\desktop"];
filename = "sim-run1-SAFT-LK-2b.txt";
outputfile = OpenWrite[filename, PageWidth → 200];
WriteString[outputfile, "Simulation of polymerisation of ethene in CO2, version 2b\n"];
WriteString[outputfile, "conv\tT[K]\tp[bar]\tw\t%CO2\tw\t
%ethene1\tw\t%ethene2\rho1[g/ml]\rho2[g/ml]\tK1\tK2\tfCO2\tfE\terror\n"];
Print["conv\tT[K]\tp[bar]\tw\t%CO2\tw\t%ethene1\tw\t%ethene2\rho1[g/ml]\rho2[g/ml]\tK1\tK2\terror\n"];
(*constants:*)
mw1 = 44.01; mw2 = 28.05; mw3 = 51000; Rgas = 83.1439; nav = 6.02 1023;
(*initial polymerization conditions; pressure, temperature, composition:*)
T = 313.15;
pstart = 207.2;(*initial pressure*)
p = 199;(*initial guess of pressure at 10 % conversion*)
vreactor = 536.0;(*mL*)
xwfeed1 = 0.9; xwfeed2 = 0.1; xwfeed3 = 0;(*initial guess feed composition*)
massethene = 3.006 mw2 10-3 vreactor;(*exact mass of ethene in reactor*)
dp = p - pstart;
K[1] = 1.6; K[2] = 0.32; K[3] = 0;(*i nitial guess distribution coeff., K[i]=y[i]/x[i]*)
(*SAFT pure component parameters:*)
nc = 3;(*number of components, 1=CO2, 2=ethene, 3=polymer*)
vo = {13.578, 18.157, 21.618}; m = {1.417, 1.464, 0.034365 mw3};
c1 = {40, 10, 10}; uo = {216.08, 212.06, 469.86};
(*SAFT constants:*)
τ = 0.74048; c0 = 0.12;
Dij = 
$$\begin{pmatrix} -8.8043 & 4.164627 & -48.203555 & 140.4362 & -195.23339 & 113.515 & 0 & 0 & 0 \\ 2.9396 & -6.0865383 & 40.137956 & -76.230797 & -133.70055 & 860.25349 & -1535.3224 & 1221.4261 & -409.10539 \\ -2.8225 & 4.7600148 & 11.257177 & -66.382743 & 69.248785 & 0 & 0 & 0 & 0 \\ 0.34 & -3.1875014 & 12.231796 & -12.110681 & 0 & 0 & 0 & 0 & 0 \end{pmatrix};$$

(*SAFT interaction parameters:*)
k = 
$$\begin{pmatrix} 0 & 0.000491 T - 0.0669 & -0.001043 T + 0.49125 \\ 0.000491 T - 0.0669 & 0 & -0.0011847 T + 0.27616 \\ -0.001043 T + 0.49125 & -0.0011847 T + 0.27616 & 0 \end{pmatrix};$$

(*SAFT equations as described in Huang & Radosz 1991,
NB strange definition of ρ: (molecules/mL in stead of mol/mL)!!!:*)
vo = Table[ $\frac{1}{8} \left( v_{iij}^{\circ} \frac{1}{3} \left( 1 - c_0 \text{Exp}\left[\frac{-3 u_{iij}^{\circ}}{T}\right] \right) + v_{jjj}^{\circ} \frac{1}{3} \left( 1 - c_0 \text{Exp}\left[\frac{-3 u_{jjj}^{\circ}}{T}\right] \right) \right)^3$ , {i, nc}, {j, nc}];
u = Table[(1 - kiij)  $\sqrt{u_{iij}^{\circ} \left( 1 + \frac{c_{1iij}}{T} \right) u_{jjj}^{\circ} \left( 1 + \frac{c_{1jjj}}{T} \right)}$ , {i, nc}, {j, nc}];
```

Appendix 1

$$d = \text{Table}\left[\sqrt[3]{\frac{6 \tau v_{[i,j]}^{\circ}}{\pi n_{av}}}, \{i, nc\}\right];$$

$$fA = \sum_{i=1}^{nc} x[i] m_{[i]};$$

$$fB = \sum_{i=1}^{nc} x[i] m_{[i]} d_{[i]};$$

$$fC = \sum_{i=1}^{nc} x[i] m_{[i]} d_{[i]}^2; \zeta^2 = \frac{\pi}{6} \rho fC;$$

$$fD = \sum_{i=1}^{nc} x[i] m_{[i]} d_{[i]}^3; \zeta = \frac{\pi}{6} \rho fD;$$

$$fE = \sum_{i=1}^{nc} x[i] m_{[i]};$$

$$fF = \sum_{i=1}^{nc} \left(x[i] (1 - m_{[i]}) \text{Log}\left[\frac{1}{1 - \zeta} + \frac{3 d_{[i]}}{2} \frac{\zeta^2}{(1 - \zeta)^2} + \frac{d_{[i]}^2}{2} \frac{\zeta^2}{(1 - \zeta)^3}\right] \right);$$

$$fG = \left(\sum_{i=1}^{nc} \sum_{j=1}^{nc} (x[i] x[j] m_{[i]} m_{[j]} \left(\frac{U_{[i,j]}}{T}\right) v_{[i,j]}^{\circ}) \right) / \left(\sum_{i=1}^{nc} \left(\sum_{j=1}^{nc} (x[i] x[j] m_{[i]} m_{[j]} v_{[i,j]}^{\circ}) \right) \right);$$

fH = 0; (* association contribution *)

$$\text{ares} = R_{\text{gas}} T \left(\frac{3 \frac{fB fC}{fD} \zeta - \frac{fC^3}{fD^2}}{1 - \zeta} + \frac{fC^3}{(1 - \zeta)^2} + \left(\frac{fC^3}{fD^2} - fA \right) \text{Log}[1 - \zeta] + fF + fE \sum_{i=1}^4 \left(\sum_{j=1}^9 \left(D_{[i,j]} fG^i \left(\frac{\zeta}{\tau} \right)^j \right) \right) + fH \right);$$

(*S AFT c ompressibility, fugacity, gibbs-free energy, stability criterium volume roots:*)

$$Z = 1 + \rho \partial_{\rho} \left(\frac{\text{ares}}{R_{\text{gas}} T} \right);$$

$$\phi = \text{Table}\left[\text{Exp}\left[Z - 1 - \text{Log}[Z] + \frac{\text{ares}}{R_{\text{gas}} T} + D\left[\frac{\text{ares}}{R_{\text{gas}} T}, x[i]\right] - \sum_{j=1}^{nc} x[j] D\left[\frac{\text{ares}}{R_{\text{gas}} T}, x[j]\right]\right], \{i, nc - 1\}\right];$$

$$g = \text{ares} + R_{\text{gas}} T (Z - 1 - \text{Log}[Z]);$$

$$\text{st1} = D[Z \rho, \rho];$$

(*Lee Kesler Plöcker (LKP) EOS*)

(*LKP pure component parameters & interaction parameters:{CO2,ethene}:*)

$$Tc = \{304.1, 282.4\}; (*Kelvin*)$$

$$Pc = \{73.8, 50.4\}; (*bar*)$$

$$\omega = \{0.225, 0.089\};$$

$$Vc = (0.2905 - 0.085 \omega) \frac{R_{\text{gas}} Tc}{Pc}; (*cm^3/mol*)$$

$$\text{mw} = \{\text{mw1}, \text{mw2}\};$$

$$kLK = \begin{pmatrix} 1 & 0.957 \\ 0.957 & 1 \end{pmatrix};$$

$$ncLK = 2;$$

(*L KP constants:*)

$$\omega R = 0.3978;$$

$$b1 = \{0.1181193, 0.2026579\}; b2 = \{0.265728, 0.331511\}; b3 = \{0.154790, 0.027655\};$$

$$b4 = \{0.030323, 0.203488\}; c1 = \{0.0236744, 0.0313385\}; c2 = \{0.0186984, 0.0503618\};$$

$$c3 = \{0.0, 0.016901\}; c4 = \{0.042724, 0.041577\}; d1 = \{0.155488 \cdot 10^{-4}, 0.48736 \cdot 10^{-4}\};$$

Programs to calculate overall pressure as function of conversion in batch precipitation polymerizations

$d2 = \{0.623689 \cdot 10^{-4}, 0.0740336 \cdot 10^{-4}\}$; $\beta = \{0.65392, 1.226\}$; $\gamma = \{0.060167, 0.03754\}$;

(*LK P module for calculation of volume roots & fugacity coefficients:*)

LK := Module[{}; Tcij = Table[$\sqrt{T_{c[i]} T_{c[j]}}$ kLK_[i,j], {i, 1, nLK}, {j, 1, nLK}];

Vcij = Table[$\frac{1}{8} (V_{c[i]}^{\frac{1}{3}} + V_{c[j]}^{\frac{1}{3}})^3$, {i, 1, nLK}, {j, 1, nLK}];

Vcm = $\sum_{i=1}^{nLK} \sum_{j=1}^{nLK} xp2[i] xp2[j] Vcij_{[i,j]}$;

Tcm = $\frac{1}{Vcm^{1/4}} \sum_{i=1}^{nLK} \sum_{j=1}^{nLK} xp2[i] xp2[j] Vcij_{[i,j]}^{1/4} Tcij_{[i,j]}$;

$\omega m = \sum_{i=1}^{nLK} xp2[i] \omega_{[i]}$;

Zcm = 0.2905 - 0.085 ωm ;

Pcm = Zcm $\frac{R_{gas} Tcm}{Vcm}$;

Tred = $\frac{T}{Tcm}$;

Pred = $\frac{p}{Pcm}$;

bb = $b1 - \frac{b2}{Tred} - \frac{b3}{Tred^2} - \frac{b4}{Tred^3}$; cc = $c1 - \frac{c2}{Tred} + \frac{c3}{Tred^3}$; dd = $d1 + \frac{d2}{Tred}$;

f = $1 + \frac{bb}{Vred} + \frac{cc}{Vred^2} + \frac{dd}{Vred^5} + \frac{c4}{Tred^3 Vred^2} \left(\beta + \frac{\gamma}{Vred^2} \right) \text{Exp}\left[-\frac{\gamma}{Vred^2}\right] - \frac{Pred Vred}{Tred}$;

ee = $\frac{c4}{2 Tred^3 \gamma} \left(\beta + 1 - \left(\beta + 1 + \frac{\gamma}{Vred^2} \right) \text{Exp}\left[-\frac{\gamma}{Vred^2}\right] \right)$;

$\ln \phi = \frac{Pred Vred}{Tred} - 1 - \text{Log}\left[\frac{Pred Vred}{Tred}\right] + \frac{bb}{Vred} + \frac{cc}{2 Vred^2} + \frac{dd}{5 Vred^5} + ee$;

(*volume roots only valid when Tred > 1:*)

rootVred0 = Vred /. FindRoot[f_[1] = 0, {Vred, Tred/Pred}, MaxIterations → 100, AccuracyGoal → 12];

rootVredR = Vred /. FindRoot[f_[2] = 0, {Vred, Tred/Pred}, MaxIterations → 100, AccuracyGoal → 12];

dH = $-R_{gas} T \left(\frac{Pred Vred}{Tred} - 1 - \frac{b2 + 2 b3/Tred + 3 b4/Tred^2}{Tred Vred} - \frac{c2 - 3 c3/Tred^2}{2 Tred Vred^2} + \frac{d2}{5 Tred Vred^5} + 3 ee \right)$;

(* = H° - H*)

dH0 = dH_[1] /. Vred → rootVred0;

dHR = dH_[2] /. Vred → rootVredR;

dH1 = $\frac{1}{\omega R} (dHR - dH0)$;

dHm = dH0 + ωm dH1;

Z0 = $\frac{Pred \text{rootVred0}}{Tred}$;

Z1 = $\frac{Pred}{Tred \omega R} (\text{rootVredR} - \text{rootVred0})$;

Zm = Z0 + ωm Z1;

vol = $\frac{Zm R_{gas} T}{p}$; (*ml/mol*)

$\ln \phi_0 = \ln \phi_{[1]} /. Vred \rightarrow \text{rootVred0}$;

$\ln \phi_R = \ln \phi_{[2]} /. Vred \rightarrow \text{rootVredR}$;

Appendix I

$$\ln\phi_1 = \frac{1}{\omega R} (\ln\phi R - \ln\phi_0);$$

$$\ln\phi_m = \ln\phi_0 + \omega_m \ln\phi_1;$$

$$\ln\phi_i = \text{Table}[\ln\phi_m + \frac{dH_m}{T R_{\text{gas}} T_{\text{cm}}} \sum_{j=1}^{\text{ncLK}} x_{p2}[j] \left(\frac{1}{V_{\text{cm}}^{1/4}} \left(2 \sum_{l=1}^{\text{ncLK}} x_{p2}[l] \left((V_{\text{cij}[l,i]}^{1/4} T_{\text{cij}[l,i]} - V_{\text{cij}[l,i]}^{1/4} T_{\text{cij}[l,i]} \right) - \left(\frac{1}{4} V_{\text{cm}}^{-3/4} T_{\text{cm}} (V_{\text{cij}[l,i]} - V_{\text{cij}[l,i]}) \right) \right) \right) \right) + \frac{Z_m - 1}{P_{\text{cm}}} \sum_{j=1}^{\text{ncLK}} x_{p2}[j] \left(P_{\text{cm}} \left(-\frac{0.085 (\omega_{[ij]} - \omega_{[il]})}{Z_{\text{cm}}} + \frac{1}{T_{\text{cm}}} \frac{1}{V_{\text{cm}}^{1/4}} \left(2 \sum_{l=1}^{\text{ncLK}} x_{p2}[l] \left((V_{\text{cij}[l,i]}^{1/4} T_{\text{cij}[l,i]} - V_{\text{cij}[l,i]}^{1/4} T_{\text{cij}[l,i]} \right) - \left(\frac{1}{4} V_{\text{cm}}^{-3/4} T_{\text{cm}} (V_{\text{cij}[l,i]} - V_{\text{cij}[l,i]}) \right) \right) \right) - \frac{2}{V_{\text{cm}}} \sum_{l=1}^{\text{ncLK}} x_{p2}[l] (V_{\text{cij}[l,i]} - V_{\text{cij}[l,i]}) \right) \right) - \ln\phi_1 \sum_{j=1}^{\text{ncLK}} x_{p2}[j] (\omega_{[ij]} - \omega_{[il]}), \{i, \text{ncLK}\}; \{i\}]$$

(*end of LK P module*)

(*Calculating starting concentrations*)

$$x_{p2}[1] = \frac{x_{\text{wtfeed1}} / m_{w1}}{x_{\text{wtfeed1}} / m_{w1} + x_{\text{wtfeed2}} / m_{w2}};$$

$$x_{p2}[2] = \frac{x_{\text{wtfeed2}} / m_{w2}}{x_{\text{wtfeed1}} / m_{w1} + x_{\text{wtfeed2}} / m_{w2}}; \text{mecalc} = 0; \text{dummy} = p; p = \text{pstart};$$

$$\text{While}[(\text{massethene} - \text{mecalc})^2 > 10^{-6}, \text{LK}; \text{mecalc} = \frac{x_{p2}[2] m_{w2}}{\text{vol}} \text{vreactor};$$

$$x_{p2}[2] = x_{p2}[2] + 0.1 \frac{(\text{massethene} - \text{mecalc})}{\text{mecalc}}; x_{p2}[1] = 1 - x_{p2}[2];$$

$$x_{\text{wtfeed1}} = \frac{x_{p2}[1] m_{w1}}{x_{p2}[1] m_{w1} + x_{p2}[2] m_{w2}}; x_{\text{wtfeed2}} = 1 - x_{\text{wtfeed1}}; p = \text{dummy};$$

Print["done"];

WriteString[outputfile, "0\t", NumberForm[T, 5], "\t", NumberForm[pstart, 5], "\t-\t-\t",

NumberForm[xwtfeed2 100, 7], "\t-\t", NumberForm[\frac{1}{\text{vol}} (x_{p2}[1] m_{w1} + x_{p2}[2] m_{w2}), 5], "\t-\t-",

NumberForm[x_{p2}[1] \text{Exp}[\ln\phi_{i[1]}] pstart, 7], "\t", NumberForm[x_{p2}[2] \text{Exp}[\ln\phi_{i[2]}] pstart, 7], "\t-\t-\t"];

Print["0\t", NumberForm[T, 5], "\t", NumberForm[pstart, 5], "\t-\t-\t", NumberForm[xwtfeed2 100, 7],

"\t-\t", NumberForm[\frac{1}{\text{vol}} (x_{p2}[1] m_{w1} + x_{p2}[2] m_{w2}), 5], "\t-\t-\t-\t-\t"];

(*Phase equilibrium calculation as a function of conversion*)

damp = 55;

Do[volerror = 1; pold = p; vold1 = 1; pold1 = 0; vold2 = 1; pold2 = 0; Secant = False;

While[volerror² > 10⁻⁴, (*Total volume correct?*)

$$x_{\text{wt2}} = x_{\text{wtfeed2}} (1 - \text{conv} / 100);$$

$$x_{\text{wt3}} = x_{\text{wtfeed2}} \text{conv} / 100;$$

$$x_{\text{wt1}} = x_{\text{wtfeed1}};$$

$$z[1] = \frac{x_{\text{wt1}} / m_{w1}}{x_{\text{wt1}} / m_{w1} + x_{\text{wt2}} / m_{w2} + x_{\text{wt3}} / m_{w3}};$$

$$z[2] = \frac{x_{\text{wt2}} / m_{w2}}{x_{\text{wt1}} / m_{w1} + x_{\text{wt2}} / m_{w2} + x_{\text{wt3}} / m_{w3}};$$

$$z[3] = \frac{x_{\text{wt3}} / m_{w3}}{x_{\text{wt1}} / m_{w1} + x_{\text{wt2}} / m_{w2} + x_{\text{wt3}} / m_{w3}};$$

Programs to calculate overall pressure as function of conversion in batch precipitation polymerizations

```

ρp1 := Sort[Select[Select[ρ /. Solve[Z ρ / nav Rgas T = p /. {x → xp1}, ρ],
  (Im[#] == 0) && (0 < Re[#] <  $\frac{n_{av}}{\sum_{i=1}^{nc} m_{[i]} v_{[i]}^\circ x[i] /. \{x \rightarrow xp1\}}$ ) &],
  ((st1 /. {x → xp1, ρ → #}) > 0) &], ((g /. {x → xp1, ρ → #1}) < (g /. {x → xp1, ρ → #2})) &][[1]];
error = 1;
iter = 0;
While[error > 10-10, (*Chemical equilibrium?*)
  βroot = Select[βr /. Solve[ $\sum_{i=1}^{nc} \frac{z[i] (K[i] - 1)}{1 + \beta r (K[i] - 1)} = 0, \beta r, 0 < \beta r < 1$  &] ;
  Do[xp1[i] = z[i] / (1 + βroot (K[i] - 1)); xp2[i] = K[i] xp1[i], {i, nc}]; dummy1 = ρp1;
  φp1 = φ /. {x → xp1, ρ → dummy1}; LK; dummy2 = vol; φp2 = Exp[ln φi]; error = 0;
  Do[K[i] = K[i]  $\left(\frac{xp1[i] \phi p1_{[i]}}{xp2[i] \phi p2_{[i]}}\right)^{\frac{1}{d_{amp}}}$ ; error = error + Log[ $\frac{xp1[i] \phi p1_{[i]}^2}{xp2[i] \phi p2_{[i]}}$ ], {i, 1, nc - 1}];
  If[Mod[iter, 50] == 0, Print[NumberForm[conv, 0], "\t", NumberForm[T, 5], "\t",
    NumberForm[p, 5], "\t", NumberForm[ $\frac{xp1[1] mw1}{xp1[1] mw1 + xp1[2] mw2 + xp1[3] mw3}$  100, 7],
    "\t", NumberForm[ $\frac{xp1[2] mw2}{xp1[1] mw1 + xp1[2] mw2 + xp1[3] mw3}$  100, 7],
    "\t", NumberForm[ $\frac{xp2[2] mw2}{xp2[1] mw1 + xp2[2] mw2 + xp2[3] mw3}$  100, 7], "\t",
    NumberForm[ $\frac{dummy1}{n_{av}}$  (xp1[1] mw1 + xp1[2] mw2 + xp1[3] mw3), 5], "\t",
    NumberForm[ $\frac{1}{dummy2}$  (xp2[1] mw1 + xp2[2] mw2), 5], "\t", NumberForm[K[1], 8],
    "\t", NumberForm[K[2], 8], "\t", ScientificForm[error, 3]]; iter = iter + 1];
  vold2 = vold1; vold1 = volerror; volerror =  $\frac{massethene / 100 \text{ conv}}{dummy1 / n_{av} xp1[3] mw3} +$ 
 $\frac{massethene / 100 \text{ conv}}{dummy1 / n_{av} xp1[3] mw3} \frac{dummy1 / n_{av} \beta root}{1 - \beta root} dummy2 - vreactor$ ;
  Print[volerror]; If[(Sign[volerror] ≠ Sign[vold1]) && (pold2 ≠ 0), Secant = True];
  Print[Secant]; If[pold2 == 0, pold2 = pold1; pold1 = p; p = p + Sign[volerror] 0.001,
  If[Secant, If[Sign[volerror] = Sign[vold1], pold1 = pold2; vold1 = vold2];
  dummy = p; p = p -  $\frac{p - pold1}{volerror - vold1} volerror$ ; pold2 = pold1; pold1 = dummy];
  Print[pold1, "\t", pold2, "\t", vold1, "\t", vold2]; Print[NumberForm[conv, 0], "\t", NumberForm[T, 5],
  "\t", NumberForm[p, 5], "\t", NumberForm[ $\frac{xp1[1] mw1}{xp1[1] mw1 + xp1[2] mw2 + xp1[3] mw3}$  100, 7],
  "\t", NumberForm[ $\frac{xp1[2] mw2}{xp1[1] mw1 + xp1[2] mw2 + xp1[3] mw3}$  100, 7],
  "\t", NumberForm[ $\frac{xp2[2] mw2}{xp2[1] mw1 + xp2[2] mw2 + xp2[3] mw3}$  100, 7], "\t",
  NumberForm[ $\frac{dummy1}{n_{av}}$  (xp1[1] mw1 + xp1[2] mw2 + xp1[3] mw3), 5],
  "\t", NumberForm[ $\frac{1}{dummy2}$  (xp2[1] mw1 + xp2[2] mw2), 5], "\t",
  NumberForm[K[1], 8], "\t", NumberForm[K[2], 8], "\t", ScientificForm[error, 3]];
  (*Output*)
  WriteString[outputfile, NumberForm[conv, 0], "\t", NumberForm[T, 5], "\t",

```

Appendix 1

```

NumberForm[p, 5], "\t", NumberForm[\frac{xp1[1] mw1}{xp1[1] mw1 + xp1[2] mw2 + xp1[3] mw3} 100, 7],
"\t", NumberForm[\frac{xp1[2] mw2}{xp1[1] mw1 + xp1[2] mw2 + xp1[3] mw3} 100, 7],
"\t", NumberForm[\frac{xp2[2] mw2}{xp2[1] mw1 + xp2[2] mw2 + xp2[3] mw3} 100, 7], "\t",
NumberForm[\frac{dummy1}{n_{av}} (xp1[1] mw1 + xp1[2] mw2 + xp1[3] mw3), 5], "\t",
NumberForm[\frac{1}{dummy2} (xp2[1] mw1 + xp2[2] mw2), 5], "\t", NumberForm[K[1], 8],
"\t", NumberForm[K[2], 8], "\t", NumberForm[xp1[1] \phi_{11} p, 7],
"\t", NumberForm[xp1[2] \phi_{12} p, 7], "\t", FortranForm[error], "\n"];
p = p + dp; dp = p - pold, {conv, 10, 90, 10}];

```

Close[outputfile];

(*Fit polynome: pressure-conversion curve*)

inputfile = OpenRead[filename];

Read[inputfile, String]

Read[inputfile, String]

data = Array[1, {10, 2}];

Do[data[[i, 2]] = Read[inputfile, Real];

 Read[inputfile, Real]; data[[i, 1]] = Read[inputfile, Real]; Read[inputfile, String]

 , {i, 10}];

data

Close[inputfile];

ffit = Fit[data, {1, x, x², x³}, x];

outputfile = OpenAppend[filename];

WriteString[outputfile, "conversion = function[x]:\n"];

WriteString[outputfile, FortranForm[ffit], "\n"];

WriteString[outputfile, "conv\tp[bar]\tcalc_conv\n"]

Do[WriteString[outputfile, NumberForm[data[[i,2]], 0], "\t",

 NumberForm[data[[i,1]], 5], "\t", NumberForm[ffit /. x -> data[[i,1]], 5], "\n"], {i, 10}];

Close[outputfile];

Null

(*End of program SAFT-LKP*)

```
(*Mathematica 4.1 notebook file;
SAFT-PR model – simulation of polymerisation run 1;
assumption: polymer insoluble in supercritical phase*)
Off[Remove::"rmnsm"]
Remove["Global*"];
Off[General::"spell1"]
(*Output directory & filename:*)
SetDirectory["C:\windows\desktop"];
filename = "sim-run1-SAFT-PR-2b.txt";
outputfile = OpenWrite[filename, PageWidth → 200];
WriteString[outputfile, "Simulation of polymerisation of ethene in CO2, SAFT-PR version 2b\n"];
WriteString[outputfile, "conv\tT[K]\tp[bar]\tw\t%CO2\twt%
ethene1\twt%ethene2\rho1[g/ml]\rho2[g/ml]\tK1\tK2\tfCO2\tfE\terror\n"];
Print["conv\tT[K]\tp[bar]\tw\t%CO2\twt%ethene1\twt%ethene2\rho1[g/ml]\rho2[g/ml]\tK1\tK2\terror\n"];
(*constants:*)
mw1 = 44.01; mw2 = 28.05; mw3 = 51000; Rgas = 83.1439; nav = 6.02 1023;
(*initial polymerization conditions; pressure ,temperature, composition:*)
T = 313.15;
pstart = 207.2;(*initial pressure*)
p = 195.24;(*initial guess of pressure at 10 % conversion*)
vreactor = 536.0;(*mL*)
xwtfed1 = 0.8945; xwtfed2 = 0.1055; xwtfed3 = 0;(*initial guess feed composition*)
massethene = 3.006 mw2 10-3 vreactor;(*exact mass of ethene in reactor*)
dp = p - pstart;
K[1] = 1.7; K[2] = 0.31; K[3] = 0;(*i nitial guess distribution coeff., K[i]=y[i]/x[i]*)
(*pure component parameters & interaction parameter:*)
nc = 3;(*number of components, 1=CO2, 2=ethene, 3=polymer*)
vo = {13.578, 18.157, 21.618}; m = {1.417, 1.464, 0.034365 mw3};
c1 = {40, 10, 10}; uo = {216.08, 212.06, 469.86};
(*SAFT constants:*)
τ = 0.74048; c0 = 0.12;
Dij = 
$$\begin{pmatrix} -8.8043 & 4.164627 & -48.203555 & 140.4362 & -195.23339 & 113.515 & 0 & 0 & 0 \\ 2.9396 & -6.0865383 & 40.137956 & -76.230797 & -133.70055 & 860.25349 & -1535.3224 & 1221.4261 & -409.10539 \\ -2.8225 & 4.7600148 & 11.257177 & -66.382743 & 69.248785 & 0 & 0 & 0 & 0 \\ 0.34 & -3.1875014 & 12.231796 & -12.110681 & 0 & 0 & 0 & 0 & 0 \end{pmatrix};$$

(*SAFT interaction parameters:*)
k = 
$$\begin{pmatrix} 0 & 0.000491 T - 0.0669 & -0.001043 T + 0.49125 \\ 0.000491 T - 0.0669 & 0 & -0.0011847 T + 0.27616 \\ -0.001043 T + 0.49125 & -0.0011847 T + 0.27616 & 0 \end{pmatrix};$$

(*SAFT equations as described in Huang&Radosz 1991,
NB strange definition of ρ: (molecules/mL in stead of mol/mL)!!:*)
vo = Table[ $\frac{1}{8} \left( v_{ij}^{oo} \right)^{\frac{1}{3}} \left( 1 - c_0 \text{Exp}\left[ \frac{-3 u_{ij}^o}{T} \right] \right) + v_{ij}^{oo} \left( 1 - c_0 \text{Exp}\left[ \frac{-3 u_{ij}^o}{T} \right] \right)^{\frac{1}{3}}$ , {i, nc}, {j, nc}];
u = Table[(1 - k[i,j])  $\sqrt{u_{ij}^o \left( 1 + \frac{c_{1[ij]}}{T} \right) u_{ij}^o \left( 1 + \frac{c_{1[ij]}}{T} \right)}$ , {i, nc}, {j, nc}];
```

Appendix I

$$d = \text{Table}\left[\sqrt[3]{\frac{6 \tau v_{[i,j]}^{\circ}}{\pi n_{av}}}, \{i, nc\}\right];$$

$$fA = \sum_{i=1}^{nc} x[i] m_{[i]};$$

$$fB = \sum_{i=1}^{nc} x[i] m_{[i]} d_{[i]};$$

$$fC = \sum_{i=1}^{nc} x[i] m_{[i]} d_{[i]}^2; \zeta 2 = \frac{\pi}{6} \rho fC;$$

$$fD = \sum_{i=1}^{nc} x[i] m_{[i]} d_{[i]}^3; \zeta = \frac{\pi}{6} \rho fD;$$

$$fE = \sum_{i=1}^{nc} x[i] m_{[i]};$$

$$fF = \sum_{i=1}^{nc} \left(x[i] (1 - m_{[i]}) \text{Log}\left[\frac{1}{1 - \zeta} + \frac{3 d_{[i]}}{2} \frac{\zeta 2}{(1 - \zeta)^2} + \frac{d_{[i]}^2}{2} \frac{\zeta 2^2}{(1 - \zeta)^3}\right] \right);$$

$$fG = \left(\sum_{i=1}^{nc} \sum_{j=1}^{nc} (x[i] x[j] m_{[i]} m_{[j]} \left(\frac{u_{[i,j]}}{T}\right) v_{[i,j]}^{\circ}) \right) / \left(\sum_{i=1}^{nc} \left(\sum_{j=1}^{nc} (x[i] x[j] m_{[i]} m_{[j]} v_{[i,j]}^{\circ}) \right) \right);$$

fH = 0; (* association contribution *)

$$\text{ares} = R_{\text{gas}} T \left(\frac{3 \frac{fB fC}{fD} \zeta - \frac{fC^3}{fD^2}}{1 - \zeta} + \frac{fC^3}{(1 - \zeta)^2} + \left(\frac{fC^3}{fD^2} - fA \right) \text{Log}[1 - \zeta] + fF + fE \sum_{i=1}^4 \left(\sum_{j=1}^9 (D_{[i,j]} fG^j \left(\frac{\zeta}{\tau}\right)^j) \right) + fH \right);$$

(*SAFT compressibility, fugacity, gibbs-free energy, stability criterium volume roots:*)

$$Z = 1 + \rho \partial_{\rho} \left(\frac{\text{ares}}{R_{\text{gas}} T} \right);$$

$$\phi = \text{Table}\left[\text{Exp}[Z - 1 - \text{Log}[Z]] + \frac{\text{ares}}{R_{\text{gas}} T} + D\left[\frac{\text{ares}}{R_{\text{gas}} T}, x[i]\right] - \sum_{j=1}^{nc} x[j] D\left[\frac{\text{ares}}{R_{\text{gas}} T}, x[j]\right], \{i, nc - 1\}\right];$$

$$g = \text{ares} + R_{\text{gas}} T (Z - 1 - \text{Log}[Z]);$$

$$\text{st1} = D[Z, \rho];$$

(*Cubic equation of state: Peng Robinson(u=2, w=-1)*)

$$Tc = \{304.1, 282.4\}; (*Kelvin*)$$

$$Pc = \{73.8, 50.4\}; (*bar*)$$

$$\omega = \{0.225, 0.089\};$$

$$k12 = 0.0541;$$

$$\text{mw} = \{\text{mw1}, \text{mw2}\};$$

$$kPR = \begin{pmatrix} 0 & k12 \\ k12 & 0 \end{pmatrix};$$

$$\text{mPR} = \text{Table}[0.37464 + 1.54226 \omega_{[i]} - 0.26992 \omega_{[i]}^2, \{i, nc - 1\}];$$

$$a = \text{Table}\left[\frac{0.45724 R_{\text{gas}}^2 Tc_{[i]}^2}{Pc_{[i]}} \left(1 + \text{mPR}_{[i]} \left(1 - \sqrt{\frac{T}{Tc_{[i]}}} \right) \right)^2, \{i, nc - 1\}\right];$$

$$b = \text{Table}\left[0.07780 \frac{R_{\text{gas}} Tc_{[i]}}{Pc_{[i]}}, \{i, nc - 1\}\right];$$

Programs to calculate overall pressure as function of conversion in batch precipitation polymerizations

$$am = \sum_{i=1}^{nc-1} \sum_{j=1}^{nc-1} x[i] x[j] \sqrt{a_{[i]} a_{[j]}} (1 - kPR_{[i,j]});$$

$$bm = \sum_{i=1}^{nc-1} x[i] b_{[i]};$$

$$As = \frac{am \text{ pset}}{R_{\text{gas}}^2 T^2}; Bs = \frac{bm \text{ pset}}{R_{\text{gas}} T};$$

$$ZPR = \frac{\text{pset } v}{R_{\text{gas}} T};$$

$$\delta = \text{Table}\left[\frac{2\sqrt{a_{[i]}}}{am} \sum_{j=1}^{nc-1} x[j] \sqrt{a_{[j]}} (1 - kPR_{[i,j]}), \{i, nc - 1\}\right];$$

$$PPR = \frac{R_{\text{gas}} T}{v - bm} - \frac{am}{v^2 + uEOS bm v + wEOS bm^2}; uEOS = 2; wEOS = -1;$$

$$\phi PR = \text{Table}\left[\text{Exp}\left[\frac{b_{[i]}}{bm} (ZPR - 1) - \text{Log}[ZPR - Bs] +\right.\right.$$

$$\left.\frac{As}{Bs \sqrt{uEOS^2 - 4 wEOS}} \left(\frac{b_{[i]}}{bm} - \delta_{[i]}\right) \text{Log}\left[\frac{2 ZPR + Bs (uEOS + \sqrt{uEOS^2 - 4 wEOS})}{2 ZPR + Bs (uEOS - \sqrt{uEOS^2 - 4 wEOS})}\right]\right], \{i, nc - 1\};$$

$$gPR = \frac{am}{bm \sqrt{uEOS^2 - 4 wEOS}} \text{Log}\left[\frac{2 ZPR + Bs (uEOS - \sqrt{uEOS^2 - 4 wEOS})}{2 ZPR + Bs (uEOS + \sqrt{uEOS^2 - 4 wEOS})}\right] -$$

$$R_{\text{gas}} T \text{Log}\left[\frac{ZPR - Bs}{ZPR}\right] - R_{\text{gas}} T \text{Log}\left[\frac{1}{\text{pset}}\right] + RT (Z - 1);$$

st1PR := ∂_v PPR;

(*Calculating starting concentrations:*)

$$xp[1] = \frac{xw\text{feed}1 / mw1}{xw\text{feed}1 / mw1 + xw\text{feed}2 / mw2}; xp[2] = \frac{xw\text{feed}2 / mw2}{xw\text{feed}1 / mw1 + xw\text{feed}2 / mw2}; \text{mecalc} = 0;$$

While[(massethene - mecalc)² > 10⁻⁶,

vp = Sort[Select[Select[v /. Solve[PPR == pstart /. x → xp, v], (Im[#] == 0) &],
(st1PR /. {x → xp, v → #}) < 0] &],

((gPR /. {x → xp, v → #1, pset → pstart}) < (gPR /. {x → xp, v → #2, pset → pstart})) &][[1]];

$$\text{mecalc} = \frac{xp[2] mw2}{vp} v_{\text{reactor}}; xp[2] = xp[2] + 0.1 \frac{(\text{massethene} - \text{mecalc})}{\text{mecalc}}; xp[1] = 1 - xp[2];$$

$$xw\text{feed}1 = \frac{xp[1] mw1}{xp[1] mw1 + xp[2] mw2}; xw\text{feed}2 = 1 - xw\text{feed}1;$$

dummy ϕ = ϕPR /. {x → xp, v → vp, pset → pstart};

WriteString[outputfile, "0\t", NumberForm[T, 5], "\t", NumberForm[pstart, 5], "\t-\t-\t",

NumberForm[xwfeed2 100, 7], "\t-\t", NumberForm[\frac{1}{vp} (xp[1] mw1 + xp[2] mw2), 5], "\t-\t-\t",

NumberForm[xp[1] dummy $\phi_{[1]}$ pstart, 7], "\t", NumberForm[xp[2] dummy $\phi_{[2]}$ pstart, 7], "\t-\t-\t";

Print["0\t", NumberForm[T, 5], "\t", NumberForm[pstart, 5], "\t-\t-\t", NumberForm[xwfeed2 100, 7],

"\t-\t", NumberForm[\frac{1}{vp} (xp[1] mw1 + xp[2] mw2), 5], "\t-\t-\t-\t-\t";

(*Phase equilibrium calculation as a function of conversion*)

damp = 55;

Do[volerror = 1; pold = p; vold1 = 1; pold1 = 0; vold2 = 1; pold2 = 0; Secant = False;

Appendix I

```

While[volerror2 > 10-4, (*Total volume correct?*)
  xwt2 = xwtfeed2 (1 - conv / 100);
  xwt3 = xwtfeed2 conv / 100;
  xwt1 = xwtfeed1;
  z[1] =  $\frac{xwt1 / mw1}{xwt1 / mw1 + xwt2 / mw2 + xwt3 / mw3}$ ;
  z[2] =  $\frac{xwt2 / mw2}{xwt1 / mw1 + xwt2 / mw2 + xwt3 / mw3}$ ;
  z[3] =  $\frac{xwt3 / mw3}{xwt1 / mw1 + xwt2 / mw2 + xwt3 / mw3}$ ;
  vp2 := Sort[Select[
    Select[v /. Solve[PPR == p /. x → xp2, v], (Im[#] == 0) &], ((st1PR /. {x → xp2, v → #}) < 0) &],
    ((gPR /. {x → xp2, v → #1, pset → p}) < (gPR /. {x → xp2, v → #2, pset → p})) &][[1]];
  pp1 := Sort[Select[Select[ρ /. Solve[Z ρ / nav Rgas T = p /. {x → xp1}, ρ],
    ((Im[#] == 0) && (0 < Re[#] <  $\frac{n_{av}}{\sum_{i=1}^{nc} m_{[i]} v_{[i]}^\circ x[i] /. {x \rightarrow xp1}$ )} &)],
    ((st1 /. {x → xp1, ρ → #}) > 0) &], ((g /. {x → xp1, ρ → #1}) < (g /. {x → xp1, ρ → #2})) &][[1]];
  error = 1;
  iter = 0;
  While[error > 10-10, (*Chemical equilibrium?*)
    βroot = Select[β /. Solve[ $\sum_{i=1}^{nc} \frac{z[i] (K[i] - 1)}{1 + \beta (K[i] - 1)} = 0, \beta], 0 < \#1 < 1 \& ]$  ;
    Do[xp1[i] = z[i] / (1 + βroot (K[i] - 1)); xp2[i] = K[i] xp1[i], {i, nc}]; dummy1 = pp1;
    φp1 = φ /. {x → xp1, ρ → dummy1}; dummy2 = vp2; φp2 = φPR /. {x → xp2, v → dummy2, pset → p};
    error = 0; Do[K[i] = K[i]  $\left(\frac{xp1[i] \phi p1_{[i]}}{xp2[i] \phi p2_{[i]}}\right)^{\frac{1}{\alpha_{amp}}}$ ; error = error + Log[ $\frac{xp1[i] \phi p1_{[i]}^2}{xp2[i] \phi p2_{[i]}}$ ], {i, 1, nc - 1}];
    If[Mod[iter, 50] = 0, Print[NumberForm[conv, 0], "\t", NumberForm[T, 5], "\t",
      NumberForm[p, 5], "\t", NumberForm[ $\frac{xp1[1] mw1}{xp1[1] mw1 + xp1[2] mw2 + xp1[3] mw3}$  100, 7],
      "\t", NumberForm[ $\frac{xp1[2] mw2}{xp1[1] mw1 + xp1[2] mw2 + xp1[3] mw3}$  100, 7],
      "\t", NumberForm[ $\frac{xp2[2] mw2}{xp2[1] mw1 + xp2[2] mw2 + xp2[3] mw3}$  100, 7], "\t",
      NumberForm[ $\frac{dummy1}{n_{av}}$  (xp1[1] mw1 + xp1[2] mw2 + xp1[3] mw3), 5], "\t",
      NumberForm[ $\frac{1}{dummy2}$  (xp2[1] mw1 + xp2[2] mw2), 5], "\t", NumberForm[K[1], 8],
      "\t", NumberForm[K[2], 8], "\t", ScientificForm[error, 3]]]; iter = iter + 1];
    vold2 = vold1; vold1 = volerror; volerror =  $\frac{massethene / 100 \text{ conv}}{dummy1 / n_{av} xp1[3] mw3} +$ 
       $\frac{massethene / 100 \text{ conv}}{dummy1 / n_{av} xp1[3] mw3} \frac{dummy1 / n_{av}}{1 - \beta root} dummy2 - vreactor$ ;
    Print[volerror]; If[(Sign[volerror] ≠ Sign[vold1]) && (pold2 ≠ 0), Secant = True];
    Print[Secant]; If[pold2 = 0, pold2 = vold1; pold1 = p; p = p + Sign[volerror] 0.001,
      If[Secant, If[Sign[volerror] = Sign[vold1], pold1 = pold2; vold1 = vold2]];
    dummy = p; p = p -  $\frac{p - pold1}{volerror - vold1}$  volerror; pold2 = vold1; pold1 = dummy];
    Print[pold1, "\t", pold2, "\t", vold1, "\t", vold2]; Print[NumberForm[conv, 0], "\t", NumberForm[T, 5],

```

Programs to calculate overall pressure as function of conversion in batch precipitation polymerizations

```

\t", NumberForm[p, 5], "\t", NumberForm[\frac{xp1[1] mw1}{xp1[1] mw1 + xp1[2] mw2 + xp1[3] mw3} 100, 7],
\t", NumberForm[\frac{xp1[2] mw2}{xp1[1] mw1 + xp1[2] mw2 + xp1[3] mw3} 100, 7],
\t", NumberForm[\frac{xp2[2] mw2}{xp2[1] mw1 + xp2[2] mw2 + xp2[3] mw3} 100, 7], "\t",
NumberForm[\frac{dummy1}{n_{av}} (xp1[1] mw1 + xp1[2] mw2 + xp1[3] mw3), 5],
\t", NumberForm[\frac{1}{dummy2} (xp2[1] mw1 + xp2[2] mw2), 5], "\t",
NumberForm[K[1], 8], "\t", NumberForm[K[2], 8], "\t", ScientificForm[error, 3]]];
(*Output*)
WriteString[outputfile, NumberForm[conv, 0], "\t", NumberForm[T, 5], "\t",
NumberForm[p, 5], "\t", NumberForm[\frac{xp1[1] mw1}{xp1[1] mw1 + xp1[2] mw2 + xp1[3] mw3} 100, 7],
\t", NumberForm[\frac{xp1[2] mw2}{xp1[1] mw1 + xp1[2] mw2 + xp1[3] mw3} 100, 7],
\t", NumberForm[\frac{xp2[2] mw2}{xp2[1] mw1 + xp2[2] mw2 + xp2[3] mw3} 100, 7], "\t",
NumberForm[\frac{dummy1}{n_{av}} (xp1[1] mw1 + xp1[2] mw2 + xp1[3] mw3), 5], "\t",
NumberForm[\frac{1}{dummy2} (xp2[1] mw1 + xp2[2] mw2), 5], "\t", NumberForm[K[1], 8],
\t", NumberForm[K[2], 8], "\t", NumberForm[xp1[1] \phi p_{11} p, 7],
\t", NumberForm[xp1[2] \phi p_{12} p, 7], "\t", FortranForm[error], "\n"];
p = p + dp; dp = p - pold, {conv, 10, 90, 10}];

```

Close[outputfile];

*(*Fit polynome: pressure–conversion curve*)*

inputfile = OpenRead[filename];

Read[inputfile, String]

Read[inputfile, String]

data = Array[1, {10, 2}];

Do[data[[i, 2]] = Read[inputfile, Real];

Read[inputfile, Real]; data[[i, 1]] = Read[inputfile, Real]; Read[inputfile, String], {i, 10}];

data

Close[inputfile];

ffit = Fit[data, {1, x, x², x³}, x];

outputfile = OpenAppend[filename];

WriteString[outputfile, "conversion = function[x]:\n"];

WriteString[outputfile, FortranForm[ffit], "\n"];

WriteString[outputfile, "conv\tp[bar]\tcalc_conv\n"];

Do[WriteString[outputfile, NumberForm[data[[i, 2]], 0], "\t",

NumberForm[data[[i, 1]], 5], "\t", NumberForm[ffit /. x -> data[[i, 1]], 5], "\n"], {i, 10}];

Close[outputfile];

*(*End of program SAFT–PR*)*

Appendix 2: Program for calculation of sorption and swelling of polymers.

(*Program calculates sorption in and swelling of polymers by mixtures of CO₂ and ethylene using either SAFT or a hybrid SAFT-LKP model

For use with other polymer-gas systems:

- adjust pure component parameters
- adjust binary interaction parameters
- Initial (guess) values for phase compositions
- when calculation does not converge:

carefully check parameters and initial guesses or increase value for damp

NB assumption: polymer does not dissolve in the gas phase*)

(*prevent annoying warning messages:*)

Off[Remove::"rmnsm"]; Remove["Global *"]; Off[General::"spell"]; Off[General::"spell1"];

(*Set directory for the results file *)

SetDirectory["C:\windows\desktop"];

outputfile = OpenWrite["output.txt", PageWidth -> 200];

(*Input:*)

model = 2; (*1=SAFT, 2=SAFT-LKP*)

damp = 1; (*default=1, equilibrium calculation converges slower and more stable at higher values*)

outfreq = 10; (*default=10: every x iterations is printed on screen; set to 1 to check convergence*)

kCO2PEP = 0.043; (*CO2-PEP binary interaction parameter for SAFT*)

T = 323.15; (*Temperature*)

pstart = 10; pend = 200; pstep = 10; (*Pressure range; first, last and stepsize, respectively*)

modelName = {"SAFT", "SAFT-LKP"};

Print["Model used for calculations: ", modelName[model]];

WriteString[outputfile, "Model used for calculations: ", modelName[model], "\n"];

WriteString[outputfile, "Binary interaction parameter CO2-PEP: ", kCO2PEP, "\n"];

WriteString[outputfile, "T[K]\tp[bar]\tw%CO2\tw%ethene\rho1[g/ml]\rho2[g/ml]\tSwelling[%]\terror\n"];

Print["T[K]\tp[bar]\tw%CO2\tw%ethene\rho1[g/ml]\rho2[g/ml]\tSwelling[%]\terror\n"];

(*SAFT:*)

(*Pure component SAFT parameters:*)

nc = 3; (*number of components, 1=CO₂, 2=ethylene, 3=polymer*)

mw1 = 44.01; mw2 = 28.05; mw3 = 51000;

v^o = {13.578, 18.157, 21.618}; m = {1.417, 1.464, 0.034365 mw3}; c₁ = {40, 10, 10}; u^o = {216.08, 212.06, 469.86};

(*SAFT constants:*)

τ = 0.74048; R_{gas} = 83.1439; c₀ = 0.12; n_{av} = 6.02 10²³;

$$D_{ij} = \begin{pmatrix} -8.8043 & 4.164627 & -48.203555 & 140.4362 & -195.23339 & 113.515 & 0 & 0 & 0 \\ 2.9396 & -6.0865383 & 40.137956 & -76.230797 & -133.70055 & 860.25349 & -1535.3224 & 1221.4261 & -409.10539 \\ -2.8225 & 4.7600148 & 11.257177 & -66.382743 & 69.248785 & 0 & 0 & 0 & 0 \\ 0.34 & -3.1875014 & 12.231796 & -12.110681 & 0 & 0 & 0 & 0 & 0 \end{pmatrix};$$

(*Binary interaction parameters for SAFT:*)

$$k = \begin{pmatrix} 0 & 0.000491 T - 0.0669 & kCO2PEP \\ 0.000491 T - 0.0669 & 0 & -0.0011847 T + 0.27616 \\ kCO2PEP & -0.0011847 T + 0.27616 & 0 \end{pmatrix};$$

(*SAFT equations as described in Huang & Radosz 1991,

NB strange definition of ρ: (molecules/mL in stead of mol/mL)!!!*)

$$v^o = \text{Table}\left[\frac{1}{8} \left(v_{i,ij}^{o,ij} \frac{1}{3} \left(1 - c_0 \text{Exp}\left[\frac{-3 u_{i,ij}^o}{T} \right] \right) + v_{j,ij}^{o,ij} \frac{1}{3} \left(1 - c_0 \text{Exp}\left[\frac{-3 u_{j,ij}^o}{T} \right] \right) \right)^{1/3}, \{i, nc\}, \{j, nc\}\right];$$

$$u = \text{Table}\left[\left(1 - k_{i,ij} \right) \sqrt{\left(u_{i,ij}^o \left(1 + \frac{c_{1,ij}}{T} \right) \right) u_{j,ij}^o \left(1 + \frac{c_{1,ij}}{T} \right)}, \{i, nc\}, \{j, nc\}\right];$$

$$d = \text{Table}\left[\sqrt[3]{\frac{6 \tau v_{i,ij}^o}{\pi n_{av}}}, \{i, nc\}\right];$$

$$fA = \sum_{i=1}^{nc} x[i] m_{[ij]};$$

$$fB = \sum_{i=1}^{nc} x[i] m_{[ij]} d_{[ij]};$$

Appendix 2

$$fC = \sum_{i=1}^{nc} x[i] m_{[i]} d_{[i]}^2; \zeta^2 = \frac{\pi}{6} \rho fC;$$

$$fD = \sum_{i=1}^{nc} x[i] m_{[i]} d_{[i]}^3; \zeta = \frac{\pi}{6} \rho fD;$$

$$fE = \sum_{i=1}^{nc} x[i] m_{[i]};$$

$$fF = \sum_{i=1}^{nc} \left(x[i] (1 - m_{[i]}) \text{Log} \left[\frac{1}{1 - \zeta} + \frac{3 d_{[i]}}{2} \frac{\zeta^2}{(1 - \zeta)^2} + \frac{d_{[i]}^2}{2} \frac{\zeta^2}{(1 - \zeta)^3} \right] \right);$$

$$fG = \left(\sum_{i=1}^{nc} \sum_{j=1}^{nc} \left(x[i] x[j] m_{[i]} m_{[j]} \left(\frac{u_{[i,j]}}{T} \right) v_{[i,j]} \right) \right) / \left(\sum_{i=1}^{nc} \left(\sum_{j=1}^{nc} x[j] m_{[j]} v_{[i,j]} \right) \right);$$

$$fH = 0; (* \text{ association contribution} *)$$

$$\text{ares} = R_{\text{gas}} T \left(\frac{3 \frac{fB fC}{fD} \zeta - \frac{fC^3}{fD^2}}{1 - \zeta} + \frac{fC^3}{(1 - \zeta)^2} + \left(\frac{fC^3}{fD^2} - fA \right) \text{Log}[1 - \zeta] + fF + fE \sum_{i=1}^4 \left(\sum_{j=1}^9 D_{[i,j]} fG^j \left(\frac{\zeta}{\tau} \right)^j \right) + fH \right);$$

(*Compressibility, fugacity, gibbs-free energy, stability criterium for volume roots(st1):*)

$$Z = 1 + \rho \partial_{\rho} \left(\frac{\text{ares}}{R_{\text{gas}} T} \right);$$

$$\phi = \text{Table}[\text{Exp}[Z - 1 - \text{Log}[Z]] + \frac{\text{ares}}{R_{\text{gas}} T} + D \left[\frac{\text{ares}}{R_{\text{gas}} T}, x[i] \right] - \sum_{j=1}^{nc} x[j] D \left[\frac{\text{ares}}{R_{\text{gas}} T}, x[j] \right]], \{i, nc - 1\}];$$

$$g = \text{ares} + R_{\text{gas}} T (Z - 1 - \text{Log}[Z]);$$

$$\text{st1} = D[Z, \rho];$$

(*Lee Kesler Plöcker EOS*)

(*Pure component LKP parameters:*)

$$Tc = \{304.1, 282.4\}; (*\text{Kelvin}*)$$

$$Pc = \{73.8, 50.4\}; (*\text{bar}*)$$

$$Vc = \{93.9, 130.4\}; (*\text{cm}^3/\text{mol}*)$$

$$\omega = \{0.225, 0.089\};$$

$$\omega R = 0.3978;$$

$$\text{mw} = \{\text{mw1}, \text{mw2}, \text{mw3}\};$$

$$\text{kLK} = \begin{pmatrix} 1 & 0.957 \\ 0.957 & 1 \end{pmatrix};$$

$$\text{ncLK} = 2;$$

(*Lee Kesler constants:*)

$$b1 = \{0.1181193, 0.2026579\}; b2 = \{0.265728, 0.331511\}; b3 = \{0.154790, 0.027655\}; b4 = \{0.030323, 0.203488\};$$

$$c1 = \{0.0236744, 0.0313385\}; c2 = \{0.0186984, 0.0503618\}; c3 = \{0.0, 0.016901\}; c4 = \{0.042724, 0.041577\};$$

$$d1 = \{0.155488 \cdot 10^{-4}, 0.48736 \cdot 10^{-4}\}; d2 = \{0.623689 \cdot 10^{-4}, 0.0740336 \cdot 10^{-4}\}; \beta = \{0.65392, 1.226\}; \gamma = \{0.060167, 0.03754\};$$

(*Lee Kesler module for calculation of ln(ϕ):*)

$$\text{LK} := \text{Module}[\{\}, \text{Tclj} = \text{Table}[\sqrt{Tc_{[i]} Tc_{[j]}} \text{kLK}_{[i,j]}, \{i, 1, \text{ncLK}\}, \{j, 1, \text{ncLK}\}];$$

$$\text{Vcij} = \text{Table} \left[\frac{1}{8} \left(Vc_{[i]}^{\frac{1}{3}} + Vc_{[j]}^{\frac{1}{3}} \right)^3, \{i, 1, \text{ncLK}\}, \{j, 1, \text{ncLK}\} \right];$$

$$\text{Vcm} = \sum_{i=1}^{\text{ncLK}} \sum_{j=1}^{\text{ncLK}} \text{xp2}[i] \text{xp2}[j] \text{Vcij}_{[i,j]};$$

$$\text{Tcm} = \frac{1}{\text{Vcm}^{1/4}} \sum_{i=1}^{\text{ncLK}} \sum_{j=1}^{\text{ncLK}} \text{xp2}[i] \text{xp2}[j] \text{Vcij}_{[i,j]}^{1/4} \text{Tclj}_{[i,j]};$$

$$\omega m = \sum_{i=1}^{\text{ncLK}} \text{xp2}[i] \omega_{[i]};$$

$$\text{Zcm} = 0.2905 - 0.085 \omega m;$$

$$\text{Pcm} = \text{Zcm} \frac{R_{\text{gas}} \text{Tcm}}{\text{Vcm}};$$

$$\text{Tred} = \frac{T}{\text{Tcm}};$$

$$\text{Pred} = \frac{p}{P_{cm}};$$

$$\text{bb} = b1 - \frac{b2}{\text{Tred}} - \frac{b3}{\text{Tred}^2} - \frac{b4}{\text{Tred}^3}; \text{cc} = c1 - \frac{c2}{\text{Tred}} + \frac{c3}{\text{Tred}^3}; \text{dd} = d1 + \frac{d2}{\text{Tred}};$$

$$f = 1 + \frac{\text{bb}}{\text{Vred}} + \frac{\text{cc}}{\text{Vred}^2} + \frac{\text{dd}}{\text{Vred}^5} + \frac{c4}{\text{Tred}^3 \text{Vred}^2} \left(\beta + \frac{\gamma}{\text{Vred}^2} \right) \text{Exp} \left[-\frac{\gamma}{\text{Vred}^2} \right] - \frac{\text{Pred Vred}}{\text{Tred}};$$

$$\text{ee} = \frac{c4}{2 \text{Tred}^3 \gamma} \left(\beta + 1 - \left(\beta + 1 + \frac{\gamma}{\text{Vred}^2} \right) \text{Exp} \left[-\frac{\gamma}{\text{Vred}^2} \right] \right);$$

$$\ln \phi = \frac{\text{Pred Vred}}{\text{Tred}} - 1 - \text{Log} \left[\frac{\text{Pred Vred}}{\text{Tred}} \right] + \frac{\text{bb}}{\text{Vred}} + \frac{\text{cc}}{2 \text{Vred}^2} + \frac{\text{dd}}{5 \text{Vred}^5} + \text{ee};$$

(*Volume roots always valid when Tred>1 (supercritical region)

When Tred<1 wrong volume root may be found:*)

If[Tred < 1, Print["Warning: Tred<1 ! Possibly wrong volume roots!"]];

rootVred0 = Vred /. FindRoot[f_{[1]} = 0, {Vred, Tred/Pred}, MaxIterations -> 100, AccuracyGoal -> 12];

rootVredR = Vred /. FindRoot[f_{[2]} = 0, {Vred, Tred/Pred}, MaxIterations -> 100, AccuracyGoal -> 12];

$$dH = -R_{\text{gas}} T \left(\frac{\text{Pred Vred}}{\text{Tred}} - 1 - \left(b2 + \frac{2 b3}{\text{Tred}} + \frac{3 b4}{\text{Tred}^2} \right) / (\text{Tred Vred}) - \frac{c2 - 3 c3 / \text{Tred}^2}{2 \text{Tred Vred}^2} + \frac{d2}{5 \text{Tred Vred}^5} + 3 \text{ee} \right); (* = H^{\circ} - H^*)$$

$$dH0 = dH_{[1]} /. \text{Vred} \rightarrow \text{rootVred0};$$

$$dHR = dH_{[2]} /. \text{Vred} \rightarrow \text{rootVredR};$$

$$dH1 = \frac{1}{\omega R} (dHR - dH0);$$

$$dHm = dH0 + \omega m dH1;$$

$$Z0 = \frac{\text{Pred rootVred0}}{\text{Tred}};$$

$$Z1 = \frac{\text{Pred}}{\text{Tred} \omega R} (\text{rootVredR} - \text{rootVred0});$$

$$Zm = Z0 + \omega m Z1;$$

$$\text{vol} = \frac{Zm R_{\text{gas}} T}{p}; (*\text{ml/mol}^*)$$

$$\ln \phi 0 = \ln \phi_{[1]} /. \text{Vred} \rightarrow \text{rootVred0};$$

$$\ln \phi R = \ln \phi_{[2]} /. \text{Vred} \rightarrow \text{rootVredR};$$

$$\ln \phi 1 = \frac{1}{\omega R} (\ln \phi R - \ln \phi 0);$$

$$\ln \phi m = \ln \phi 0 + \omega m \ln \phi 1;$$

$$\ln \phi i = \text{Table}[\ln \phi m +$$

$$\frac{dHm}{T R_{\text{gas}} T_{cm}} \sum_{j=1}^{\text{ncLK}} x_{p2}[j] \left(\frac{1}{V_{cm}^{1/4}} \left(2 \sum_{l=1}^{\text{ncLK}} x_{p2}[l] \left((V_{cjl}[l,j])^{1/4} T_{cjl}[l,j] - V_{cjl}[l,j]^{1/4} T_{cjl}[l,j] \right) - \left(\frac{1}{4} V_{cm}^{-3/4} T_{cm} (V_{cjl}[l,j] - V_{cjl}[l,j]) \right) \right) \right) +$$

$$\frac{Zm - 1}{P_{cm}} \sum_{j=1}^{\text{ncLK}} x_{p2}[j] \left(P_{cm} \left(-\frac{1}{Z_{cm}} (0.085 (\omega_{[j]} - \omega_{[i]})) +$$

$$\frac{1}{T_{cm}} \frac{1}{V_{cm}^{1/4}} \left(2 \sum_{l=1}^{\text{ncLK}} x_{p2}[l] \left((V_{cjl}[l,j])^{1/4} T_{cjl}[l,j] - V_{cjl}[l,j]^{1/4} T_{cjl}[l,j] \right) - \left(\frac{1}{4} V_{cm}^{-3/4} T_{cm} (V_{cjl}[l,j] - V_{cjl}[l,j]) \right) \right) -$$

$$\frac{2}{V_{cm}} \sum_{l=1}^{\text{ncLK}} x_{p2}[l] (V_{cjl}[l,j] - V_{cjl}[l,j]) \right) - \ln \phi 1 \sum_{j=1}^{\text{ncLK}} x_{p2}[j] (\omega_{[j]} - \omega_{[i]}), \{i, \text{ncLK}\}; \{i\}$$

(* (initial guess) compositions for both phases; 1=CO2, 2=ethene, 3=polymer:*)

(*Gas phase:*)

$$\text{xwtgas1} = 1; \text{xwtgas2} = 0;$$

$$x_{p2}[1] = \text{xwtgas1} / \text{mw1} / (\text{xwtgas1} / \text{mw1} + \text{xwtgas2} / \text{mw2});$$

$$x_{p2}[2] = \text{xwtgas2} / \text{mw2} / (\text{xwtgas1} / \text{mw1} + \text{xwtgas2} / \text{mw2}); x_{p2}[3] = 0;$$

(*Swollen polymer phase:*)

$$\text{xwt}[1] = 0.033; \text{xwt}[2] = 0; \text{xwt}[3] = 1 - \text{xwt}[1] - \text{xwt}[2];$$

(*Swelling equilibrium calculation*)

```

ρpolymer = Sort[Select[Select[ρ /. Solve[Z ρ / nav Rgas T = 1 /. {x[1] → 0, x[2] → 0, x[3] → 1}, ρ],
  ((Im[#] == 0) && (0 < Re[#] <  $\frac{n_{av}}{m_{[3]} v_{[3,3]}})$ ) &], ((st1 /. {x[1] → 0, x[2] → 0, x[3] → 1, ρ → #}) > 0) &],
  ((g /. {x[1] → 0, x[2] → 0, x[3] → 1, ρ → #1}) < (g /. {x[1] → 0, x[2] → 0, x[3] → 1, ρ → #2})) &][[1]];
Do[If[model = 1, dummy2 = Sort[Select[Select[ρ /. Solve[Z ρ / nav Rgas T = p /. {x → xp2}, ρ],
  ((Im[#] == 0) && (0 < Re[#] < nav /  $(\sum_{i=1}^{nc} m_{[i]} v_{[i,i]}^0 x[i] /. {x \rightarrow xp2})$ )) &], ((st1 /. {x \rightarrow xp2, ρ \rightarrow #}) > 0) &],
  ((g /. {x \rightarrow xp2, ρ \rightarrow #1}) < (g /. {x \rightarrow xp2, ρ \rightarrow #2})) &][[1]]; φp2 = φ /. {x \rightarrow xp2, ρ \rightarrow dummy2}];
If[model = 2, LK; dummy2 = vol; φp2 = Exp[ln φ]];
ρp1 := Sort[Select[Select[ρ /. Solve[Z ρ / nav Rgas T = p /. {x \rightarrow xp1}, ρ],
  ((Im[#] == 0) && (0 < Re[#] < nav /  $(\sum_{i=1}^{nc} m_{[i]} v_{[i,i]}^0 x[i] /. {x \rightarrow xp1})$ )) &],
  ((st1 /. {x \rightarrow xp1, ρ \rightarrow #}) > 0) &], ((g /. {x \rightarrow xp1, ρ \rightarrow #1}) < (g /. {x \rightarrow xp1, ρ \rightarrow #2})) &][[1]];
error = 1;
iter = 0;
While[error > 10-10, Do[xp1[[i]] =  $\frac{xwt[[i]] / mw_{[i]}}{\sum_{j=1}^{nc} xwt[[j]] / mw_{[j]}}$ , {i, nc}]; dummy1 = ρp1;
  φp1 = φ /. {x \rightarrow xp1, ρ \rightarrow dummy1}; error = 0; Do[If[xp1[[i]] > 0, error = error + Log[ $\frac{xp2[[i]] \phi p2_{[i]}}{xp1[[i]] \phi p1_{[i]}}$ ]2], {i, ncLK}];
  If[Mod[iter, outfreq] = 0 ∨ error ≤ 10-10, Print[NumberForm[T, 5], "\t", NumberForm[p, 5], "\t", NumberForm[xwt[1] 100, 7],
    "\t", NumberForm[xwt[2] 100, 7], "\t", NumberForm[ $\frac{dummy1}{n_{av}} (xp1[1] mw1 + xp1[2] mw2 + xp1[3] mw3)$ , 5],
    "\t", NumberForm[ $\frac{1}{dummy2} (xp2[1] mw1 + xp2[2] mw2)$ , 5], "\t",
    NumberForm[ $(\frac{\rho_{polymer}}{dummy1 xp1[3]} - 1)$  100, 5], "\t", ScientificForm[error, 3]]];
  Do[If[xp1[[i]] > 0, xwt[[i]] = xwt[[i]]  $(\frac{xp2[[i]] \phi p2_{[i]}}{xp1[[i]] \phi p1_{[i]}})^{\frac{1}{damp}}$ ], {i, 1, ncLK}]; iter++; xwt[3] = 1 - xwt[1] - xwt[2];];
WriteString[outputfile, NumberForm[T, 5], "\t", NumberForm[p, 5], "\t", NumberForm[xwt[1] 100, 7], "\t",
  NumberForm[xwt[2] 100, 7], "\t", NumberForm[ $\frac{dummy1}{n_{av}} (xp1[1] mw1 + xp1[2] mw2 + xp1[3] mw3)$ , 5],
  "\t", NumberForm[ $\frac{1}{dummy2} (xp2[1] mw1 + xp2[2] mw2)$ , 5], "\t",
  NumberForm[ $(\frac{\rho_{polymer}}{dummy1 xp1[3]} - 1)$  100, 5], "\t", FortranForm[error], "\n"];
xwt[1] = xwt[1]  $\frac{p+10}{p}$ ; xwt[2] = xwt[2]  $\frac{p+10}{p}$ ; xwt[3] = 1 - xwt[1] - xwt[2], {p, pstart, pend, pstep}];
Close[outputfile];

```

Dankwoord

Yes! Het laatste stukje schrijfwerk voor een dr. in spé! Daar wil ik graag wat mensen voor bedanken, want zonder hen zou ik misschien wel gepromoveerd zijn, maar ik zou niet weten hoe...

Allereerst Jos Keurentjes, bedankt voor de mogelijkheid om onderzoek te kunnen doen en de vrijheid die je me daar in gaf. Het in recordtempo becommentariëren van allerlei publicaties en uiteindelijk dit proefschrift heb ik zeer gewaardeerd. Naast de begeleiding van Jos ben ik ook Marius Vorstman veel dank verschuldigd voor de begeleiding, de discussies en hulp bij het opstarten van de superkritische groep tijdens de eerste helft van mijn promotie. Vervolgens nam Maartje Kemmere het stokje succesvol van je over, Maartje bedankt!

Mijn eerste afstudeerder, Peter Somers, bedankt voor het geweldige experimentele werk dat je verzet hebt in Delft. Je scherpe inzicht in de theorie leverde leuke diepgaande discussies op over wat er allemaal mis is met SAFT! Hierbij wil ik graag ook Theo de Loos bedanken voor de goede samenwerking en voor de interessante discussies op het gebied van fasengedrag. Naveen Koak wil ik bedanken voor het Flash-algoritme in Fortran code voor de SAFT berekeningen.

Mark van Ginneken, mijn tweede afstudeerder, bedankt voor het uitvoeren van de vaak lastige polymerisatie experimenten.

Chris Luyk en Vincent Arts, zonder jullie werkplaats en inzet had ik geen werkende pompen, veilige reactoren en andere hogedrukopstellingen gehad, bedankt!

Voor de vele GPC metingen en hulp bij de NMR metingen ben ik Wieb Kingma en Marcel van Genderen zeer dankbaar. Henny Bruinewoud, ook jij ontzettend bedankt voor alle DSC metingen!

De leden van mijn kerncommissie, Leon Janssen, Gert-Jan Gruter en Cor Koning wil ik graag bedanken voor het doorlezen en becommentariëren van mijn proefschrift.

Rob Duchateau, voordat ik bij je kwam vond ik dat synthesewerk maar niks, van die enge, stinkende, explosieve stoffjes... Je hebt me heel wat bijgebracht en ik begon het zowaar leuk te vinden! Bedankt voor de goede samenwerking!

En dan m'n kamergenoten, eerst met Earl Goetheer en Stefan van der Sanden op een kamer, later alleen met Earl. Het is altijd een zeer gezellige rotzooi geweest met jullie. Earl, ik kan

me geen betere wetenschappelijke sparringpartner bedenken. Je stelling, dat uit chaos creatie volgt, gaat zeker voor jou op! Ook de andere (ex-)SPD leden, bedankt voor de gezellige werksfeer, waardoor vooral de koffiepauzes wel eens uit konden lopen.

Mijn familie, vrienden en kennissen wil ik graag bedanken voor de interesse in de voortgang van mijn onderzoek en voor de aangename onderbrekingen hiervan.

Tot slot, lieve Maaïke, bedankt voor je steun, liefde, kritiek en geduld!

Curriculum Vitae

Tjerk de Vries is op 14 januari 1973 geboren in De Bilt. Na het behalen van het VWO diploma aan het Alberdink Thym College te Hilversum in 1991 begon hij Scheikundige Technologie te studeren aan de Technische Universiteit Eindhoven. Het afstudeerwerk werd verricht op het gebied van dynamische simulatie van driewegkatalysatoren voor auto's in de vakgroep van prof.dr.ir. G.B. Marin. In 1997 werd het ingenieursdiploma behaald. Aansluitend werkte hij als wetenschappelijk medewerker bij dezelfde vakgroep aan het opzetten en begeleiden van een computerpracticum over chemische reactoren. In 1998 werd gestart met het promotieonderzoek aan de Technische Universiteit Eindhoven, in de Procesontwikkelingsgroep van prof.dr.ir. J.T.F. Keurentjes.